BUREAU OF RECLAMATION

Technical Report No. ENV-2021-121

Best Practices of Numerically Simulating Hydraulic Flushing – Progress Report

U.S. Department of the Interior

September 2021

Mission Statements

The U.S. Department of the Interior protects and manages the Nation's natural resources and cultural heritage; provides scientific and other information about those resources; and honors its trust responsibilities or special commitments to American Indians, Alaska Natives, and affiliated Island Communities.

The mission of the Bureau of Reclamation is to manage, develop, and protect water and related resources in an environmentally and economically sound manner in the interest of the American public.

Cover photo: A photo of Paonia Reservoir in Colorado after the reservoir was drawn down, showing how a channel incised through a portion of the reservoir sediments.

Technical Report No. ENV-2021-121

Best Practices of Numerically Simulating Hydraulic Flushing – Progress Report

Prepared by:

YONG LAI
Digitally signed by YONG LAI
Date: 2021.09.08 11:39:17 -06'00'

Yong G. Lai, Ph.D., Hydraulic Engineer
Sedimentation and River Hydraulics Group
Technical Service Center

JIANCHUN HUANG
Digitally signed by JIANCHUN HUANG
Date: 2021.09.08 13:06:55 -06'00'

Jianchun Victor Huang, Ph.D., P.E., Hydraulic Engineer
Sedimentation and River Hydraulics Group
Technical Service Center

Reviewed by:

BLAIR GREIMANN
Digitally signed by BLAIR GREIMANN
Date: 2021.09.09 16:24:31 -06'00'

Blair P. Greimann, Ph.D., Hydraulic Engineer
Sedimentation and River Hydraulics Group
Technical Service Center

Table of Contents

List of Figures

Tables

Summary

The document provides best practices in numerically simulating hydraulic flushing for reservoir sediment management. Three types of hydraulic sediment removal methods are discussed: drawdown flushing, pressure flushing and turbidity current venting.

The document first discusses the need for reservoir sediment management along with various ways that have been in use at present. Specifically, hydraulic flushing is introduced and presented as one of the widely used practices in moving the reservoir sediments to downstream. Each type is described in terms of its basic physical processes along with empirical and analytical methods for a quick assessment of the flushing operations. In addition, a brief review is provided with regard to the laboratory and field studies that have been used to investigate the physical processes of each flushing method and for specific sediment management applications.

The primary focus of this document is on the numerical modeling of various hydraulic flushing options. Therefore, a literature study has been carried out focusing on the numerical models and their use in practice. Three categories of numerical models are described and reviewed separately: the 1D, 2D depth-averaged or layer-averaged, and 3D CFD models. A Chapter is devoted also to the theory and numerical methods of the three categories. Due to the time and funding constraint, however, only 3D CFD models are presented. The theory and numerical methods of 1D and 2D models will be added in future.

Finally, general guidelines are given on how to select a proper model category given a specific type of reservoir and flushing method. More specific guidelines are also presented and discussed once a specific model is selected - 1D, 2D or 3D model. For each category, case studies are presented and discussed to provide guidelines on how specific project study questions are addressed using the numerical models, how to apply the models, determination of model domain and mesh, model input requirements, model performance, and results interpretation.

It is cautioned that this document is in its first version and will be updated continuously in the future when more cases are simulated and experience gained. At present, the guidelines are mostly based on the experiences of using the Reclamation models and projects. In the future, guidelines will be expanded based on experiences reported by other researchers and agencies when more literature is reviewed.

1. Introduction

Reservoirs have been built on natural rivers by humans to provide power, flood protection, water supply for irrigation and municipal use, recreation, and navigation. They increase the water surface level and reduce the water velocity, leading to undesirable and even detrimental consequences. One of them is reservoir sedimentation – a large amount of inflowing sediments are blocked by a dam, causing deposition within the reservoir and starvation of sediment supply to downstream. Reservoir sedimentation in general reduces the reservoir capacity, increases the risk of plugging the water intake, and alters ecology negatively.

It has been estimated that the loss rate of worldwide annual reservoir storage is between 0.5 to 1%, relative to the initial designed capacity (Mahmood 1987; Morris and Fan 1998; Annandale 2001; White 2001; Basson 2009; Wisser et al. 2013). Reservoir sustainability becomes a much-researched topic in the last decade and is required for most reservoirs. Sustainability requires actions to either remove sediments out of a reservoir or pass them through or around the reservoir. Failure to manage reservoir sediment today can be consequential in the future: dams may eventually lose their benefits and/or even need to be decommissioned - a substantial cost to future generation.

At Reclamation, most dam facilities are approaching to the age of 100 years –often the design lifespan of the space allocated for reservoir sedimentation. Reservoir sedimentation will limit Reclamation's ability to meet the agency mission of water delivery unless active sediment management plans are employed. Many Reclamation reservoirs have already been affected by sedimentation. Often, the outlets of most dams were set at levels based on the 100-year sedimentation. This level is being reached and exceeded at some reservoirs. For example, Paonia Reservoir in Colorado has had difficulty in meeting the project water deliveries because of the sediment and debris blockage at its intake. There is currently an appraisal level study underway to develop alternatives to pass sediments through the reservoir so that a sustainable alternative may be found and implemented. Buffalo Bill Dam in Wyoming, a hydropower generation facility, is another example. There are currently two dam outlets - hydropower and river outlets; they are near each other and at the same elevation. They have used the river outlet for the drawdown sediment flushing. Operation has been successful in creating a big-enough scour cone to maintain unobstructed hydropower intake. Reservoir drawdown, however, is not feasible most of the times due to the need of water for power generation. In other reservoirs, reservoir sediments are beginning to approach to the intake elevation for a penstock or water diversion. These facilities have witnessed the reduced project benefits due to reservoir sedimentation benefits, such as Black Canyon in Idaho, Elephant Butte in New Mexico, Summer in New Mexico, Arrowrock in Idaho, and Horseshoe Dam in Arizona, among others.

Various sediment removal measures may be adopted; among them are upstream watershed management, sediment bypass tunnels, hydraulic flushing, turbidity current venting, and mechanical dredging (Shen 1999). Upstream watershed management may be accomplished

through land-use practices to reduce the sediment delivery to a reservoir; sediment bypass is to divert sediments through channels or tunnels to downstream before they reach the dam; hydraulic flushing is to flush or sluice sediments within and near the dam to downstream through increased water release; turbidity current venting is to pass the inflowing fine sediments out of a dam directly through low-level outlets (Shen 1999; Randle et al. 2015a,b). Reservoir sediment removal has also been achieved using all types of dredging: mechanical, hydraulic and hydrosuction; however, their costs are usually high.

This document focuses specifically on the hydraulic flushing as it is one of the mostly adopted methods for reservoir sediment management. Hydraulic flushing is an economically attractive mean to manage sedimentation when low-level outlets exist at a dam. It is also one of the best methods through which the previously deposited sediment in the reservoir may be removed by opening the bottom outlets of a dam (Shen 1999; Madadi et al. 2017).

In this document, the term hydraulic flushing includes three types: drawdown flushing or sluicing, pressure flushing, and turbidity current venting. Drawdown flushing is carried out by lowering the reservoir pool elevation, partially or fully; it is the most effective technique for sediment entrainment and removal among the three. Drawdown flushing, however, is not always considered economically, socially, or politically viable for large reservoirs as the stored water may be needed for delivery commitment and/or power generation. For such reservoirs, pressure flushing or current venting is instead adopted. Pressure flushing refers to the process where sediment flushing is carried out when the reservoir water is maintained at a constant level well above the outlet. The benefit of the pressure flushing is that much less water is released; the effectiveness of pressure flushing, however, is limited to the vicinity of the outlet (Fan and Morris 1992; Kantoush 2008). Pressure flushing has been widely used at reservoirs due to the minimal amount of water needed and it is sufficient for reservoirs which do not experience large amount of sedimentation. Pressure flushing is effective in clearing out the debris and deposits in front of the gates, maintaining the clearance needed by the gate operation. Finally, turbidity current venting refers to the operation that sluices out the suspended fine sediments while they are moving towards the dam face during a large storm event. Venting can be very effective in venting the sediment current out of the reservoir before it deposits.

In practice, reservoir managers are faced with not only the decision of what hydraulic flushing method to use, but also the determination of an optimized flushing operation such as the timing, sequence, duration and release rate with the flushing operation. For drawdown flushing, the pool level needs to be optimized to balance the water needed and the sediment removable; for the pressure flushing, release rate, sequence and duration may be optimized to achieve efficient sediment removal; for current venting, the gate opening timing, size and duration need to match the storm event as well as the moving current characteristics. Further, all three flushing operations may significantly impact the downstream turbidity level, which is often regulated in the U.S. In the past, numerical models have been widely used to not only assist the planning and design, but also to determine the flushing operation schedule, although field data and empirical relations are also widely used. When new reservoir gates need to be added, numerical models are often used to assist the gate design and operation rules.

At Reclamation, a number of numerical models (1D, 2D and 3D) have been developed and applied to reservoirs for hydraulic flushing studies. Most modeling studies have been carried out based on engineers' own experience and expertise. There are currently no guidelines or best-practices that may be used to guide the sediment flushing modeling properly and consistently. In the literature, an increasing number of modeling studies have also been reported and lessons have been learnt. The situation motivated the development of this best practice document.

In this document, the best-practice guidelines are developed on selecting appropriate numerical models for a specific hydraulic flushing study. The issues include: the type and theory of numerical models available; selection of a proper numerical model for a given type of flushing; the study questions that may be answered; and reliability of numerical models. Sample application cases are also presented to illustrate various guidelines.

2. Literature Review

Hydraulic flushing is a cost-effective way to managing sediments in reservoirs. Sometime, the term of sluicing and flushing is used for different processes. Sediment sluicing passes incoming sediment directly to the downstream of the dam, while sediment flushing resuspends the previously deposited sediment and transports them downstream. Both methods involve the opening of low-level gates in a dam to allow increased flow velocity to transport sediments out of a reservoir. In many cases, sluicing and flushing occur simultaneously so the definition is not always clear.

In this document, three types of hydraulic flushing are considered: drawdown flushing, pressure flushing, and turbidity current venting. Drawdown flushing is carried out by lowering the reservoir pool elevation by releasing a large amount of water out of the reservoir. Pressure flushing is performed by opening low-level outlets while maintaining the relatively high reservoir pool level. Current venting sluices out the suspended fine sediments while it is moving towards the dam. The three hydraulic flushing types are illustrated in Figure 1 through Figure 3. For drawdown flushing with a wide reservoir, an eroded flushing channel is typically generated during as illustrated in Figure 1b. For pressure flushing, however, the eroded area is usually limited to a scour cone near the outlet (Figure 2b), leading to a much-reduced amount of sediments flushed in comparison with the drawdown flushing. A comparison of the two was discussed by Lai and Shen (1996) and Shen (1999) and a sample result is reproduced in Figure 4. For a turbidity current, it forms when a turbid stream flows into a less turbid reservoir as shown in Figure 3. Once plunged, the current may attach to the bed as an underflow propagating down a slope; but it may also stay along the neutrally buoyant interface above the bed if the reservoir is stratified due to temperature.

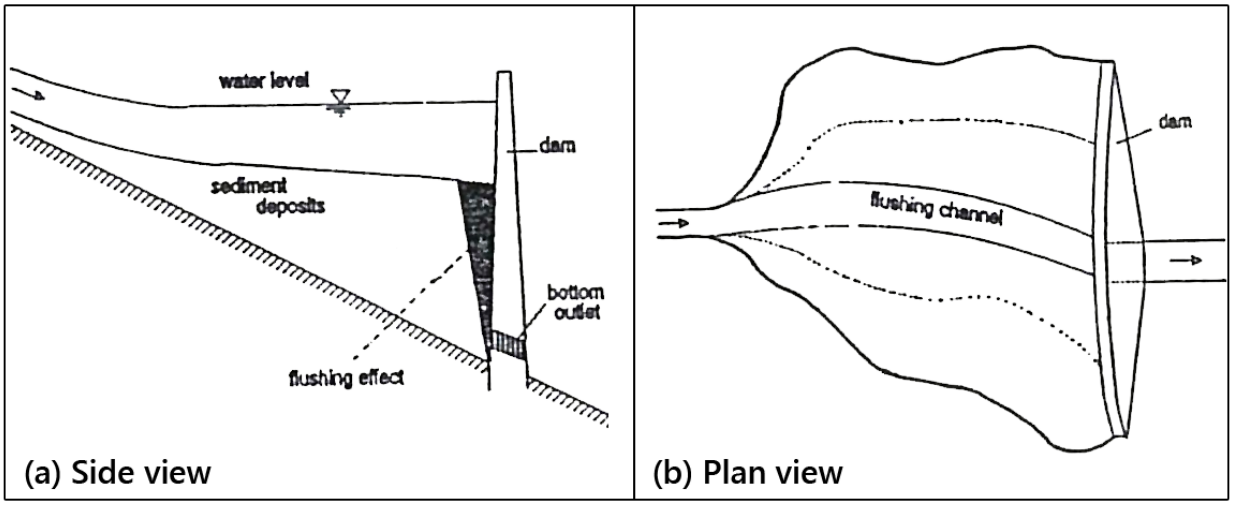

Figure 1. Sediment erosion and movement in drawdown flushing (source: Shen 1999).
Note that the side view is highly vertically exaggerated.

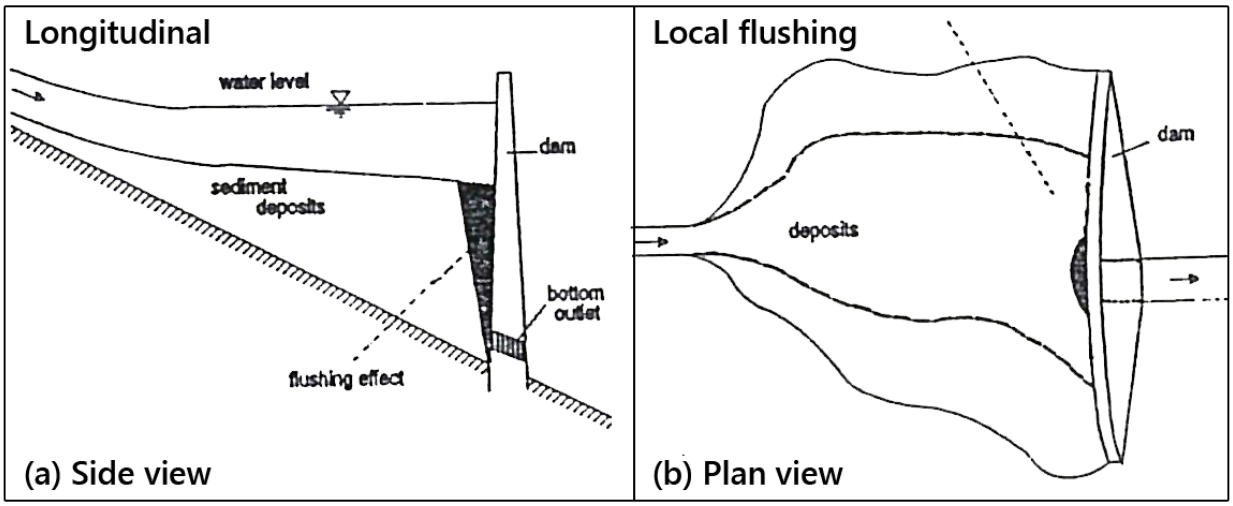

Figure 2. Sediment erosion in pressure flushing (source: Shen 1999).

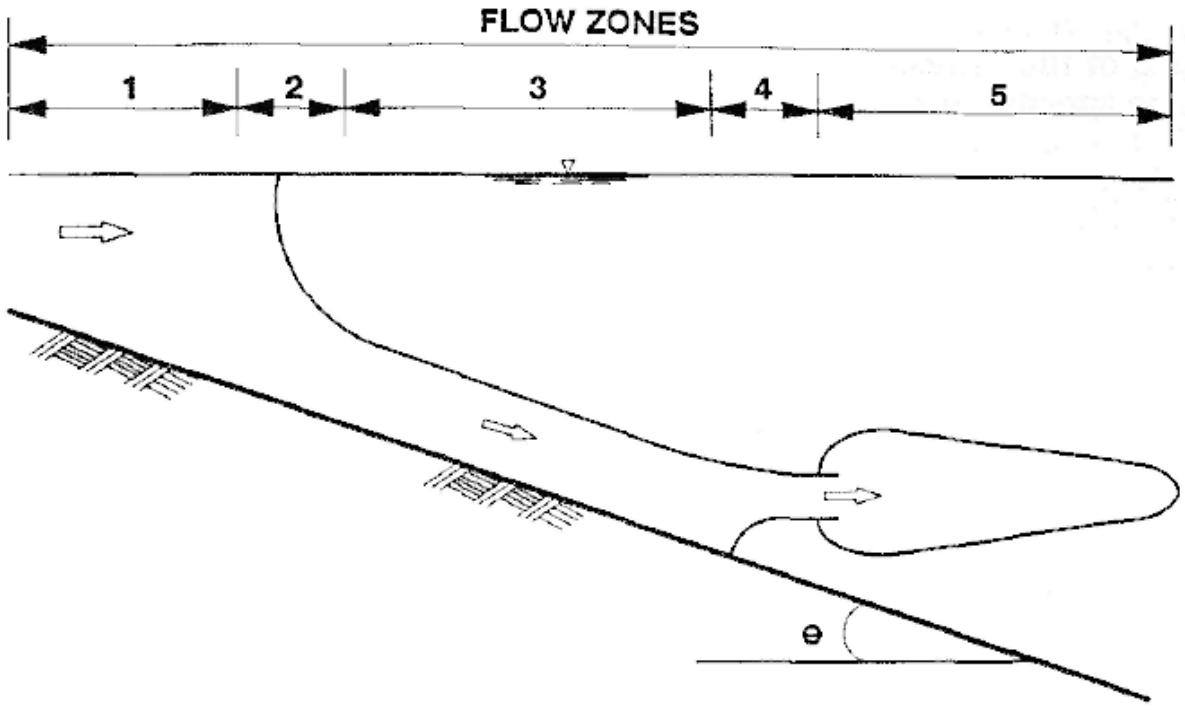

Figure 3. Sketch for a typical turbidity current (Source: Alavian et al. 1992).

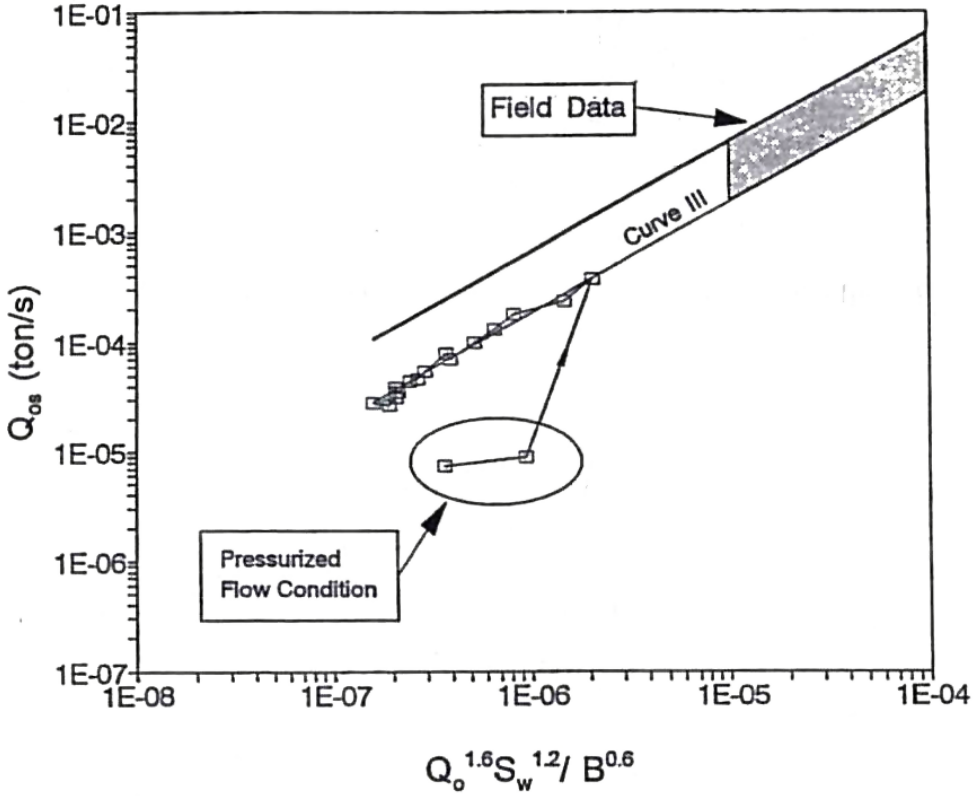

Figure 4. Sediment outflow and flow characteristics based on the field data with the pressure and drawdown flushing (source: Lai and Shen 1996; Shen 1999); note that the sediment rate is only for a short period of time while the cone is still being eroded.

2.1 Hydraulic Flushing Analysis

2.2.1 Drawdown Flushing

Drawdown flushing lowers the pool elevation, creating a larger energy gradient and increased flow velocity, resulting in the erosion of sediments from the reservoir and transport of sediments to downstream. This technique has been most effective in reservoirs where water storage requirement allows sufficient water release. Drawdown flushing is also most effective for narrow reservoirs. It may involve a large volume of water passing through the dam; sometimes it may even require the reservoir emptied (Atkinson 1996). When it is poorly managed, sediments from the upstream delta may move towards deeper portion of the reservoir and then deposit, rather than be routed past the dam (Dahl and Ramos-Villanueva 2019). Note that drawdown flushing may be the only long-term option for sediment management in many reservoirs.

Drawdown flush can best practiced under the following conditions (Morris and Fan 1998, Kondolf et al. 2014, White 1990):

- narrow valleys with steep sides,
- steep longitudinal slope,
- river flow above a threshold to mobilize and transport sediment,
- low-level gates large enough to pass flows, and
- strongly seasonal flow patterns.

There are many proposed flushing criteria for determining whether flushing at a particular reservoir will be successful. Dahl and Ramos-Villanueva (2019) presented some guidelines for reservoir drawdown flushing. Three factors were considered: total capacity of the reservoir (CAP), mean annual runoff to the reservoir (MAR), and mean annual inflow of sediments to the reservoir (MAS). Low ratios of CAP/MAR (<0.1) and CAP/MAS (<30) were recommended for a successful drawdown sediment flushing. Others provided similar guidelines. For example, the ratio of reservoir capacity to mean annual runoff should be less than 1/50 according to Annandale (1987). A value of 1/25, however, was suggested for reservoirs with a half-life shorter than 100 years by Ackers and Thompson (1987). Discussion of the same topic was also reported by Atkinson 1996), Sumi (2008), and Kondolf et al. (2014).

Figure 5 summaries the drawdown flushing projects from diverse environments; it shows that for drawdown flushing to be successful the ratio CAP/MAR should not exceed 4% (Kondolf et al. 2014). Note that the flushing efficiency is defined as the ratio between the volume of sediment flushed out and the volume of water employed. The cost of operation is defined as the ratio between the expenses of mechanical excavation and the loss of water and hydropower.

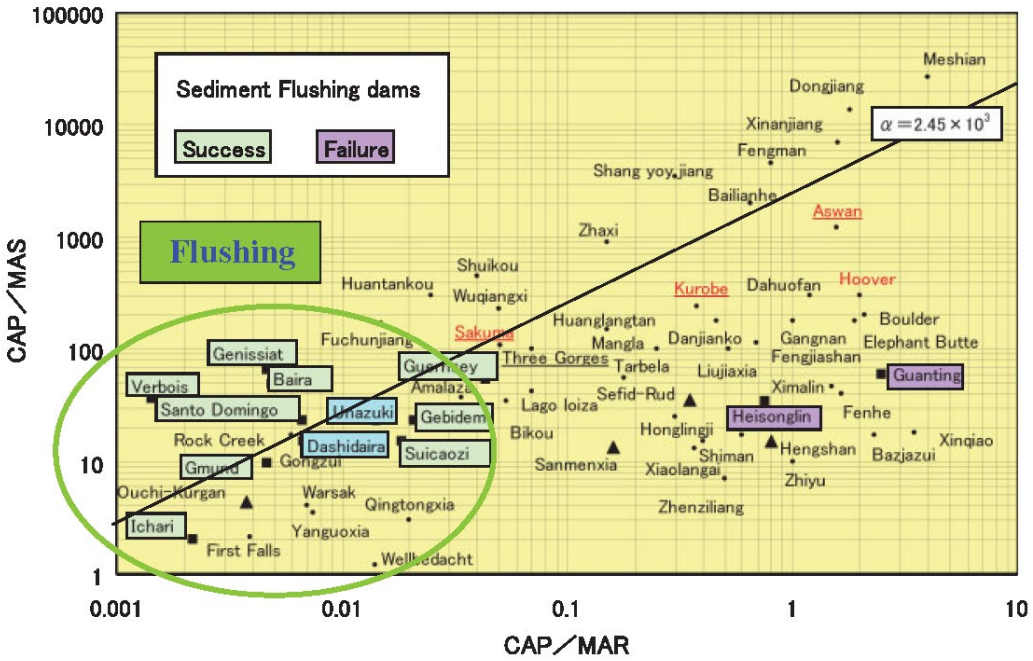

Figure 5. Plot of drawdown flushing project with CAP/MAR and CAP/MAS (source: Kondolf et al. 2014).

The physical processes of reservoir sediment flush depend on many factors and some are listed below:

1. Geometry of reservoir: width, depth, and area-capacity table,
2. Reservoir sediment particle size and sediment distribution,
3. Annual flow and flow hydrographs,
4. Incoming sediment load and sediment class sizes and concentration of sediment hydrography,
5. Outlet opening size, sill elevation, and location,
6. Reservoir operation rules,
7. Sediment concentration magnitude and duration constraint placed on the reservoir release, and
8. Restriction of sand deposition in the downstream gravel-bed channel (e.g., Chang et al. 1996).

Of the above, factors 1-6 should be known before designing a reservoir sediment flush operation and information in 7-8 may be obtained by a numerical/physical model or from sediment monitoring and in some cases are optional depending on the environmental constraints.

When drawdown flushing is used for a reservoir much wider than the original width of the river, only a relatively narrow channel will be created, not the entire width of the reservoir lake (see Figure 1). This was observed, e.g., at the Paonia Reservoir in Colorado (Figure 6) and many other reservoirs.

Figure 6. A photo of Paonia Reservoir in Colorado after the reservoir was drawn down: a channel incised through a portion of the reservoir sediments.

The concept of sustainable reservoir capacity was discussed by Atkinson (1996), who defined it as the storage capacity of a reservoir which can be sustained by hydraulic flushing in a long term. If a reservoir is narrower than the width of a self-formed channel produced by the drawdown flushing flow, most of the sediments could be flushed out of the reservoir. If the flushing channel width is much narrower than the reservoir width, the sustainable reservoir capacity would be smaller than the original designed or initial storage capacity. A rough estimation of the sustainable reservoir capacity was possible by using the long-term estimated bed profile and side slope. The long-term or final channel slope may be estimated from the initial bed profile and the difference between the dam outlet and initial bed elevation at the dam. The channel side slope can also be obtained from the sediment dry density. According to Atkinson (1996), the flushing channel width B may be related to the flushing discharge and approximated by an empirical function as $B = 12.8{Q_f}^{0.5}$ (B is the width in meter and Q_f is the flushing discharge in m^3/s). This relation may be applicable when reservoir sediments have reached near the dam. It is, however, cautioned that the flushing channel width may vary widely depending on the local conditions. Randle et al. (2015a), for example, found that the channel width might vary significantly in both spatial and temporal dimensions based on the data from the drawdown and dam decommissioning study at the Elwha Dam and Glines

Canyon Dam on the Elwha River, Washington. The channel was found narrower where it came in contact with more cohesive sediments and wider where it contacted coarser and non-cohesive sediments. The channel in the upstream half of the reservoir became highly braided and changed course daily while reworking non-cohesive coarse delta sediments.

Four sediment transport stages are generally involved in a drawdown flush:

1. When the low-level outlets are first opened, local high velocity flow entrains the fine material deposits close to the outlet, resulting in a short period of high sediment concentration outflow. This is stage is similar to pressure flushing.
2. After the local deposits are removed, the velocity becomes too small to even move the fine material. This stage is similar to the final stage of pressure flushing.
3. When the reservoir level is lowered further, the sediment depositions near the reservoir entrance are being entrained. At this stage, the entrained fine sediments are being carried downstream towards and out of the dam, the coarse sediments may be redeposited in the reservoir close to the dam.
4. In the final stage when water stage is at its lowest similar to typical riverine channel flow, sediments previous deposited in the reservoir may be resuspended and transported downstream of the dam.

2.2.2 Pressure Flushing

Pressure flushing in this report refers to the process where flushing is carried out using low-level outlets when the reservoir water is maintained at a constant and relatively high level well above the outlet. Pressure flushing is usually used in reservoirs where water storage is of high value, and has been widely used for reservoirs in the U.S. where water storage is important and the inflowing sediment rate is relatively small. Sediments eroded from the reservoir are usually limited to a small area immediately upstream of the gates (see Figure 2). It is also used to clean the sediments and debris near the gate(s) and to prevent the outlets from being buried or clogged. The effectiveness of pressure flushing, however, has long been viewed as low: only sediments in the vicinity of the outlet are removed (Fan and Morris 1992; Kantoush 2008). Jansson and Erlingsson (2000), e.g., found that the scouring cone was limited in an area in the vicinity of the bottom outlet. Further, the pressure flushing schedule adopted – the timing, duration and release discharge - may impact the flushing efficiency significantly. Our understanding of pressure flushing is limited at present and often the design of an efficient flushing schedule is not science-based.

Empirical relations for the scour cone estimate have been proposed (see discussion by Lai and Greimann 2020). For the flow field upstream of an orifice in a reservoir. Shammaa et al. (2005) used potential flow solutions to analyze the velocity contours upstream of orifices and found that the computed decay of the velocity with distance from the orifice matched previous experimental and numerical analysis of flow fields upstream of unbounded orifices. They also found that the particular shape of the orifice is only important close to the orifice. For orifices of different geometries, they found this distance typically did not exceed 2 to 3 times of $\sqrt{A}$, where A is the area of the orifice opening. They found that maximum velocity upstream of an

unbounded orifice where the flow depth (H) is much greater than the orifice diameter (D) ($H \gg D$) can be described by the following equation:

$$\frac{u_{max}}{U_0} = 1 - [1 + 0.25(D/x)^2]^{-0.5}$$

where x = distance along centerline from orifice, D = orifice diameter, U_0 is the average velocity within the orifice. This equation is only valid for $x > 0$, and the maximum velocity becomes approximately proportional to x^{-2} for x/D greater than 2. The equation also predicts that for x/D equal to 2, the maximum velocity is 3% of the average velocity at the orifice. The analysis demonstrates that velocity decreases rapidly upstream of orifices in reservoirs and therefore the effect of the orifice on erosion will be limited to a relatively small area upstream of the orifice.

Powell and Khan (2012; 2015) studied the flow field upstream of a bounded orifice with both a fixed bed and a mobile bed. The analyzed circular orifices with the fixed bed or the initial sediment level at the elevation of the invert of the orifice. The flow field was similar to the unbounded orifice case, but the maximum velocity decreased slightly slower due to smaller area from which to draw flow into the orifice. They developed equations of the same form as predicted from Shammaa et al. (2005), but with slight modification to coefficients:

$$\frac{u_{max}}{U_0} = 1 - [1 + a(D/x)^b]^{-c}$$

The a, b, and c values are 0.332, 1.679, and 0.515, and 0.145, 1.493, and 0.913 for the fixed bed and mobile bed cases, respectively.

An idealized conceptual figure of the scour upstream of an orifice is shown in Figure 7. The scoured area upstream of the orifice is assumed to form at a depth of D_s below the invert of the orifice. There is an approximate flat area projecting from the wall and then the scoured area is assumed to project upward at a constant angle θ.

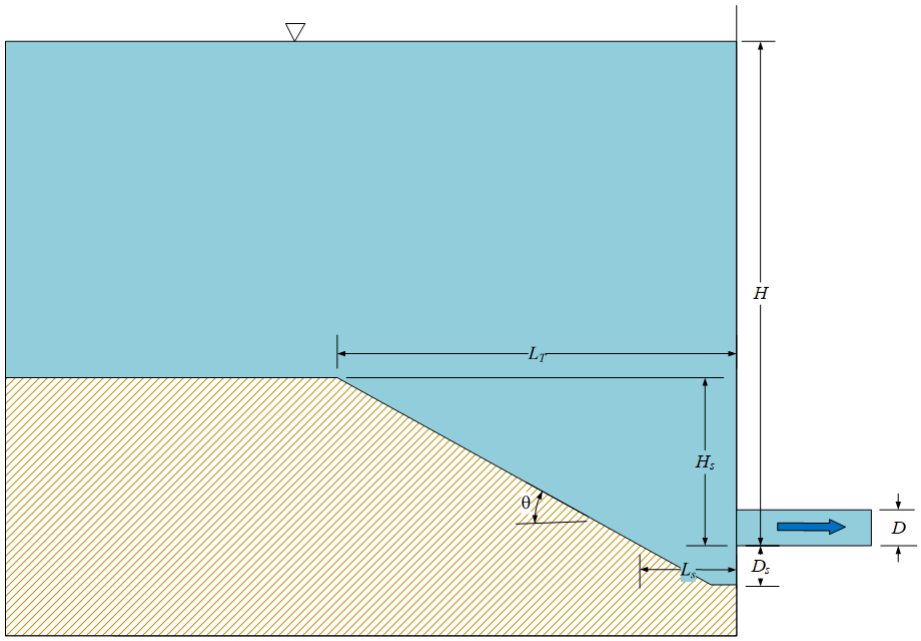

Figure 7. Idealized profile view of equilibrium scour upstream of orifice.

Fathi-Moghadam et al. (2010) performed physical modelling of scour in non-cohesive sediment upstream of circular orifices. They found that the non-dimensional volume (V/D^3) and non-dimensional total length (L_T/D) of the equilibrium scour hole governed by the following non-dimensional equations:

$$\frac{V}{D^3} = 5.28\left(\frac{U_0}{\sqrt{g(s-1)d_{50}}}\right)^{0.1}\left(\frac{H_s}{H}\right)^{0.046}$$

$$\frac{L_T}{D} = 8.19\left(\frac{U_0}{\sqrt{g(s-1)d_{50}}}\right)^{0.1}\left(\frac{H_s}{H}\right)^{0.033}$$

Here H_s is the depth of sediment above the invert of the orifice and they did not report the depth of scour below the orifice. The first term in the equation is typically called the particle densimetric Froude Number and u is the average velocity through the orifice, s is the specific gravity and d_{50} is the median particle diameter. The experiments did not vary sediment depth (H_s) or orifice diameter (D), but had variable water depth (H), sediment diameter (d_{50}) and orifice flow velocity (u). They found that the angle of the scour cone was relatively constant and was close to the angle of repose for submerged particles: θ varied between 27 to 33, 29 to 34, and 30 to 35 degrees, for the fine, medium and coarse sand, respectively. The slope of the cone in the flow direction was only 2 to 6 % larger than the slope perpendicular to the flow. Like most empirical equations, it should only be applied within the range of the experimental data upon which it was based. The value of H_s/H varied between 0.25 to 0.45, and this equation cannot be applied to estimate depth of scour when H_s= 0.

Kamble et al. (2017) choose to non-dimensionalize the length of scour with the water depth and developed the following equation:

$$\frac{L_T}{H} = 2.9\left(\frac{H_s}{H}\right)^{0.51}\left(\frac{A_0}{H^2}\right)^{0.31}\left(\frac{u}{\sqrt{g(s-1)d_{50}}}\right)^{-0.44}$$

They only used one sediment size (0.25 mm) in their experiments so the dependency on the sediment size is uncertain. Because velocity is directly dependent on water depth, every non-dimensional parameter is dependent upon depth, and some hesitation is warranted in applying this equation.

Powell and Khan (2012) performed experiments in non-cohesive material with grain size varying between 0.29 and 0.89 mm. The orifice diameter was 15.2 cm and the head above the center of the orifice varied between 45.72 cm and 76.20 cm. The experiments were all run with H_s= 0. Powell and Khan (2015) performed tests and found scour hole length (L_s) varied between $1.5D$ to $2.17D$, with the highest head resulting in the longer scour hole length. The depth of the scour hole varied between $0.5D$ and $0.71D$, again with head resulting in the deepest scour hole. They describe the shape of the scour hole with the following non-dimensional equation:

$$\frac{d}{D_s} = \begin{cases} 1, & \text{if } x/L_s < 0.15 \\ 1.2(1 - x/L_s), & \text{if } 0.15 \leq x/L_s < 1 \end{cases}$$

where d is the local depth of scour and x is distance from orifice.

Hajikandi et al. (2018) compared different equilibrium scour conditions between square and circular orifices. They found very similar non-dimensional scour shapes as Powell and Khan, but that the scour length was 10 to 15 percent longer for a square orifice of the small cross-sectional area as a circular orifice. Similar to Powell and Khan (2012), the length and the width of the scour hole showed weak dependency on particle size. Their results also extend the results of Powell and Khan to higher values of H/D. The results for the length of the scour hole as a function of hydraulic head are shown in Figure 8.

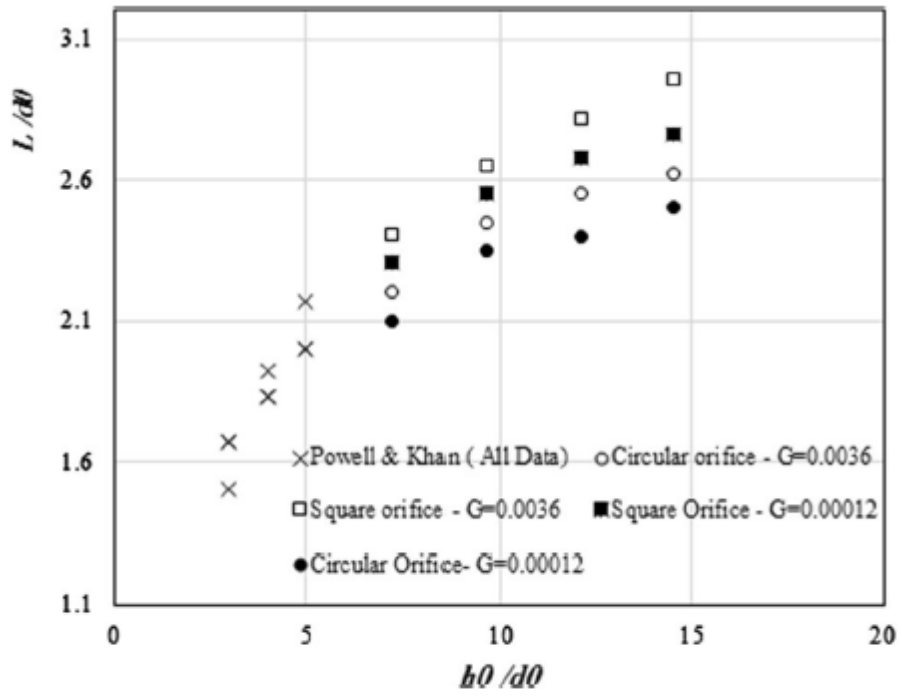

Figure 8. Measured scour length upstream of orifices as a function of hydraulic head (source: Hajikandi et al. 2018). To convert their notation to present notation: *h0* = *H*, *d0* = *D*, and *L* = L_s.

Emamgholizadeh and Fathi-Moghdam (2014) developed equations using experiment with cohesive soil and found that the densimetric Froude number was not significant compared to the bulk density of the sediment and the non-dimensional volume and total length:

$$\frac{V}{D^3} = 0.99\left(\frac{H_s}{H}\right)^{0.59}[(1-\eta)(s-1)]^{-2.85}$$
$$\frac{L_T}{D} = 0.33\left(\frac{H_s}{H}\right)^{0.4}[(1-\eta)(s-1)]^{-1.44}$$

where η is the sediment porosity. The side slope of the scour cones for five classes of the bulk density were measured as 55.4, 46.7, 43.2, 37.8, and 32.1 lb/ft^3 with an average of 43°. In their report, they noted significant discrepancy of the side slope of the scour cones with field measurements and stated that the field measurement of the reservoirs in China had measured scour cone side slopes ranging between 4 to 17° (Fang and Cao, 1996). This difference in the measured side slopes is significant and indicates that the laboratory results on scour length cannot be directly scaled to the field. It is likely that for cohesive soils the equilibrium angle of repose could be significantly different in the laboratory scale and field scale. Larger scale slumping processes could be important at the field scale than the laboratory scale.

Empirical equations will be useful in designing and evaluating expected scour in pressurized flushing scenarios. However, there are several limitations:

1. The equations may not apply outside of the range of parameters used in the development of the equation.

2. The equations do not describe all the characteristics of the scour hole.
3. The equations only apply for simple geometric conditions. Other structures added to increase scour or more complex geometries will have an unknown effect.
4. The sediment size and cohesive properties were not scaled from the field to the laboratory. Therefore, the typically non-dimensional parameters related to sediment size will be much different in the laboratory than the field.

The last point requires additional explanation. The shear strength of a soil is commonly computed as (Reclamation 1998):

$$\tau_s = c' + (\sigma - u)\tan\phi'$$

where τ_s = shear strength of soil

c' = effective cohesive strength

σ = normal stress on sliding surface

u = pore water fluid pressure

ϕ' = internal friction angle

Assuming a uniform thickness of submerged sediment on a slope, the equation for the critical stable depth (h_c) on slope, β, is:

$$(1-\eta)(\gamma_s - \gamma_w)h_c \tan\beta = c' + (1-\eta)(\gamma_s - \gamma_w)h_c \tan\phi'$$

For non-cohesive soil ($c' = 0$), this equation simplifies to a simple angle of repose condition meaning that if $\beta > \phi'$, the slope is unstable and fails. The depth of sediment is not important for non-cohesive soil. For cohesive soil, it is more complicated. Typically, the sediment used in the laboratory and that is present in the field will have similar values of c' and ϕ'. Therefore, the critical depth for the same slope will be similar in the laboratory as in the field. However, the depth of sediment in the laboratory may be below the critical depth, whereas the depth of sediment in the field is much greater the critical depth. The result is that field observations of the stable slopes in the field are significantly less than in the laboratory.

A more reliable method of estimating scour hole size would be to perform two analysis steps:

1. Estimate the length of the scour hole at or below the invert of the orifice (L_s) using data from Hajikandi et al. (2018) and Powell and Kahn (2012). Typical values of L_s are expected to be about 1.5 to 3 times the equivalent orifice diameter.

2. Estimate stable profile outside of scour hole using geotechnical principles. For non-cohesive soils, assume that the stable slope will be near the submerged angle of repose for that material. For cohesive soil, determine the stable profile based upon the measured effective cohesive strength and internal friction angle for that material.

The two stages of empirical analysis results from the likely scenario that there is a two-step process of evacuating sediment in front of the intake. First hydraulic forces are dominant near the intake and rather quickly remove sediment within approximately 1.5 to 3 intake diameters. Then the over-steepened area created by the sediment may fail through geotechnical processes until it reaches a stable profile.

2.2.3 Turbidity Current Venting

Turbidity current may be formed if the incoming sediments are very fine while concentration is high. It is the result of a sediment-laden flow plunging beneath the clear water in the reservoir. Once plunged, the turbidity current moves along the bed of the reservoir towards the dame face. Such bottom-moving turbidity current may be vented out of reservoir if there are low-level outlets that may be opened. While turbidity current is being vented, the reservoir sediments on the bed may also be entrained and passed out of the reservoir. Since turbidity current moves near the bed with a finite thickness, venting can be an effective sediment management tool and has been used extensively in, e.g., Taiwan (Lai 2014; Huang et al. 2019).

Detailed empirical and analytical analysis have been carried out and available for understanding the turbidity current characteristics, plunging criteria, mixing rate, entrainment from the upper clear water layer, and a number of simple models. Readers are referred to Lai (2014) for details and they are omitted herein.

2.2 Field and Laboratory Studies

Field and laboratory studies have been widely used in the past. Majority of the literature was concerned with the drawdown flushing. For a good review, refer to Shen (1999) and Randle (2015a;b). Turbidity current was also widely studied; Lai (2014) may be referred for a detailed review concerning the field and lab studies. Herein, some reviews are provided for the pressure flushing as it is less documented. Some of the literature of the turbidity current field and lab studies are also reviewed.

There are limited studies of pressure flushing. Most relied on the experimental approach, using the physical model studies, to optimize the layout and design of a hydraulic structure (Isaac et al. 2014). Some of the experimental studies are discussed below, among others.

Talebbeydokhti and Naghshineh (2004) conducted an experimental work using the physical model. They found that the amount of sediment flushed was a function of the release discharge, the water level and the flushing channel width. Emamgholizadeh et al. (2006) investigated the scour cone development with varying release flow and water depth above the outlet. It was observed that the scour cone volume and size increased with the release discharge and decreased with the water depth. Meshkati et al. (2009; 2012) studied the time dependent process of the scour cone in a water storage reservoir and developed a set of non-dimensional relationships for the temporal variations of the scour cone dimensions. The effect of the outlet cross-section size was also investigated on the cone development. It was found that the cone size was a strong function of the outlet diameter. Powell and Khan (2012, 2015) reported laboratory studies using circular outlets. They investigated the flow characteristics and the sediment transport, primarily the formation of vortices near the outlet. Ahadpour

Dodaran et al. (2012) conducted an experimental study to understand the effect of the frequency and location of a vibrating plate on the scour cone sized. They concluded that the vibrating plate had a positive effect on the scour cone size. Most experiments were carried out using the non-cohesive sediments. An exception was the work of Emamgholizadeh and Fathi-Moghadam (2014) who studied the cohesive sediment cone development. They reported that the scour cone volume and size decreased with an increase in the sediment bulk density. The bulk density reflects the compaction of the cohesive materials and produces different erodibility. It was found to be the most important parameter in comparison with discharge and water depth.

In recent studies, Kamble et al. (2017) reported hydraulic modeling to understand the scour cone development during pressure flushing for a run-of-the-river hydro-electric project. The experiment was done in a flume fitted with a single spillway bay; flushing discharge and water depth were varied. Using the dimensional analysis and measured data, special relations were developed for computing the dimensionless parameters of flushing cone geometry (depth and length) in the vicinity of outlet. These relations may be useful for project design purpose. In another study, Madadi et al. (2017) used the laboratory experiment to investigate whether a new outlet configuration might increase the pressure flushing efficiency. A projecting semicircular structure was connected to the upstream edge of the bottom outlet. It demonstrated that the proposed new outlet increased the sediment removal efficiency significantly in comparison with the traditional flushing without the projecting structure.

Hajikandi et al. (2018) compared different equilibrium scour conditions between square and circular orifices. They found very similar non-dimensional scour shapes as Powell and Khan, but that the scour length was 10 to 15 percent longer for a square orifice of the small cross-sectional area as a circular orifice. Similar to Powell and Khan (2012) the length and the width of the scour hole showed weak dependency on particle size. There results also extend the results of Powell and Khan to higher values of water depth to orifice diameter.

In the area of turbidity current lab and field studies, a brief review is provided.

Field study of turbidity currents faces challenges such as large uncertainties associated with existing data collection instrumentation, limited amount of field variables that can be measured, hazardous conditions during periods of active turbidity currents, and high cost in data collection. Therefore, laboratory experiments are typically performed (Paull et al. 2003). Early experiments concentrated on the initiation mechanisms and configuration of currents, especially the head and the body (e.g., Kuenen and Migliorini 1950; Ellison and Turner 1959; Middleton 1966). The first laboratory experiments to investigate 3D structures of density currents were carried out by Fietz and Wood (1967). Subsequent studies have focused further on the body (e.g., Garcia 1993; Buckee et al. 2001; Sequeiros et al. 2009), on the head (e.g., Lambert et al. 1976; Huppert and Simpson 1980; Marino et al. 2005), and on the erosion and deposition patterns (e.g., Parker et al. 1987; Garcia 1994). Field studies of turbidity currents have been limited owning to the difficulties mentioned above, but some historical data measurements in larger reservoirs are available (BOR 1954). Turbidity currents may reach velocities of tens of meters per second and heights of hundreds of meters. Even some modest currents have damaged deployed equipment. Limited field studies have been reported, for example, by Chikita (1990), Paull et al. (2003) and Xu et al. (2004). A detailed review of key advancements (both measurement technology and science theory) in the field measurement of currents in submarine canyons was reported by Xu (2011).

Laboratory experiments, however, are only roughly applicable to the field due to scaling issues.

2.3 Numerical Modeling Studies

Numerical models have been widely used in sediment hydraulic flushing study. The model complexity varied widely, ranging from 1D, 2D and 3D models. A literature review is provided concerning all three models. It is generally commented that numerical modeling study has been limited mostly to drawdown flushing and density current venting; few studies have been found for the pressure flushing.

2.3.1 1D Numerical Models

1D numerical models offer a balance between the limited empirical models and more complex and computationally expensive 2D and 3D models. 1D models are appropriate in run-of-the-river reservoirs, where flow is highly channelized and transverse mixing is well accomplished.

Chang et al. (1996) used a 1D model, FLUVIAL-12, to evaluate the feasibility and effectiveness of sediment passing through reservoirs through drawdown flushing during flood events. The model was applied to a series of reservoirs (Poe, Cresta, and Rock Creek) on the North Fork Feather River in Northern California. In their study, the numerical modeling showed that sediments could be flushed out of the reservoirs and the reservoir capacity could be maintained by an extended drawdown flushing operation during flood. In addition, the reservoir drawdown and sediment in the reservoir can be controlled so that no sand would deposit on the gravel bed downstream of the reservoirs for fish habitat purpose.

Morris and Hu (1992) used a 1D HEC-6 model to simulate sediment flushing in the Loíza Reservoir in Puerto Rico. The numerical modeling indicted that the conversion of the reservoir from continuous high-pool operation to low-pool operation during flood periods would decrease sediment trap efficiency by 65%.

Liu et al. (2004) developed a 1D numerical model to simulate the 2001 sediment flushing operation at two reservoirs in a series: the Dashidaira reservoir and Unazuki reservoir on the Kurobe River in Japan. The model was used to compute the bed evolutions, suspended sediment concentrations, and sediments flushed from or deposited in the two reservoirs.

Ahn (2012) and Ahn et al. (2013) used a 1D model (GSTAR4) to simulate the sediment flushing in Xiaolangdi Reservoir of the Yellow River and in Lewis and Clark Lake of the Missouri River.

Guertault et al. (2014) applied the 1D flow and sediment transport model, Mage-AdisTS, to simulate the 2012 sediment flushing at the Genissiat reservoir on the French Upper Rhone River. During the flushing operations, water and sediment were released in different levels in order to maintain an average concentration downstream of Genissiat below 5 g/L throughout the operation. This was implemented by different gate opening combinations of hydraulic

outlets located at three different levels (a bottom gate, a half-depth gate, and a surface spillway). To calculate the sediment concentration released from the dam, the numerical model first calculated total sediment concentration in the reach, then transferred it into the vertical concentration profile based on the mass conservation and steady state vertical diffusion equation, finally calculated the average concentration passing through the gate. The model reproduced the sediment concentrations at the bottom, half-depth, and surface well, but not the peak suspended sediment concentration in the bottom gate. This would be expected because 1D models are cross sectionally average and cannot predict complex flow field near the low-level gates in reservoirs.

Boyd and Gibson (2016) used the 1D HEC-RAS model to simulate 2014 fall flush of the reservoir at Spencer Dam, 40 miles upstream of the confluence of the Niobrara River and the Missouri River. The reservoir has been flushed twice annually, in the spring and in the fall, in the last 60 years in an effort to remove sediment in the reservoir. However, no spring flush was performed in 2014 and it provided an opportunity to flush sediment deposited in the reservoir in an entire year. Cross sections were survey upstream and downstream of the dam, with approximately 250 ft spacing in the reservoir. Suspended sediment and bed material samples were also collected during the flush at three locations downstream of the dam. The numerical model was calibrated with the reservoir sediment volume channel and downstream sediment concentration. It was reported that the model underpredicted the delta scour by about 50% and over-predicted the peak sediment concentration downstream of the dam. The authors attributed the difference to the channel widening process which could not be simulated correctly by the 1D model and anticipated that a lateral process model, such as Bank Stability and Toe Erosion Model (BSTEM), would improve the model result.

Brignoli (2017) applied SRH-1D's unsteady flow and sediment transport modules to simulate the controlled sediment flush in Isolato and Madesimo Reservoirs in Italy for a total of 66 hours operation. Madesimo Dam in Scalcoggia River, a tributary of Liro River, locates about 1.4 km upstream of the conference of Scalcoggia and Liro rivers. Isolato Dam locates about 1.4 km upstream of the same conference in the Liro River. Mechanical equipment was used to help remove the reservoir sediment once the reservoirs are empty. The numerical model was mainly used to predict the sediment impact in the downstream of the two dams and downstream of the conference. The author found that a satisfactory agreement between the computed and the observed depositional pattern was obtained.

Huang et al. (2019) updated SRH-1D to simulate a sediment flushing plan for the Paonia reservoir, located on Muddy Creek in western Colorado. A proposed sediment lushing plan was conceptualized to lower the reservoir pool in the early spring, and to flush the sediment with high spring runoff flows through the outlet works before closing the gates to refill the pool for the irrigation season. SRH-1D was modified to include a user-defined set of reservoir operation rules. Unsteady flow and sediment solutions within SRH-1D were used to simulate the reservoir filling and emptying process. The model was first calibrated with 3 years of field data and then used to predict short-term sediment management under different reservoir operations. The goal of the reservoir operations was to maximize the flushing of sediment, but still fill the reservoir with the water from the spring snowmelt. To simulate actual operational conditions in which the future flows are unknown, a forecasted spring snow melt volume was used to set the reservoir operations. The flushing period was continued until it was necessary

to start capture the flow and ensure the reservoir filled. The numerical model results showed that reservoir trap efficiency strongly depended on the whether the 10%, 50% or 90% exceedance value for the inflow volume forecasted was used. For the year 2016, the reservoir trap efficiency was predicted to range from 20% when using 90% exceedance forecast to -3% (net erosion) when using the 10% exceedance forecast.

Artruc (2020) developed a numerical model to simulate the rate, magnitude, and timing of lateral erosion of Lake Aldwell on the Elwha River in Washington state under the effects of drawdown rate and grain size. The numerical model calculated the bank erosion due an excess shear stress on the bank and a geotechnical failure due to a discrepancy between the water in the channel and the water within the bank; however, the hydraulic model is simplified as 1D steady flow at normal depth.

2.3.2 2D Numerical Models

2D depth-averaged numerical models provide more detailed representations of hydraulic characteristics of a reservoir lake which might be missed in a cross sectionally averaged 1D model. 2D models may be used to simulate a reservoir with a relatively large width-to-depth ratio in which sediment deposition and resuspension may vary widely along a cross section.

Olsen (1999) presented a 2D numerical modeling for the reservoir sediment flush study. The numerical model solves 2D depth-averaged equations for flow and 3D convection-diffusion equation for the sediment concentration with the extrapolated flow field. The grid is adaptive in the vertical direction and changes according to the calculated water and bed levels. The numerical model was assessed by comparing with the bathymetric cross-sections from a physical model study of Kali Gandaki Hydropower Reservoir in Nepal.

Dewals et al. (2004) used WOLF 2D to simulate the sediment flush in an unknown reservoir in India. WOLF 2D is a free-surface flow and sediment solver using the multi-block rectangular grids, developed by the Division of Applied Hydrodynamics and Hydraulic Engineering of the University of Liege in Belgium. The numerical model predicted that only a narrow channel was generated by the flushing that was unable to be extended to a very board part of the reservoir width. The presented results demonstrated the ability of the model to simulate sediment entrainment during a sediment flush; no field data, however, were available and used to validate the numerical results.

Boeriu et al. (2011) presented case studies where 2D models are used for simulation of the reservoir drawdown flush. 2D depth-averaged flow and sediment transport modules of Delft3D, a morphological software developed by WL/Delft Hydraulics in corporation with Delft University of Technology, was used for the propose. The erosion flush was calculated differently for cohesive and non-cohesive sediments and the bed level was calculated using the Exner equation. Case studies were provided to predict the sediment erosions in an unnamed reservoir in Sri Lanka where several 5 to 10 days of flushing were simulated and in the Koga reservoir in Ethiopia where a 35 days of reservoir drawdown eroded sediment at the reservoir entrance and deposited some of them in the reservoir near the dam and transported some to the downstream of the dam. No field data were available and used to validate the results.

Minami et al. (2012) applied a 2D width-averaged numerical model to simulate the coordinated sediment flushing and sluicing at Dashidaira and Unazuki dams on the Kurobe River in Japan. The suspended sediment concentrations just downstream of both dams were calculated and compared with measurements well. The numerical model confirmed that the higher suspended sediments released from both dams during flushing operation.

Chen and Tsai (2017) developed a 2D model to estimate sediment erosion/deposition, bed evolution, and sediment flushing efficiency of A-Gong-Dian reservoir in southern Taiwan. The reservoir is wide making it the longest dam in Taiwan with a dam length of 2.4 km. The reservoir collects water from both Joushui River and Wanglai River. The simulated efficiency of the empty reservoir flushing was similar to that obtained from a laboratory model. The numerical modeling found that sediment erosion upstream of the outlet in the Joushui river side and deposition in the Wanglai river side and they proposed a relocation of the outlet toward the upstream of the Wanglai river side to improve the flushing efficiency.

Iqbal et al. (2019) used the 2D numerical model BASEMENT, developed by the Laboratory of Hydraulics, Hydrology and Glaciology at ETH Zurich, to simulate two sediment flushing test cases. The numerical model employs a finite volume technique to solve the 2D shallow water equations over an unstructured triangular mesh. The transition from subcritical to supercritical during the rapid sediment flushing process is handled by solving the Riemann problem at each cell interface with Godunov scheme. The model was used to simulated two sediment flushing testing cases: 1:40 physical model of the reservoir of the Gulpur Hydropower Plant which was being constructed on the Poonch river in Pakistan-administrated Kashmir and the laboratory flushing experiment by Lai and Shen (1995). The model reproduced the bed longitudinal and lateral erosions after flushing and flushed sediment volume well.

Chaudhary et al. (2019) used the MIKE21C to simulate the reservoir flush for the proposed reservoir on the Dibang River in east Asia. The reservoir will collect waters from Dri and Tangon River. A 1D model, MIKE 11, was used to calculate the long-term sediment distribution in the reservoir. MIKE21C, a 2D model over a curvilinear grid, was used to simulate the sediment deposition/flush of the reservoir with a constate incoming flow rate and an initial bathymetry obtained from 1D model. The reservoir flushing would be carried out through the low level spillway crest and the downstream water surface were obtained from the flow rates over the spillway. The numerical model was used to estimate how much sediment can be flushed out with various flushing discharges and durations.

The modeling of turbidity current has also been simulated with 2D models. The models have been developed to overcome the limitations of the empirical models. Most numerical models adopt the layer-averaged approach. A complete set of layer-averaged governing equations was derived by Parker et al. (1986) for unsteady flows. Most early models are 1D in nature. And only a few 2D layer-averaged models have been reported that deal with unsteady, non-conservative turbidity currents. Bradford and Katopodes (1999) studied turbidity undercurrents in deep sea environment. They developed a high-resolution, total variation diminishing, finite-volume numerical model to capture the current front with the predictor-corrector time-stepping scheme. Structured quadrilateral meshes were used to represent geometry suitable to deep sea applications. The model was verified by comparison with

experimental data for turbidity currents driven by uniform and non-uniform sediment. Groenenberg (2007, 2009) developed a 2D model that used a combination of the explicit fractional-step MacCormack scheme and a high-resolution shock-capturing technique. The model was solved numerically on a rectangular grid by means of a second-order finite-difference approximation. The model was tested and verified using a number of laboratory cases and reasonable agreement with the measured data was obtained.

At Reclamation, a comprehensive 2D layer-averaged model is developed into SRH-2D which is suitable to both narrow and wide reservoirs (Lai et al. 2015; Lai and Wu 2018; Huang et al. 2019). The objective is to advance existing 2D models so that an engineering numerical tool may be developed. Comprehensive test and verification cases have been reported which highlighted the applicability range of the model, along with the calibration process. We believe that the 2D layer-averaged model is a good compromise between the empirical models that are over simplified and the 3D models (Reynolds-averaged, LES or DNS) that are still at the research stage and yet to be demonstrated for field applications.

2.3.3 3D Numerical Models

Three-dimensional (3D) numerical models have also been reported in simulating the reservoir drawdown flush. In this document, the 3D models belong to the category of those based on the solution of the full NS equations without the hydrostatic assumption.

Ghoreishi and Tabatabai (2010) used a 3D hydrodynamic model to simulate the reservoir sediment flushing experiments by Lai and Shen (1995). The experiments were conducted in a rectangular flume with dimensions 50 m long, 2.44 m wide, and 1.52 m high with sediment paved in a 9 m reach upstream from the dam. The numerical model predicted the channel erosion near the dam well; however, it did not reproduce the observed eroded channel developed longitudinally upstream. The authors attributed the deviation to the limitation of the 3D model that treated the water surface as a rigid lid. The 3D model reproduced the erosion patten in the first stage of the sediment flush (mainly pressure flush) and showed differences in the second stage (drawdown flush).

Esmaeili et al. (2015) employed a fully 3D numerical model to simulate the 2012 sediment flushing operation in Dashidaira reservoir in Japan. Sediment flushing operation has been performed through the bottom outlets every year during the first major flood event in the rainy season since 1991. The finite volume approach is employed using unstructured and adaptive gird which moves vertically with changes in the bed and the free-water surface. The model was first calibrated to reduce the difference between the computed and measured total volume of the flushed-out sediment. The simulated reservoir bathymetry after flushing operation was then compared with measured one. The results showed that the 3D model can properly simulated the flushing channel evolutionary pattern. The numerical modeling found that smaller size sediment tends to be eroded and flushed out earlier than larger sediment sizes, and coarser sediment is mainly flushed out at the end of the preliminary drawdown and during the free-flow state. Esmaeili et al. (2017) presented additional calculations based on the same model, such as additional artificial discharge during the free-flow state, increasing the drawdown speed, and the construction of an auxiliary longitudinal channel.

Haun and Olsen (2012) applied the 3D model, SSIIM 2, to predict the reservoir sediment flushing process. The numerical model uses structured multiblock grid in the horizontal directions and adaptive grid in the vertical direction where the number of vertical cells depends on the water depth. Only one cell is spanning the water depth in shallow areas and a 2D calculation is done and up to 11 cells are generated in deep areas. The numerical model was applied to a physical model study of the Kali Gandaki hydropower reservoir in Nepal to reproduce the sediment volume flushed out and the bed deformation in six cross-sections. The numerical model improved the channel erosion in a bend due to the secondary currents. Olsen and Haun (2018) updated the 3D model SSIIM to include bank failure algorithm to find the location and the depth of the slides during reservoir flushing. The domain is divided into water, soil, and slide cells. The soil domain uses a 2D depth-averaged grid and the water grid and the slide grid are 3D. The bank failure algorithm was tested with the 2014 reservoir sediment flush on the Bodendorf reservoir in Austria. The numerical model reproduced number and magnitude of the slides well, but the locations were not always correct. The updated implemented algorithms worked well for thick sediment layers, but instabilities occurred for thin layers. The numerical model SSIIM was also used by Saam et al. (2019) to simulated the efficiency of flush of the Schwarzenbach reservoir in the Black Forest, Germany, with partial and full drawdown.

Numerical modeling of pressure flushing processes is rare, as only 3D CFD model is adequate for such a numerical modeling study. At Reclamation, a 3D CFD model with scour module was developed to simulate the pressure flushing process at the Cherry Creek Reservoir, Denver, Colorado (Lai and Greimann 2020). The 3D model is based on the solution of the Navier-Stokes equations along with sediment transport and mobile-bed modules. The numerical model results are compared with the field measurement results, which allows evaluating the suitability of the 3D model for pressure flushing simulation. It was found that the 3D model worked well in simulating the pressure flushing process. The predicted sediment release concentration compared well with the measured data downstream in the river for both 2017 and 2018 releases. The reasonable agreement points to the potential of the 3D model for future pressure flushing application. The numerical results suggested that the existing five-gate release schedule in 2017 was effective in removing the limited amount of sediments in front of the gates. If the maximum discharge would be much higher like the 2018 release schedule, a 3-gate release would be more efficient than the 5-gate schedule. Other options to consider are to maximize the flushing efficiency would be to flush every other year or to decrease the flushing duration.

3. Theory and Numerical Methods

This Chapter is reserved to describe the basic theory of the 1D, 2D and 3D models are presented, based on the Reclamation models. At present, however, only 3D model is described in a limited way.

In the past, Reclamation, at the Sedimentation and River Hydraulics Group, has developed several flow and sediment transport models that have been used for many Reclamation projects. SRH-1D (Huang and Greimann, 2012) is a 1D hydraulic and sediment transport numerical model that simulates the cross-sectionally averaged sediment transport, erosion and deposition. It is useful for large scale river studies and for reservoirs where drawdown sediment sluicing is the primary mechanism for sediment erosion. It has been applied to the Paonia reservoir studies where drawdown sediment sluicing is currently being used to simulate a sustainable reservoir sediment management strategy. It has also been applied to dam removal studies where the dam is permanent removed.

SRH-2D (Lai, 2008; 2010; Lai 2020) is a 2D depth-averaged hydraulic and sediment transport model that simulates the depth-averaged sediment transport, erosion and deposition with a horizontal 2D mesh. SRH-2D has been widely used for numerous projects at Reclamation and also nationally and internationally. SRH-2D model has been applied to drawdown sluicing at reservoirs such as on the Klamath River, Elwha River, Ventura River in the US. A version of SRH-2D has also been developed to predict the pressure flushing of the turbidity current that can occur in large reservoirs with high incoming sediment concentrations. Successful applications of the model to turbidity current venting has been demonstrated at the Shihmen Reservoir, Taiwan, where sediment bypasses around reservoirs are being designed.

3.1 3D CFD Model Theory

3.1.1 Governing Equations

We start with the most general 3D CFD model as the equations of 1D and 2D models are derived from 3D theory. The 3D flow model theory is based on Lai et al. (2003) and described recently also by Lai and Greimann (2020).

The governing equations of the 3D CFD flow model is based on the unsteady Reynolds-Averaged Navier-Stokes (URANS) equations expressed in tensor form as:

$$\frac{\partial U_j}{\partial x_j} = 0$$

$$\frac{\partial U_i}{\partial t} + \frac{\partial \left(U_j U_i\right)}{\partial x_j} = \frac{\partial}{\partial x_j}\left(\upsilon \frac{\partial U_i}{\partial x_j} + \tau_{ij}\right) - \frac{\partial P}{\rho \partial x_i} + g_i$$

In the above, t is time; x_j is j-th Cartesian coordinate; U_j is mean velocity component along coordinate x_j; $\tau_{ij} = -\overline{u_i u_j}$ is turbulence stress (u_j is j-th turbulent fluctuating velocity component); P is mean pressure; ρ is water density; υ is water kinematic viscosity; and g_i is an i-th component of the acceleration due to gravity. Repeated subscript (e.g., j) means summation over the three Cartesian coordinates.

The turbulent stress τ_{ij} is related to the mean velocity strain rate using the Boussinesq approximation as:

$$\tau_{ij} = \upsilon_t \left(\frac{\partial U_i}{\partial x_j} + \frac{\partial U_j}{\partial x_i} \right) - \frac{2}{3} k \delta_{ij}$$

In the above, υ_t is the turbulence eddy viscosity to be computed with a turbulence model, and δ_{ij} is the Kronecker delta (a unit tensor). In this study, the two-equation k-ε model of Launder and Spalding (1974) is adopted. That is, the eddy viscosity is computed by:

$$\upsilon_t = C_\mu \frac{k^2}{\varepsilon}$$

In the above, k is the turbulence kinetic energy and ε is the turbulence dissipation rate which are solved as:

$$\frac{\partial k}{\partial t} + \frac{\partial (U_j k)}{\partial x_j} = \frac{\partial}{\partial x_j} \left(\left(\upsilon + \frac{\upsilon_t}{\sigma_k} \right) \frac{\partial k}{\partial x_j} \right) + G - \varepsilon$$

$$\frac{\partial \varepsilon}{\partial t} + \frac{\partial (U_j \varepsilon)}{\partial x_j} = \frac{\partial}{\partial x_j} \left(\left(\upsilon + \frac{\upsilon_t}{\sigma_\varepsilon} \right) \frac{\partial \varepsilon}{\partial x_j} \right) + C_{\varepsilon 1} \frac{\varepsilon}{k} G - C_{\varepsilon 2} \frac{\varepsilon^2}{k}$$

where $G = \tau_{ij} \frac{\partial U_i}{\partial x_j}$ is the rate of the turbulence kinetic energy production. The standard turbulence model constants take the following values: $C_\mu = 0.09, C_{\varepsilon 1} = 1.44, C_{\varepsilon 2} = 1.92, \sigma_k = 1.0,\ \sigma_\varepsilon = 1.3$.

3.1.2 Sediment Transport Equations

Sediment transported in rivers and reservoirs may be divided into four categories: wash load, suspended load, mixed load, or bed load. Wash load is transported through the modeling domain without interaction with those on the bed and is normally ignored. The suspended load is transported through the system in "suspended" mode in water column, but it has a non-zero fall velocity and may exchange sediments with the bed leading to a net effect of bed erosion or deposition. The bed load refers to the sediment that saltates and/or rolls along the bed as opposed to the suspended load in water column. The mixed load is defined as the sediment sizes that are transported in between the suspended and bed load forms. In terms of

modeling effort, the mixed load is most demanding, followed by suspended load, wash load, and bed load.

A special suspended load module is developed into U^{2}RANS. Only suspended load transport is considered as sediment deposits near the dam face are usually very fine. In general, suspended sediment may be divided into a number of size classes although only a single fine size is tested and applied in the present study. In general, each size class is transported in the system separately and independent of each other. The 3D transport of a suspended sediment size class, say size *k*, is governed by the following advection-diffusion equation derived from mass conservation:

$$\frac{\partial C_k}{\partial t}+\frac{\partial UC_k}{\partial x}+\frac{\partial VC_k}{\partial y}+\frac{\partial (W-\omega_k)C_k}{\partial z}=\frac{\partial}{\partial x}\left(D_k\frac{\partial C_k}{\partial x}\right)+\frac{\partial}{\partial y}\left(D_k\frac{\partial C_k}{\partial y}\right)+\frac{\partial}{\partial z}\left(D_k\frac{\partial C_k}{\partial z}\right)$$

In the above, C_k is the volume concentration for sediment size class k (defined as ρ_k/ρ_S with ρ_k the mass concentration of size k and ρ_S the specific sediment density); ω_k is the fall velocity for size k; D_k is the diffusivity. The specific density is assumed to be the same for all size classes.

The diffusivity is computed by:

$$D_k=\frac{\upsilon_T}{\sigma_{Ck}}$$

In the above σ_{Ck} is the Schmidt parameter. For fine sand and cohesive sediments ($\leq 150\mu m$) σ_{Ck} is usually found to be 1.0.

The unhindered fall velocity for non-cohesive sediments may be computed by a number of ways. One method is based on van Rijn (1993) as:

$$\omega_k=\frac{(\gamma-1)gd_k^2}{18\nu} \qquad 65\mu m<d_k\leq 100\mu m$$

$$\omega_k=\frac{10\nu}{d_k}\left(\sqrt{1+\frac{0.01(\lambda-1)gd_k^3}{\nu^2}}-1\right) \qquad 100\mu m<d_k\leq 1000\mu m$$

$$\omega_k=1.1\sqrt{(\gamma-1)gd_k} \qquad 1000\mu m<d_k$$

where

γ = specific gravity of sediment ($=\rho_s/\rho_w$)

ν = kinematic water viscosity (m^2/s)

The unhindered fall velocity for cohesive sediments can be either the same as the non-cohesive sediments or a user provided value.

Boundary conditions are needed to solve the above suspended sediment concentration equation. At free surfaces, the net sediment concentration flux is set to zero; i.e.,

$$\omega_k C_k + D_{Vk} \frac{\partial C_k}{\partial z} = 0$$

At the stream or reservoir bed, the net sediment flux reflects the net sediment exchange rate with the bed; it is non-zero unless the flow has reached equilibrium. The net sediment flux with the bed is computed by:

$$\omega_k C_k + D_{Vk} \frac{\partial C_k}{\partial z} = D_k - E_k$$

where $D_k = \omega_k C_k$ is the deposition rate and E_k is the sediment entrainment rate, respectively. The entrainment rate for the non-cohesive size class may be computed by:

$$E_k = \begin{cases} \omega_k C_k^* & loose\ bed\ with\ unlimted\ supply \\ min(\omega_k C *_k,\ \omega_k C_k) & fixed\ bed\ without\ supply \end{cases}$$

In the above, the entrainment rate is proportional to the local equilibrium concentration (C_k^*) near the bed. The equilibrium concentration is determined by an empirical equation derived from experimental data. For a fixed bed without sediment supply, only deposition is allowed. The equilibrium concentration equation proposed by Zyserman and Fredsøe (1994) may be adopted. It computes the equilibrium concentration as follows:

$$C_{b*} = \frac{0.331(\theta - 0.045)^{1.75}}{1 + \frac{0.331}{0.46}(\theta - 0.045)^{1.75}}$$

$$\delta = 2d$$

$$\theta = \frac{{u_\tau}^2}{(\gamma - 1)gd} \qquad \text{(Shields parameter)}$$

In the above, d is the sediment diameter, δ is the reference height which is made to be twice the sediment diameter.

In the present study, the bed is primarily cohesive. For cohesive sediment, the sediment entrainment rate is computed as:

$$E_k = p_k \varepsilon (\tau_b - \tau_c)$$

where p_k is the volume fraction of the cohesive size class on the bed, ε is the erodibility and τ_c is the critical shear stress of the cohesive bed, and τ_b is the bed shear stress.

It is noted that the erodibility may not be a constant for cohesive sediment. For example, two erosion modes may exist, one is the surface erosion and the other is the mass erosion (Partheniades 1965). Surface erosion has a smaller erodibility and occurs when bed shear stress is just above a relatively critical value. At higher bed shear stress levels, mass erosion may occur when a layer of bed material is lifted and eroded once bed shear stress exceeds the bulk shear strength of the bed material. The erodibility can be much higher than the surface erosion mode. Only a single erodibility is implemented in the present study.

Deposition of cohesive sediments depend on several processes and it occurs when bed shear stress is less than a critical value. According to the laboratory study of cohesive sediment depositional behaviors by Mehta and Partheniades (1973), deposition is controlled by shear stress on the bed, turbulence near the bed, settling velocity, sediment type, flow depth, suspended concentration, and ionic constitution. Two deposition processes may be modeled: full and partial. The deposition rate is computed as follows:

$$\begin{cases} D_k = \omega_k \left(1 - \frac{\tau_b}{\tau_{ref}}\right) & if\ \ \tau_b \le \tau_f \\ D_k = \omega_k \left(1 - \frac{\tau_b}{\tau_p}\right)\left(1 - \frac{C_{eq}}{C_k}\right) & if\ \ \tau_f < \tau_b < \tau_p\ and\ C_k > C_{eq} \\ D_k = 0 & if\ \ \tau_b \ge \tau_p\ \ or\ \ C_k \le C_{eq} \end{cases}$$

$$\tau_{ref} = \frac{\tau_f\, \tau_p}{\chi\, \tau_f + (1-\chi)\tau_p} \qquad \chi = 1 - \frac{C_{eq}}{C_k}$$

In the above, τ_f is the critical bed shear stress below which full deposition dominates, τ_p is the critical stress above which no deposition happens (deposition rate is zero), C_{eq} is the equilibrium cohesive sediment concentration consisting of relatively weak flocks that are broken apart before reaching the bed or eroded immediately after deposition. Full deposition allows the concentration to reduce to zero and is appropriate for low shear areas such as floodplains. Partial deposition allows concentration to approach to an equilibrium value (C_{eq}) and is appropriate for high shear main channel areas. If $\tau_f = \tau_p$, only the first equation, i.e., the full deposition, is applied and C_{eq} is ignored. If $C_{eq} = 0$, the first two equations collapse into one and it is meaningless to separate full and partial deposition modes. Under such scenarios, only the partial mode critical shear stress is used. Not that the first equation was due to Krone (1962) and the second equation was due to van Rijn (1993).

Many experiments were preformed to determine the full deposition critical shear stress. There was quite a scatter and it may range from 0.06 to 1.1 Pa. As an example, Krone (1962)

conducted a series of flume experiments for the San Francisco Bay sediment. He found that $\tau_f = 0.06\ Pa$ when $C_k < 0.3\frac{kg}{m^3}$ and $\tau_f = 0.078\ Pa$ when 0.3 <C_k<10 *kg/m*^{3}. Mehta and Partheniades (1973) found that $\tau_f = 0.15\ Pa$ for kaolinite in distilled water. There are no relationships that reliably predict the values of τ_f, τ_p and C_{eq} for general field applications. Thus, they should be either determined through laboratory and field measurements, or through calibration. As a reference, in the study of the erosion upstream of the San Acacia Dam on the Rio Grande River (Lai and Bauer 2007), the laboratory measured data were determined to be $\tau_f = 0.005\frac{lb}{ft^2}$, $\tau_p = 0.021\frac{lb}{ft^2}$ and $C_{eq} = 1.0\frac{kg}{m^3}$. In modeling the Cherry Creek pressure flushing, erosion is the dominant process and deposition is not important. It is found that results are not sensitive to the choice of deposition rate formulation.

3.1.3 Bed Dynamics

Bed dynamics concerns with how sediments in the bed interact with those in the water column. On one hand, sediment movement in the river modifies the bed topography and the sediment contents on the bed. On the other hand, the flow and sediments in the water column are altered due to bedform changes. Therefore, modeling of the bed dynamics is an integral part of alluvial modeling.

Bed sediments may be divided into an active layer and a number of subsurface layers. The volume or mass fractions of sediments within each layer, i.e., the bed gradation, are inputs at the beginning of the modeling and may change during bed evolution. It may be shown that the volume and mass fractions are equivalent if the specific gravity is the same for all sediment size classes (this is assumed in our study).

The elevation of bed surface (Z_b) is changing due to net erosion and deposition. Change in bed elevation is contributed from all sediment size classes. The change in Z_b due to sediment size class *k* is governed by the following equation:

$$\eta_{ak}\left(\frac{\partial Z_b}{\partial t}\right)_k = -\dot{V}_k = -\frac{1}{L}(p_k q_{bk}^* - q_{bk})$$

where $\eta_{ak} = 1 - \sigma_{ak}$ is the porosity parameter, σ_{ak} is the porosity for the *k*-th size class in the active layer, $\dot{V}_k$ is the net volumetric erosion rate per unit bed area (or net rate of eroded depth) for size class *k*., q_{bk} is the bedload flux per unit width, and $q_{bk}^*$is the equilibrium capacity of q_{bk}. Note that $\dot{V}_k$ is computed from the net exchange rate. The above equation provides the net erosion and deposition of the sediments which would alter the sediment contents in the active layer. The value of porosity for natural systems range from 0.25 to 0.55; a typical good value for spherical grains is 0.36 as given by random close packing.

The active layer is defined to be the top bed layer participating in the sediment exchange between water column and alluvial bed, while subsurface layers provide sediments to or receive sediments from the active layer. The thickness of the active layer is a user input. A

constant thickness may be reasonably used. As reviewed by Merkel and Kopmann (2012), the selection of active layer thickness is empirical at present and inconclusive. A number of formulas for the active layer thickness was also discussed by Malcherek (2007).

The volume fraction of each sediment size class and the porosity of the active layer and subsurface layers are chosen as the two primitive variables. The governing equations for the two are needed within each bed layer. In our approach, the mass conservation equation is used to determine the volume fraction of sediment class in the active layer; it can be written as:

$$\frac{\partial m_a p_{ak}}{\partial t} = -\dot{V}_k + p_{2k} \sum_i \dot{V}_i \qquad \text{if net erosion } (\sum_i \dot{V}_i \geq 0)$$

$$\frac{\partial m_a p_{ak}}{\partial t} = -\dot{V}_k + p_{ak} \sum_i \dot{V}_i \qquad \text{if net deposition } (\sum_i \dot{V}_i < 0)$$

where m_a is the total volume per unit area without void (or mass) of sediments in the active layer, p_{ak} is the volume fraction of *k*-th class in the active layer ($\sum_k p_{ak} = 1$), p_{2k} is the volume fraction of *k*-th class in the first subsurface layer (beneath the active layer). In the modeling the total volume (or mass) per unit area (m_a) remains constant throughout the simulation, while the thickness of the active layer may change.

The m_a value is computed at the beginning of the computation based on the thickness of the active layer (δ_a). The thickness, δ_a, is a function of flow and sediment conditions as well as the bedform evolution. But δ_a can also be a user supplied parameter. By default, δ_a is set as $N_a d_{90}$ with N_a ranging from 1.0 for large boulders to more than 14.0 for fine sediments.

The porosity of the active layer is governed by the volume conservation equation derived from the kinematic constraint and may be expressed as:

$$\frac{\partial \delta_{ak}}{\partial t} = -\frac{\dot{V}_k}{\tilde{\eta}_k} + p_{2k} \frac{\sum_i \dot{V}_i}{\eta_{2k}} \qquad \text{if } \sum_i \dot{V}_i \geq 0$$

$$\frac{\partial \delta_{ak}}{\partial t} = -\frac{\dot{V}_k}{\tilde{\eta}_k} + p_{ak} \frac{\sum_i \dot{V}_i}{\eta_{ak}} \qquad \text{if } \sum_i \dot{V}_i < 0$$

where δ_{ak} is the volume per unit area for size *k* of the active layer thickness including voids; relation between δ_{ak} and η_{ak}:$\delta_{ak}\eta_{ak} = p_{ak} m_a$. In the above, $\tilde{\eta}_k$ is computed as:

$\tilde{\eta}_k = \eta_{ak}$ if $\dot{V}_k \geq 0$ (*k*-th size is eroded from active layer)

$\tilde{\eta}_k = \eta_{sk}$ if $\dot{V}_k < 0$ (*k*-th size is deposited into active layer)

and η_{sk} is the porosity parameter for the suspended sediment. The above equations may be more conveniently written as:

$$\frac{\partial \delta_{ak}}{\partial t} = -\frac{\dot{V}_k}{m_a p_{ak}}\delta_{ak} + p_{2k}\frac{\sum_i \dot{V}_i}{\eta_{2k}} \quad \text{if } \sum_i \dot{V}_i \geq 0 \text{ and } \dot{V}_k \geq 0$$

$$\frac{\partial \delta_{ak}}{\partial t} = -\frac{\dot{V}_k}{\eta_{sk}} + p_{2k}\frac{\sum_i \dot{V}_i}{\eta_{2k}} \quad \text{if } \sum_i \dot{V}_i \geq 0 \text{ and } \dot{V}_k < 0$$

$$\frac{\partial \delta_{ak}}{\partial t} = \frac{p_{ak}\sum_i \dot{V}_i - \dot{V}_k}{m_a p_{ak}}\delta_{ak} \quad \text{if } \sum_i \dot{V}_i < 0 \text{ and } \dot{V}_k \geq 0$$

$$\frac{\partial \delta_{ak}}{\partial t} = -\frac{\dot{V}_k}{\eta_{sk}} + \frac{\sum_i \dot{V}_i}{m_a}\delta_{ak} \quad \text{if } \sum_i \dot{V}_i < 0 \text{ and } \dot{V}_k < 0$$

The volume fraction (p_{Lk}), the porosity parameter (η_{Lk}), and the thickness (t_L) of subsurface layers are also updated. In the model, the subsurface layer underneath the active layer ($L = 2$) exchanges sediments with the active layer so that the mass of each size class is maintained in the active layer. In the process, the thickness of layer 2 may increase or decrease. The remaining subsurface layer remains unchanged until the thickness of layer 2 is reduced to zero. Under such a circumstance, layer 3 replaces layer 2 and the total number of subsurface layers is reduced by one at the point. For layer 2, the volume fraction (p_{2k}), the porosity parameter (η_{2k}), and its thickness are computed. If net erosion occurs ($\sum_i \dot{V}_i \geq 0$), p_{2k} and η_{2k} do not change, and the thickness change is governed by:

$$\frac{dt_{2k}}{dt} = -\left(\sum_i \dot{V}_i\right)\left(\sum_i \frac{p_{2i}}{\eta_{2i}}\right)$$

where subscript i runs through all sediment size classes. If net deposition occurs ($\sum_i \dot{V}_i < 0$), the thickness change is governed by:

$$\frac{dt_{2k}}{dt} = -\left(\sum_i \dot{V}_i\right)\left(\sum_i \frac{p_{ai}}{\eta_{ai}}\right)$$

and p_{2k} and η_{2k} are modified by fully mixing the new depositions from the active layer with the sediments already in layer 2.

4. Guidelines and Case Studies

The guidelines discussed are based on the experiences gained at Reclamation in research and development of in-house numerical models and in applying them to hydraulic flushing projects. Several numerical models have been developed and applied at Reclamation including SRH-1D (Huang and Greimann 2012), SRH-2D (Lai 2008; 2010; 2020), and U^2RANS (Lai et al. 2003; Lai and Greimann 2020). The guidelines are general at present and may be updated in future when more projects are studied and more experience gained with the numerical models. In addition, selected case studies are presented to illustrate the use and performance of the models.

4.1 General Recommendations

General recommendations for whether to select a 1D, 2D depth-averaged, or a 3D CFD model are as follows:

- For pressure flushing modeling, only 3D CFD model may be applicable. 1D and 2D models are not recommended unless the specific cases warrant their use.
    - It is recommended to simulate only a portion of the reservoir pool surrounding the flushing gates or intakes. A larger model domain is unnecessary and serves only to increase the runtime beyond practical uses of the 3D models.
- For turbidity current venting study, 2D layer-averaged model is recommended.
    - 1D models exist; their applicability, however, is limited to the run-of-the-river type of reservoirs. With the availability of 2D layer-averaged models, the use of 1D models is less needed as the latest 2D models are more general than 1D models and the requitement of computing resources is relatively low to moderate.
    - 3D CFD models are applicable; however, the runtime of 3D models may become prohibitively long that they may become impractical for project applications.
- For drawdown flushing study, 1D or 2D models are recommended for most reservoirs unless the drawdown water level is too high and processes are similar to the pressure flushing scenario.
    - 1D models are more suitable for long time scales (more than 10 years) or when the reservoirs geometry is confined to a single channel. 1D models may also be more appropriate for evaluating a number of alternative operational or design

strategies when many simulations are necessary.

- 2D models are recommended if the total length of the river is less than, e.g., 10 miles and time scale of simulation is focused on single drawdowns or less than 10 years. 2D model takes much longer to complete a simulation and therefore, limited by the spatial and time scales.

- 2D models are highly recommended is the width of the reservoir is wide (e.g., more than 4 to 5 times of the drawdown width).

4.2 1D Models

SRH-1D is a 1D hydraulic and sediment transport numerical model that simulates the cross-sectionally averaged sediment transport, erosion and deposition (Huang and Greimann 2012). The guidelines in applying 1D models such as SRH-1D are listed below:

- Applicable primarily to drawdown flushing modeling, and occasionally to turbidity current venting. The model is not suitable for pressure flushing study.

- 1D models are highly recommended is the length of the simulated river is long; for example, if it is more than 10 miles.

- The accuracy of the 1D models increases significantly if the width of the reservoir is relatively narrow. The term "narrow" is defined as when the width ratio of the largest reservoir cross section to the narrowest or drawdown section is no more than 4 to 5.

- The reliability of the 1D model results increases also with the pool level lowering depth; the highest accuracy is achieved when the flow through the reservoir pool during flushing is similar to the run-of-the-river type.

SRH-1D has been applied to several draw-down sediment flushing studies at Reclamation. One example is the application at the Paonia reservoir where drawdown flushing strategy is being developed to achieve the sustainable reservoir sediment management (Huang et al. 2019).

4.2.1 Case Study at the Paonia Reservoir (Huang et al. 2019)

Paonia Dam and Reservoir are located 16 miles northeast of Paonia, Colorado, on Muddy Creek, about one mile upstream of its junction with Anthracite Creek. The reservoir has a surface area of 1.35 km^2 (333 acres) with a total initial capacity of 25.8 million m^3 (20,950 acre-feet). Hydrology is characterized by spring snowmelt with summer thunderstorms.

Based on the bathymetric survey of the entire reservoir, conducted in June 2013, the estimated average annual rate of sedimentation has been 0.125 million m^3 (101 acre-ft) per year. Nearly

25% of the reservoir's original capacity of 25.8 million m^3 has been lost to sediment deposition (see (Reclamation, 2014a)).

In 2010, the outlet works at Paonia Dam became partially blocked with sediment and debris, indicating an impending sediment deposition issue. Following the 2010 blockage, a sediment sluicing/flushing plan was implemented. Operations were changed to include drawing the reservoir to lower levels in the early spring, allowing high spring run-off flows to flush suspended sediment through the outlet works before closing the gates to refill the pool for irrigation season.

Until Fall 2014, the flushing strategy was able to pass a measurable amount of sediment through the long, narrow reservoir and downstream (the pool is approximately 4.8 km (3 mi) long and 0.3 km (0.2 mi) wide). However, reservoir drawdown in late-October 2014 revealed the reservoir dead pool had completely filled with sediment, and the outlet works intake became partially plugged with cohesive sediment and submerged debris.

A short-term plan and a long-term plan were developed to manage inflowing and deposited sediment more efficiently. The SRH-1D model was used to provide answers regarding the reservoir sediment deposition, reservoir trap efficiency, sediment release concentration, and when the sluicing/flushing strategy could be fully implemented.

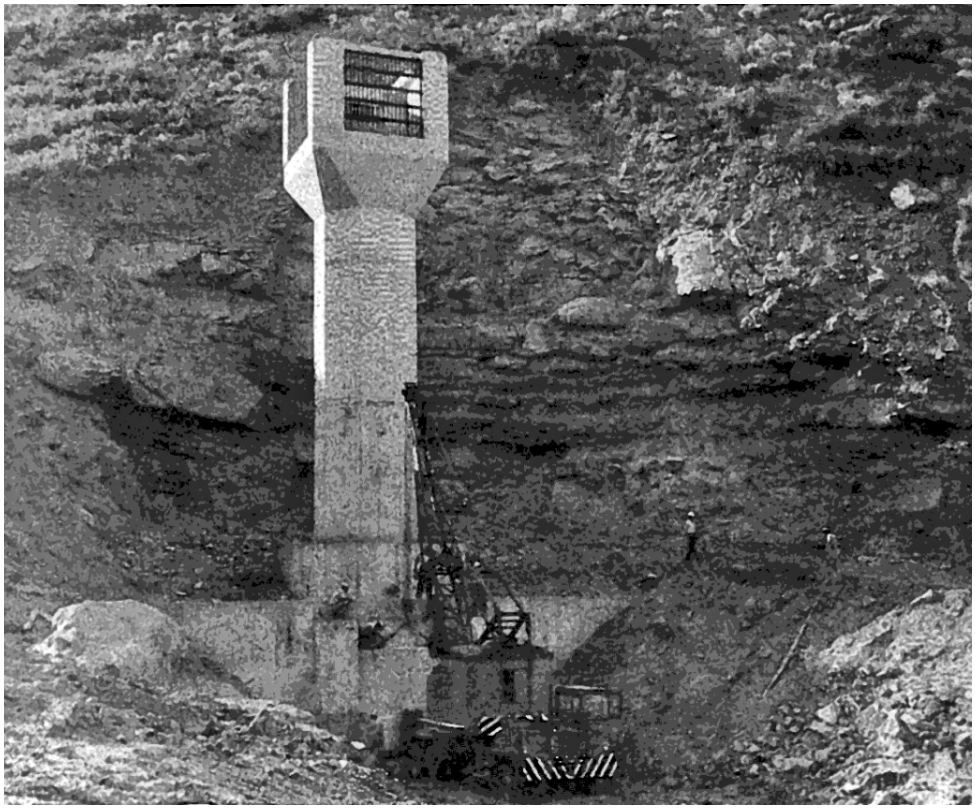

Figure 9. General view of Paonia Dam outlet structure, Bureau of Reclamation photo by E. J. Peterson on July 11, 1961.

Figure 10. Paonia Dam outlet structure during emergency actions to maintain diversion, Bureau of Reclamation photo Nov 11, 2014.

SRH-1D was updated to include a user-defined set of reservoir operation rules, which are implemented to assess the potential short-term and long-term effects of managing inflow and sediment deposition in Paonia Reservoir. The reservoir operation rules include: 1) the minimum and maximum reservoir releases associated with different reservoir water levels at each Julian day of year, 2) an algorithm to decide when to start reservoir filling based on reservoir incoming flow forecasts, 3) limitations on reservoir releases based upon gate and spillway capacity, and 4) limitations on the ramping rate of reservoir releases. The model is used to simulate reservoir sediment processing during a short-term drawdown for one season and a long-term 20-year simulation.

The required inputs to the Paonia Reservoir SRH-1D sediment model include general model parameters, cross-section geometry, upstream discharges of flow and sediment, downstream water surface elevation or discharge, channel bed and reservoir sediment gradations, channel and floodplain Manning roughness, selection of sediment transport capacity equations, and calibrated/assumed values of associated transport parameters.

The suspended sediment concentration samples were split into significant time periods of before the annual peak discharge (Pre-Peak), after the annual peak discharge (Post-Peak), and after July 4th, as shown in Figure 11. Sediment concentration is significantly higher during the rising stage of the snowmelt. Post-snowmelt peak sediment concentration is usually lower than these of pre-peak and post-July 4.

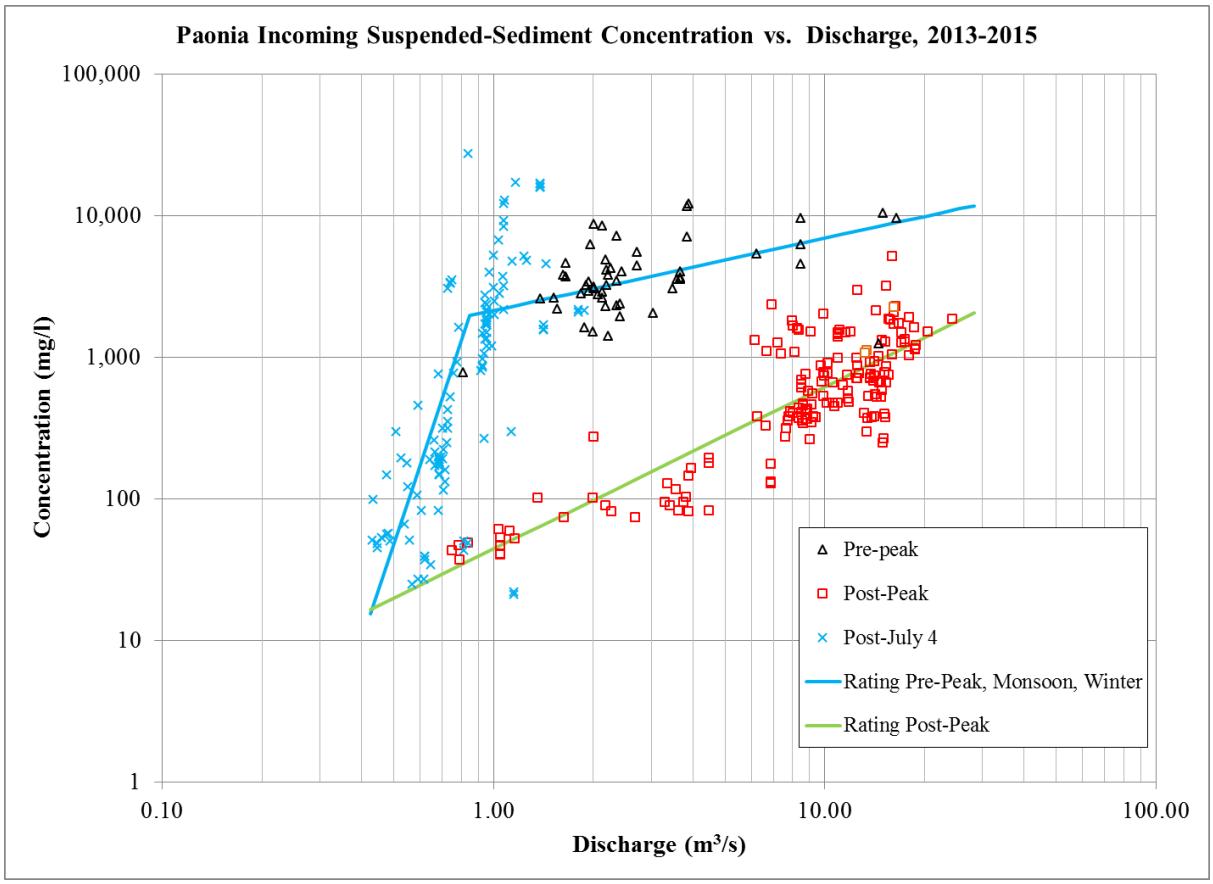

Figure 11. Suspended sediment concentration versus discharge, Paonia Reservoir (2013-2015).

The model was first calibrated with sediment flushing from 6/11/2013 to 6/30/2015. In Figure 12, a comparison between the measured and simulated sediment load exiting the reservoir is given. The model underestimates the total sediment load exiting the reservoir in 2013 by 9% (232 tons), and overestimates the total sediment load in 2014 by 19% (8,313 tons). A reasonable fit of the channel bed profile of the reservoir (Figure 13) is shown given the combination of sluicing, filling, and flushing operations of the reservoir in 2013, 2014 and 2015. The predicted outgoing suspended sediment concentration (Figure 14) reasonably fits the observations during high concentration measurements greater than 100 mg/l.

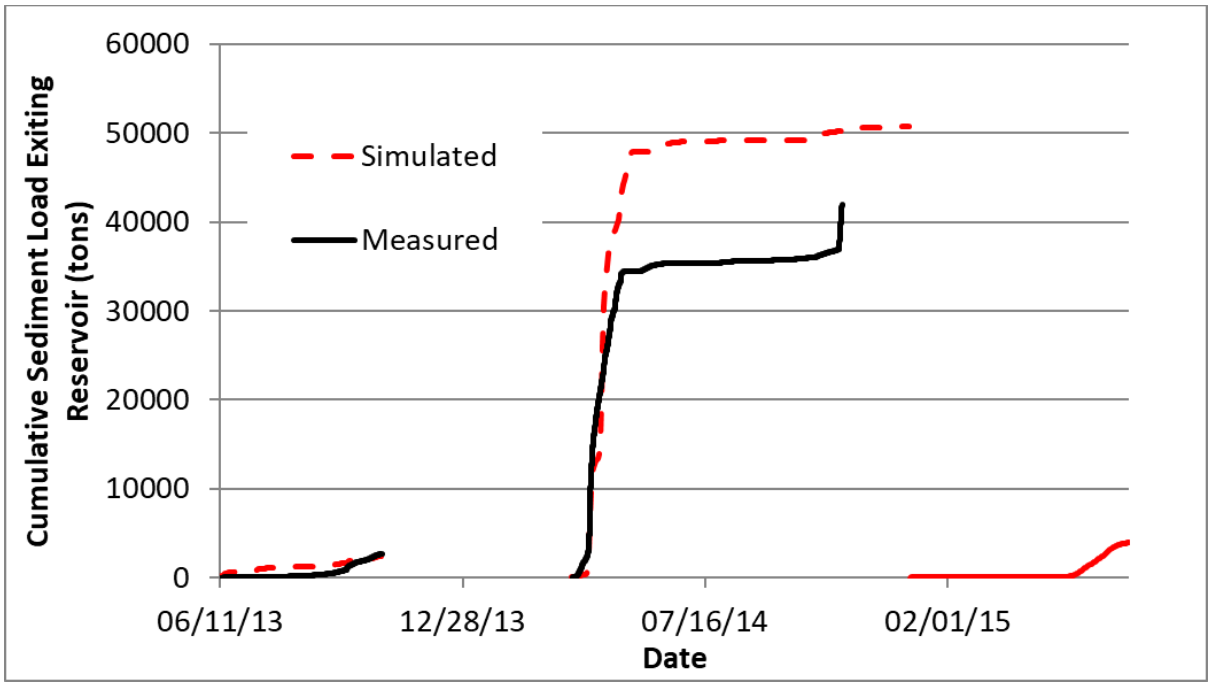

Figure 12. Model calibration comparison to measured total sediment load exiting Paonia Reservoir in 2013, 2014, and 2015.

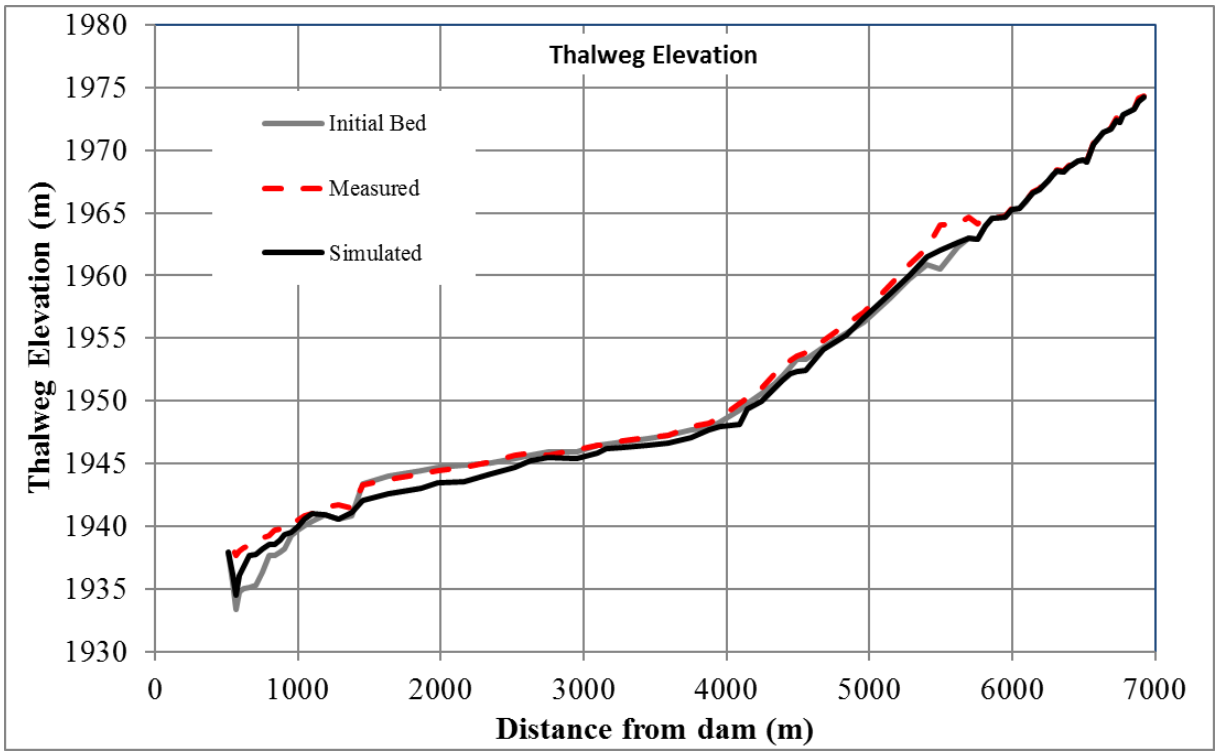

Figure 13. Model calibration comparison to the June 30, 2015 survey channel bed profile of Paonia Reservoir.

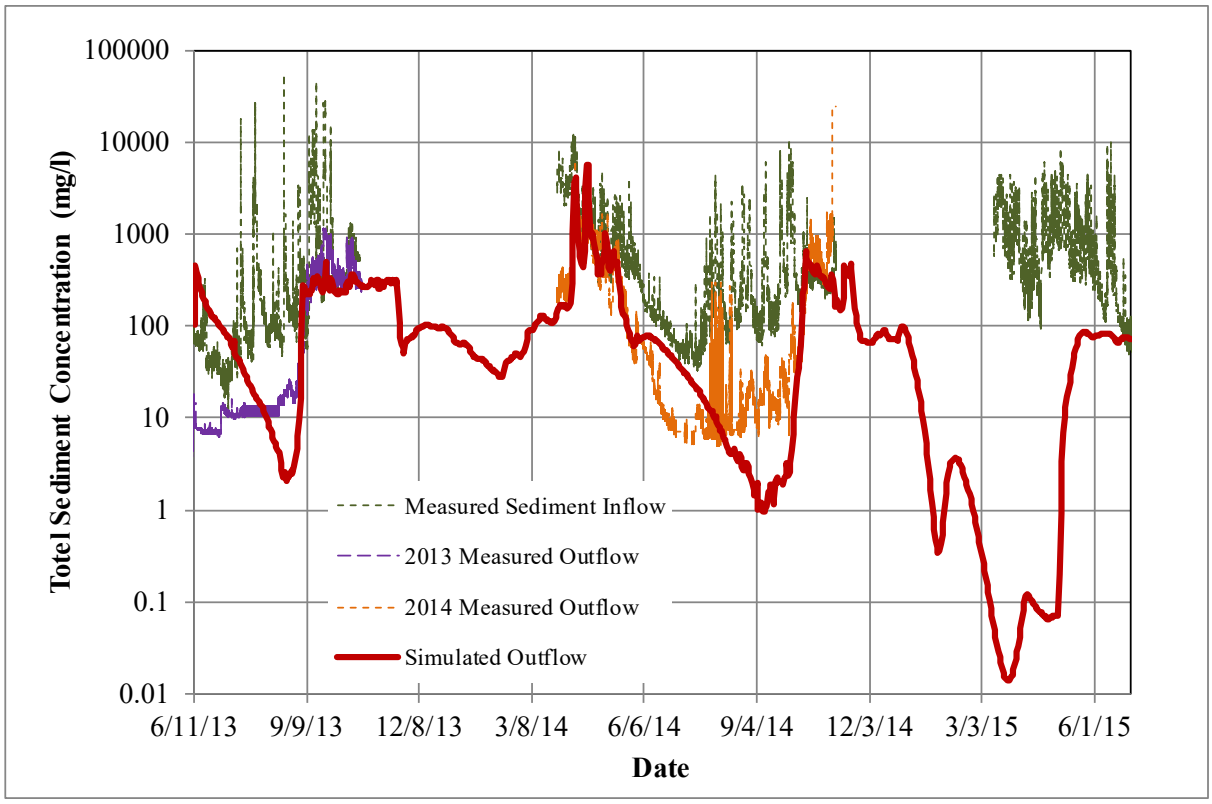

Figure 14. Simulated and observed suspended sediment concentration (mg/l) of Paonia Reservoir release.

The numerical model is then used for a short-term predictive simulation period from on March 1, 2016 to October 31, 2016 with June 2015 topography.

Figure 15 displays the simulated reservoir outflow in comparison with the reservoir inflow under the reservoir operational rules, along with reservoir water surface elevation. Before April 16 the reservoir releases as much water as possible to flush out or "sluice" reservoir sediment. Then the reservoir stores water from April 16 through April 28 to fill the reservoir to the spillway elevation. After the reservoir is full on April 29, the reservoir releases rate is equal to the inflow rate with spillway flow occurring. Beginning July 1, the reservoir enters into the irrigation season, and it releases a constant flow set as 5.7 m^3/s (200 cfs) until the reservoir is empty on August 27. After August 27, the reservoir pool is gone and the conditions are essentially riverine. The reservoir water surface elevation is also shown in Figure 15. Before April 16, the reservoir acts as a river to flush or "sluice" sediment through the outlet works and the water surface elevation remains at low stage, fluctuating with incoming flow rate. Note that current outlet works are not designed to pass debris and sediment and a new water outlet is under design. Before funding is available and the new water outlet is constructed, regular maintenance would need to be performed to clean the debris off the outlet intake to allow sediment to pass during spring flush. From April 16 to April 28, the reservoir gates are closed, maintaining a minimum flow rate, to refill the pool for the irrigation. Once the reservoir pool is full and the water surface elevation reaches crest elevation of 1965.7 m (6447.5 ft), the reservoir starts to release water and the water surface elevation remains at a high level a little above 1965.7 m. On July 1, the reservoir starts to

release water for irrigation, and the water surface falls until the reservoir is empty. After that, reservoir acts as a river and the water surface elevation remains at low stage, fluctuating with incoming flow rate.

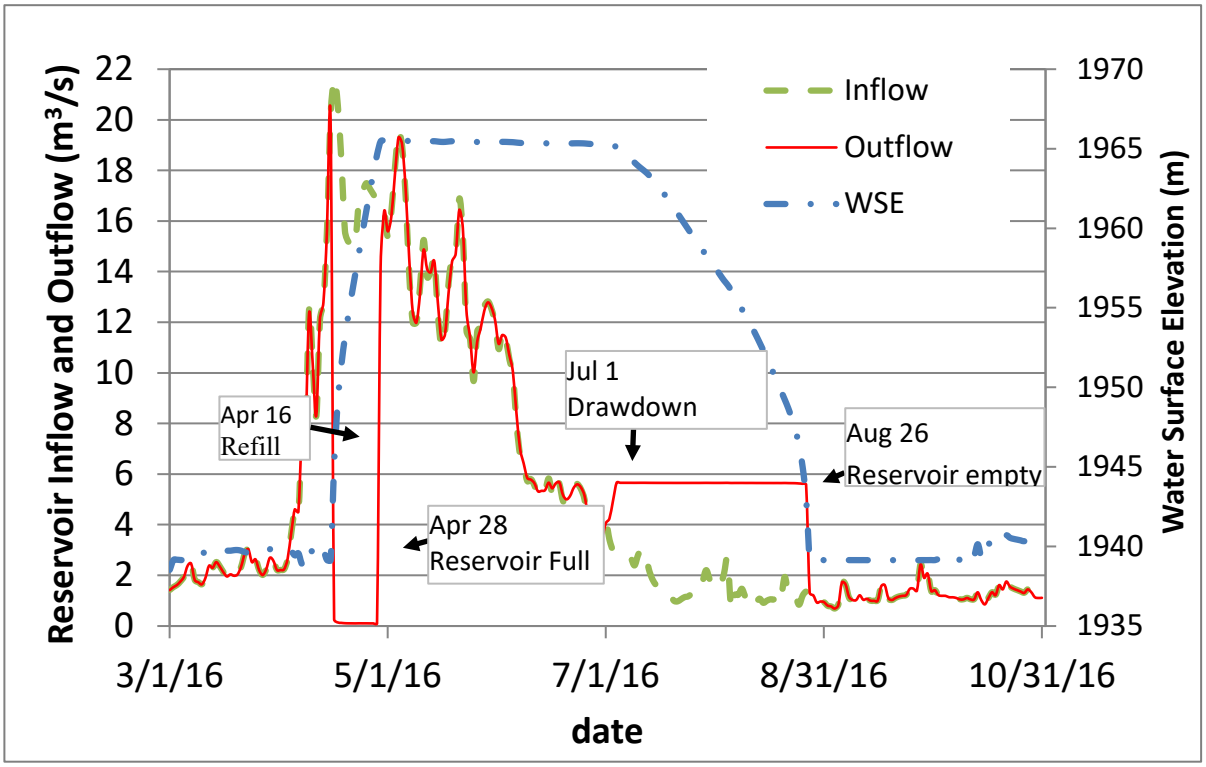

Figure 15. Paonia Reservoir inflow, outflow, and water surface elevation under reservoir operation rules.

Figure 16 show the inflow and outflow sediment balance. Before the reservoir starts to fill on April 16, the sediment is flushed out of the reservoir. About 30,000 tons of sediment are flushed out of the reservoir before April 16. After that date, reservoir starts to fill and the majority of the incoming sediment is deposited in the reservoir. After the reservoir empties on August 26, the reservoir acts as a river and sediment begins to erode from the reservoir. The numerical model predicts 40,800 tons of sediment is accumulated in the reservoir from March 1 to October 31, 2016.

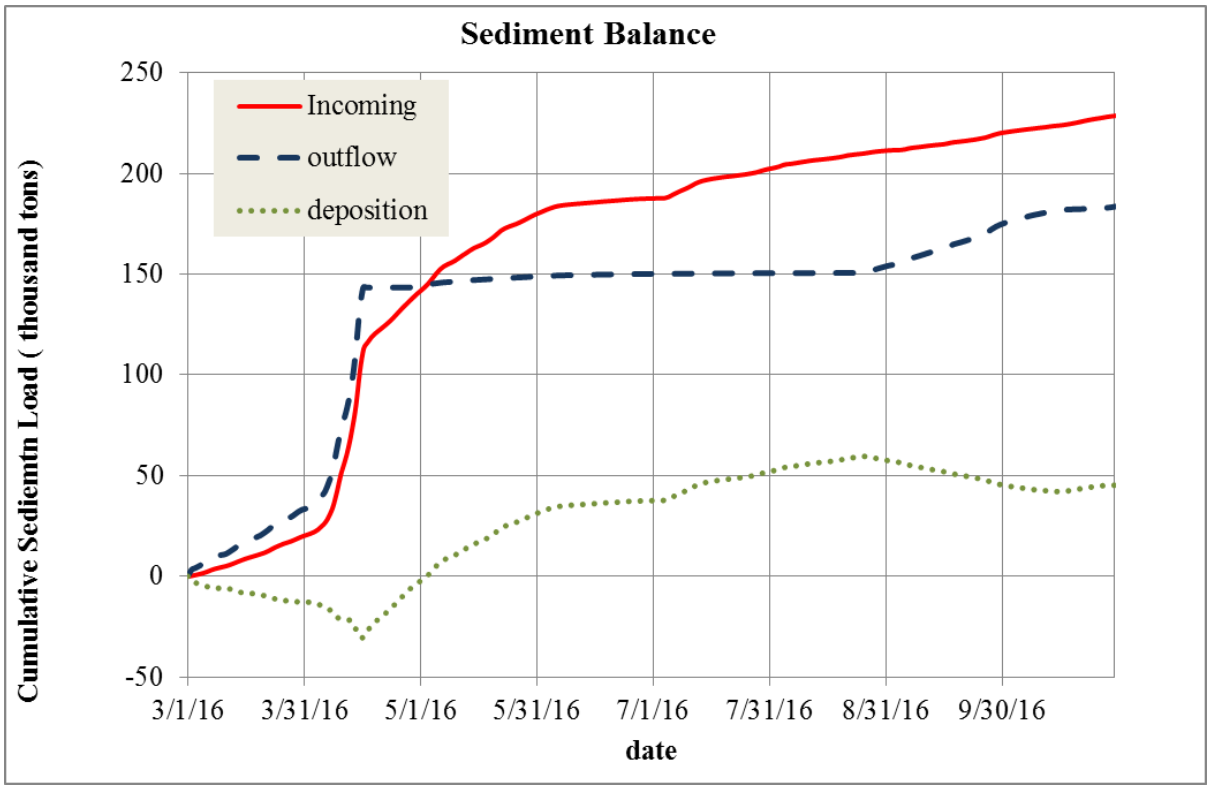

Figure 16. Cumulative inflow and outflow sediment loads and sediment deposition in the Paonia Reservoir.

The numerical model shows that a spring sediment flush is a useful method to pass and remove sediment from Paonia Reservoir. Most of the sediment erosion occurs during the spring flush when the reservoir water surface elevation is low.

4.3 2D Depth- and Layer-Averaged Models

SRH-2D (Lai, 2008; 2010; 2020) is a 2D depth-averaged hydraulic and sediment transport model that simulates the depth-averaged or layer-averaged sediment transport, erosion and deposition with a horizontal 2D mesh. The guidelines in applying 2D models such as SRH-2D are listed below:

- 2D models are applicable to both drawdown flushing and turbidity current venting. They are not suitable for pressure flushing study in general.

- For drawdown flushing simulation, following general guidelines are provided:

    - The restriction of the narrowness of the reservoir pool is lifted in theory in comparison with the 1D models. Therefore, 2D models are applicable to most reservoirs.

    - Reliability of the 2D model results is still related to the amount of pool level lowering: lower the pool level, higher the accuracy. The highest accuracy is

achieved when the flow through the reservoir pool is the run-of-the-river type.

- For turbidity current modeling, the following general guidelines are recommended:
    - Special rules and/or equations are needed in order to simulate the amount of water and sediment rates correctly at the low-level gates of the dam. See Lai et al. (2015) for a detailed discussion.
- Potential Limitations
    - The flushing-induced channel formation may be underpredicted significantly if the bed consists of cohesive materials unless the cohesive properties are properly calibrated including soil consolidation.
    - Eroded sediment from the channel may also be under-predicted due to the failure of a model to handle the bank erosion properly.

SRH-2D model has been applied to drawdown sluicing at reservoirs such as on the Klamath River, Elwha River and Ventura River. The model has also been applied to predict the density current venting and sediment bypass tunnels at the Shihmen Reservoir, Taiwan.

4.3.1 Case Study at the Klamath River

A case study is presented which use SRH-2D to understand the channel processes due to drawdown of Copco 1 reservoir on the Klamath River (Lai and Greimann 2012). It is part of a much larger effort performed at the Reclamation to support the Secretarial Determination on Klamath Dam Removal and Basin Restoration (Reclamation 2011).

Under the Dam Removal alternative, four PacifiCorp dams - JC Boyle, Copco 1, Copco 2, and Iron Gate on the Klamath River in Oregon and California - are under consideration for possible decommissioning. It was estimated that about 10 million cubic meters of sediment deposits are stored within the four reservoirs. A proposed dam removal alternative consists of two stages. First, Copco 2 dam is removed as it contains negligible deposits. Second, a concurrent drawdown of the remaining three reservoirs (JC Boyle, Copco 1 and Iron Gate) would commence in late fall or early winter. The deposits have a high water content (> 80% by volume) and the majority of the sediment particles are fine-grained (silt and clay). When the deposits are released downstream, high suspended sediment concentrations and their associated biological impacts will be the major concern, while concerns for downstream sediment deposition should be minor. A 2D modeling study was performed at the Copco 2 reservoir to address two issues: the channel form development during drawdown and an estimate of the amount of suspended sediment released downstream. The channel processes aids in determining the best strategies for revegetating the reservoir area and recovering a functional riparian corridor. The downstream sediment release helps in determining the timing and duration of the drawdown, as well as the drawdown rate.

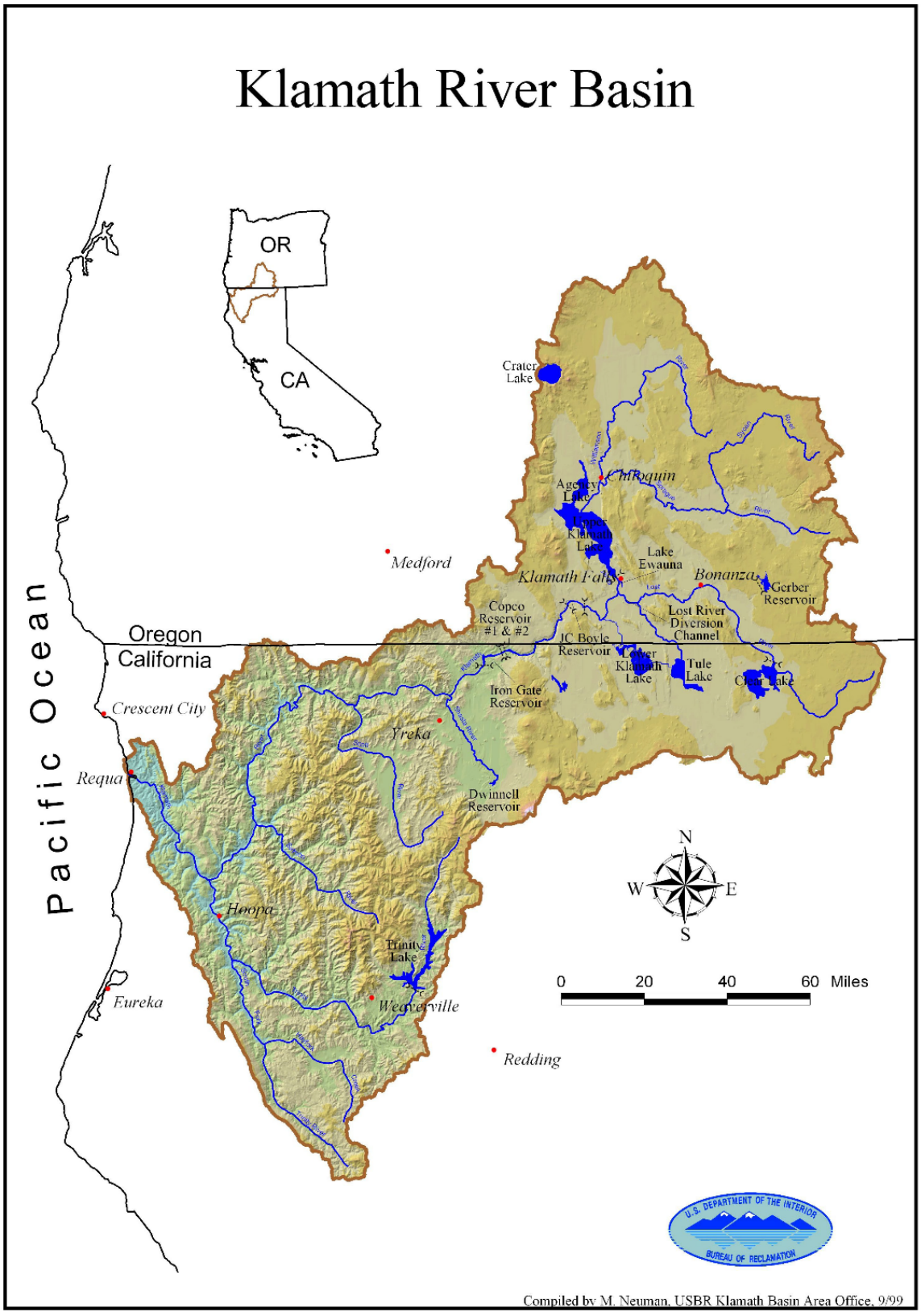

Figure 17. Overview of Klamath River from JC Boyle to Shasta.

Copco 1 dam is one of the four dams on the Klamath River in southern Oregon and northern California. These dams are located in the Upper Klamath Basin, downstream of Upper Klamath Lake (Figure 17), and on a 38-mile reach. The Klamath River begins at Lake Ewauna just south of Upper Klamath Lake and flows southwest into California. The Klamath River in the four-dam area maintains a high-energy, coarse-grained channel that is frequently confined by bedrock and is comparatively steep compared to the river downstream of the study area. Floodplain development is generally isolated to discreet reaches and wider valleys allowing more alluvial channel migration processes are rare.

Copco I dam is 126-feet high and was constructed in 1918. The upstream reservoir is 4.5-miles long (RM 203.1 to 198.6), has a surface area of 1,000 acres, an average depth of 34 feet, a maximum depth of 108 feet, and a total storage capacity of 33,724 acre-feet. Water levels in Copco reservoir are normally maintained within 6.5 feet of full pool that is elevation 2,607.5 feet. The historical channel through Copco reservoir consisted of asymmetrical meanders, controlled by bedrock on the outer bends. Deep pools were probably located in these bends. In the upper portion from the high pool to about RM 200, the channel was a mostly single-thread, sinuous channel with broad asymmetrical meanders. Terraces were located along most of the reach, and were mostly 5-10 feet above the river channel. In addition, there were areas designated with willow and brush vegetation, which could correspond to either floodplain areas or young alluvial terraces. Downstream of RM 200 to about RM 199, the channel is more sinuous, perhaps due to the canyon constriction that begins near the dam. In this reach, the channel contained a greater number of vegetated islands, some abandoned channel meanders, and wetland or floodplain environments. Most surfaces in the reach were less than 5 feet above the river channel based on historical topography. A few terraces of 5-10 feet and 15-20 feet also exist in the reach, but are more limited in extent.

A 2D numerical analysis begins by defining a solution domain and generating a mesh covering the domain. In this study, the solution domain includes the entire Copco 1 reservoir and the mesh developed consists of 10,504 mixed quadrilaterals and triangles (Figure 18a). There are surveyed topographic and bathymetric data available in the form of digital elevation model (DEM). These DEM data were interpolated to the mesh to represent the initial bed elevation of the reservoir before drawdown (see Figure 18b for the contours of the initial bed elevation).

Flow analysis requires the input of flow resistance that is calculated with the Manning's roughness equation. The Manning's coefficient (n) used in this study is 0.03, uniformly distributed in space. The value is based on our 1D model analysis, as well as previous modeling experience. The sediment transport and bed erosion modeling require information about the subsurface sediment data. These data came from a number of sources including historical aerial photography, bathymetric and topographic survey, and geomorphic study (Reclamation, 2011). In the model, the reservoir subsurface is divided into two layers. The top layer consists of mostly reservoir deposits of silt and clay with the surveyed layer thickness as shown in Figure 19a. The bottom layer consists of mostly pre-dam river sediments. Sediment

composition of the top layer was found to be different for the upstream and downstream zones (see Figure 19a) while composition of the bottom layer is assumed to be the same over the solution domain. Cumulative distributions of the bed sediment for both the top and bottom layers are shown in Figure 19b.

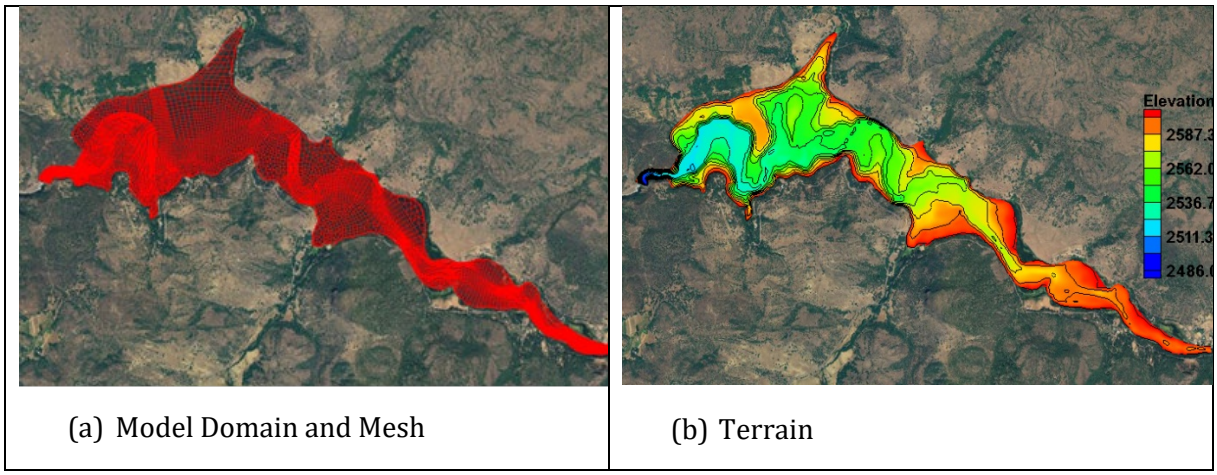

Figure 18. Model solution domain, mesh, and topography used for the numerical modeling.

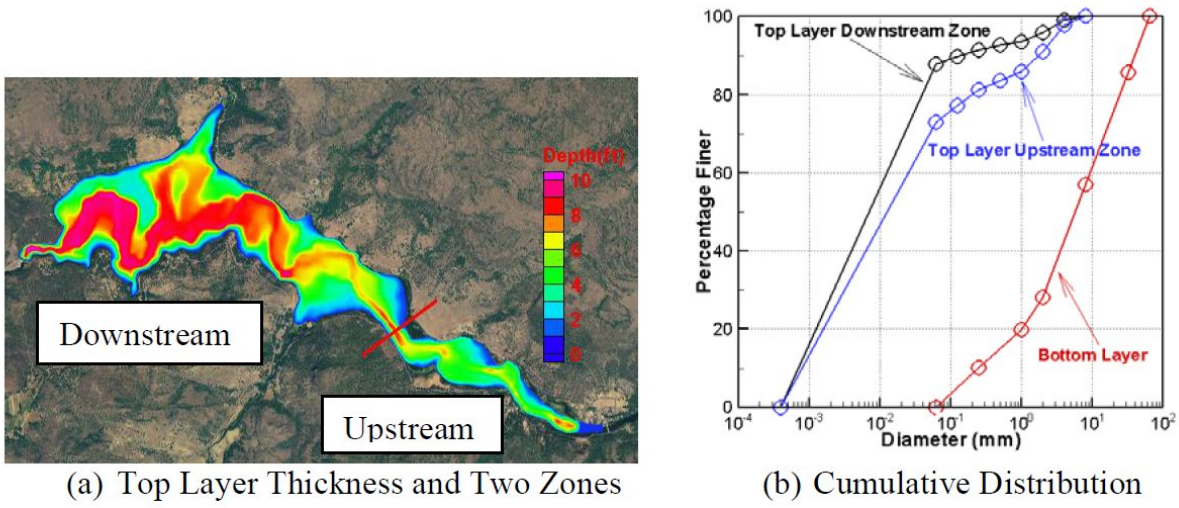

Figure 19. Subsurface sediment data in the reservoir: (a) top layer thickness and two zones of top layer sediment composition; (b) cumulative distributions of bed sediment.

Three hydrological scenarios are simulated, representing a Dry-Year (2004), Average-Year (1968), and Wet-Year (1999). All simulations start on November 15 and last for six months. Flow discharges into the reservoir over the six-month period are shown in Figure 20a. They are the recorded historical data and used as the inlet boundary condition. No sediment is assumed to enter reservoir as majority of inputs is wash load that simply passes through. The total sediment released downstream of Copco 1 may be obtained by simply adding the known wash load entering Copco 1 to the predicted sediment release from Copco 1 by the present model. Initially, the reservoir is filled with water at an elevation of 2,603 feet (invert of the

spillway). Drawdown is accomplished through release at an exit gate and the release rate is implemented as the exit boundary condition. The release rate is determined by the nominal drawdown rate of 3.0 ft/day, subject to the constraint of the gate capacity characterized by the discharge capacity curve in Figure 20b.

Seven sediment size classes are used to represent the bed sediment, as tabulated in Table 1. Size class 1 is used to model the cohesive material in the reservoir (those smaller than 0.0625 mm in diameter) while the rest of the sediment classes represent the non-cohesive sediment.

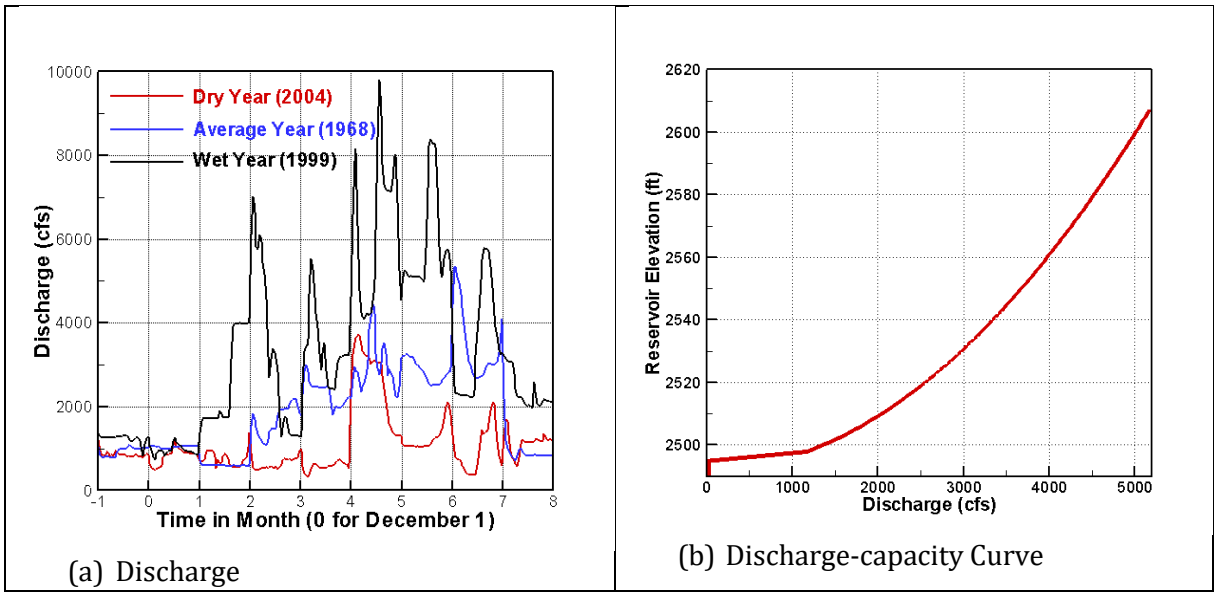

Figure 20. Flow hydrograph of three hydrological scenarios and the discharge capacity curve of exit gate at the dam face for drawdown.

Table 1. Size in diameter of each sediment size class

Size Class ID	1	2	3	4	5	6	7
Upper Bound of Diameter (mm)	Cohesive	0.125	0.5	2.0	8.0	32.0	128.0

A total of nine simulation runs have been carried out, representing three hydrological scenarios (Dry-Year, Average-Year, and Wet-Year) and three reservoir bed erodibility conditions (Easy-Erosion, Medium-Erosion, and Hard-Erosion). Each model run starts on November 15 and ends on May 15 of the following year, a duration of six months. Herein, only the model results corresponding to the Average-Year and Medium-Erosion, called baseline run, are presented unless it is stated otherwise; more results may be found in Reclamation (2011). Comparison of model results showed that the differences in most variables are small among three bed erodibility conditions.

The predicted reservoir water surface elevation and discharges into and out of the reservoir are displayed in Figure 21. With the 3 feet/day maximum drawdown rate and the constraint imposed by the gate capacity for drawdown, reservoir water elevation is lowered to below 2,500 feet within one month under all scenarios. However, only under the relatively dry year can the reservoir water level be maintained at such a low level. The reservoir would be filled with water quickly with the Wet-Year hydrology. The predicted sediment concentration delivered downstream from Copco 1 is shown in Figure 22 for the three hydrological scenarios. The predicted concentrations do not differ substantially between the Dry-Year and Average-Year, indicating that majority of the reservoir deposits has been mobilized. There is noticeable difference between the Wet-Year and the other two. The main reason is that reservoir water level remains low for both the Dry- and Medium-Year scenarios, leading to higher velocity and sediment carrying capacity than the Wet-Year scenario. With the Dry- and Medium-Year simulations, the predicted high-concentration sediment pulse has an average peak of about 6,000 ppm (occasionally exceeding 7,000 ppm) and a duration of about 1.5 months. With the Wet-Year, the average peak of pulse is lowered to 4,000 ppm (occasionally exceeding 6,000 ppm). After 45 days of drawdown, sediment concentration falls to a relatively low level (about several hundreds of ppm). The model results are not sensitive to the range of erodibility parameters used for the reservoir bed sediment.

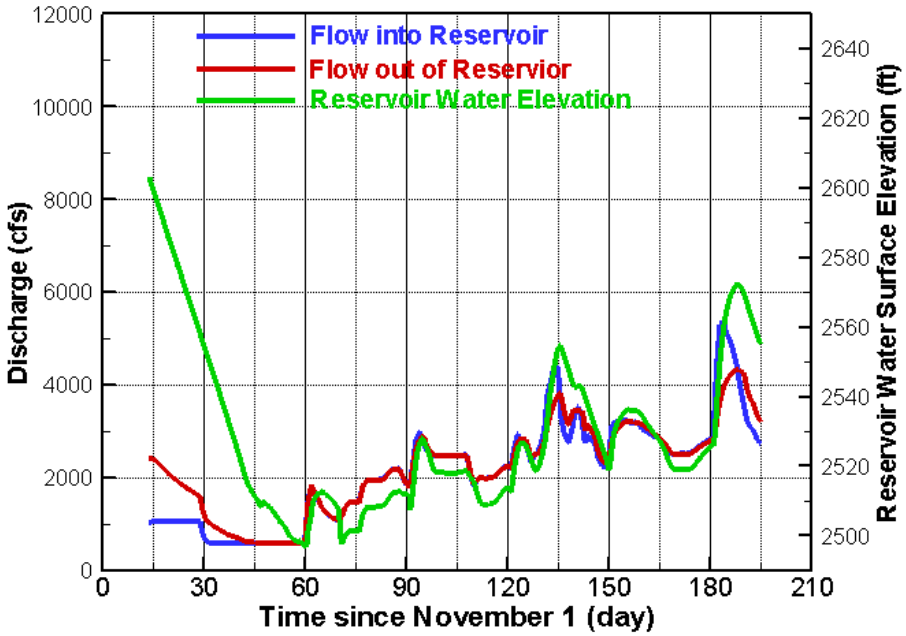

Figure 21. Simulated reservoir water surface elevation and discharges into and out of the reservoir under the baseline scenario.

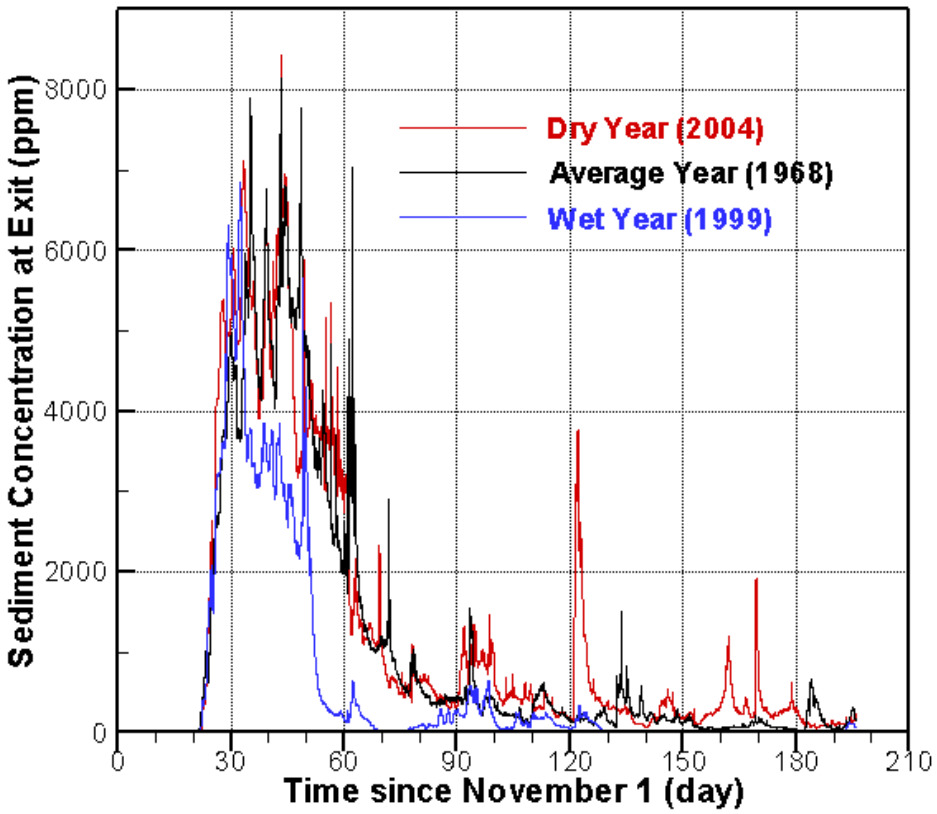

Figure 22. Predicted sediment concentration out of the drawdown gate of Copco1 under the three hydrological scenarios.

One of the primary interests of the modeling study is to investigate the channel development due to drawdown. In general, channel formation due to drawdown may occur in one of two forms: retrogressive erosion and progressive erosion. The retrogressive erosion is characterized by a zone of high slope and fast erosion that is moving upstream. The point of slope change has the highest erosion rate and is called the knickpoint. Retrogressive erosion is often initiated in instances where sediment deposits are deep and located near the dam and drawdown is rapid or an initial deep slope is created. This erosion process was observed both in laboratory flumes and in the field (Morris and Fan 1998). An example was reported by Major et al. (2008) when the Marmot Dam on the Sandy River in Oregon was decommissioned. The progressive erosion is characterized by the reemergence of channel beginning at the upstream end of the reservoir and moving and finally reaching the dam while the reservoir was emptied. Channel is often formed from upstream to downstream via fluvial processes due to increased sediment carrying capacity. Progressive erosion is often initiated when reservoirs are drawdown using some form of low-level outlet and the rate of drawdown is not very rapid.

The channel formation process due to drawdown at the Copco 1 reservoir is examined. Snapshots of predicted channel form are shown in Figure 23 on eight different days. The model predicts the occurrence of the progressive erosion with channel cutting through the reservoir deposits from upstream to downstream. The progressive erosion was expected to occur given the assumed drawdown scenario according to the studies by GEC (2006) and PWA (2009). The reservoir pool level is approximately down to the lowest level on December 29 while May 14 is at the end of simulation. The pre-dam geomorphology of the reservoir areas was delineated, as reported by Reclamation (2011); it is shown in Figure 24. The data were based on historical aerial photography and topographic maps. The predicted bed elevation and the net depth of erosion and deposition along incised channel thalweg are compared with the initial top bed layer thickness and bed elevation in Figure 25.

The model predicts the formation of an incised channel caused by progressive erosion. The predicted channel thalweg agrees well with the geomorphic delineation of the pre-dam channel (compare Figure 23h and Figure 24). Majority of the reservoir deposit within the pre-dam channel is eroded after about 45 days of drawdown, particularly for the upstream half of the reservoir. The eroded sediment provides most of the suspended sediment delivered downstream. Incision into the bottom bed layer is also predicted for the upstream half of the reservoir six months after the drawdown. In the upstream area (zone 1 and 2), channel incision decreases with increased flow into the reservoir (wet year). The trend, however, is reversed in zone 4 and 5 where incision increases with increased flow.

Deposition is predicted in the area of pre-dam floodplains located in the downstream half of the reservoir. It is particularly visible in the open area near the narrow canyon (compare Figure 23h and Figure 24). This may have implications on how revegetation and habitat restoration should be planned once the dam is decommissioned.

Finally, it is cautioned that the deposition near the drawdown gate in zone 1 may be unrealistic given that (a) only a depth-averaged model is used despite that flow is three-dimensional near the gate, and (b) “pressurized flow” is present at the gate while “open channel flow” is assumed by the model. The inaccuracy of the erosion prediction near the gate, however, is expected to have negligible effect on the predicted erosion upstream.

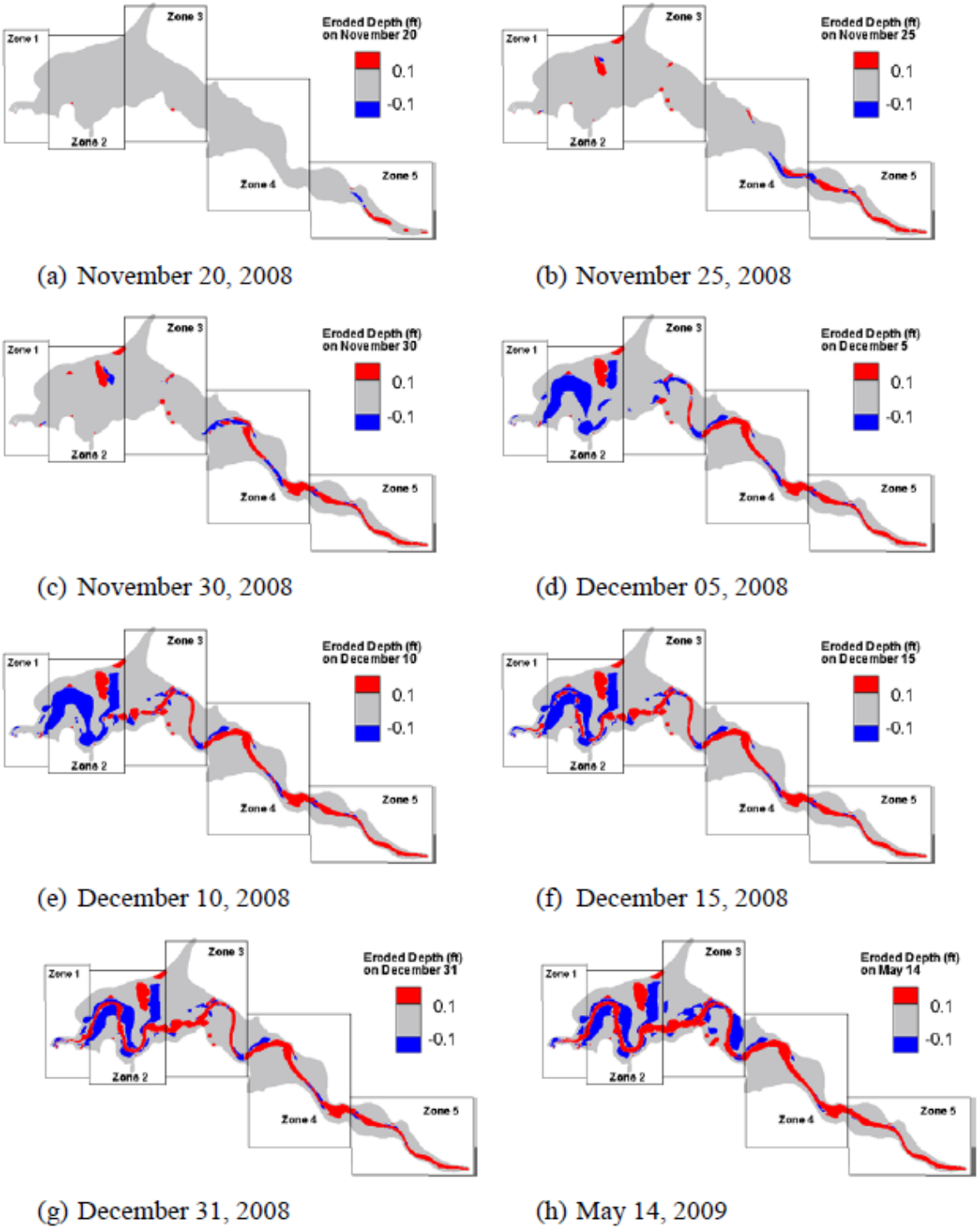

(a) November 20, 2008 (b) November 25, 2008

(c) November 30, 2008 (d) December 05, 2008

(e) December 10, 2008 (f) December 15, 2008

(g) December 31, 2008 (h) May 14, 2009

Figure 23. Predicted erosion/deposition pattern during the drawdown of Copco 1 reservoir under the Average-Year hydrology (2008) and Medium-Erosion bed sediment.

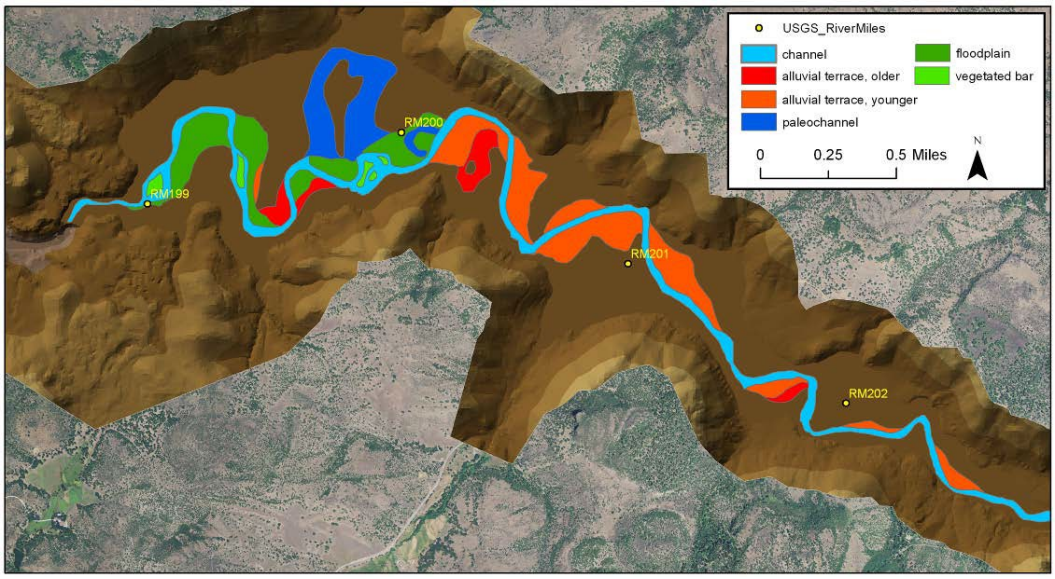

Figure 24. Geomorphic map of river corridor prior to construction of Copco I Dam.

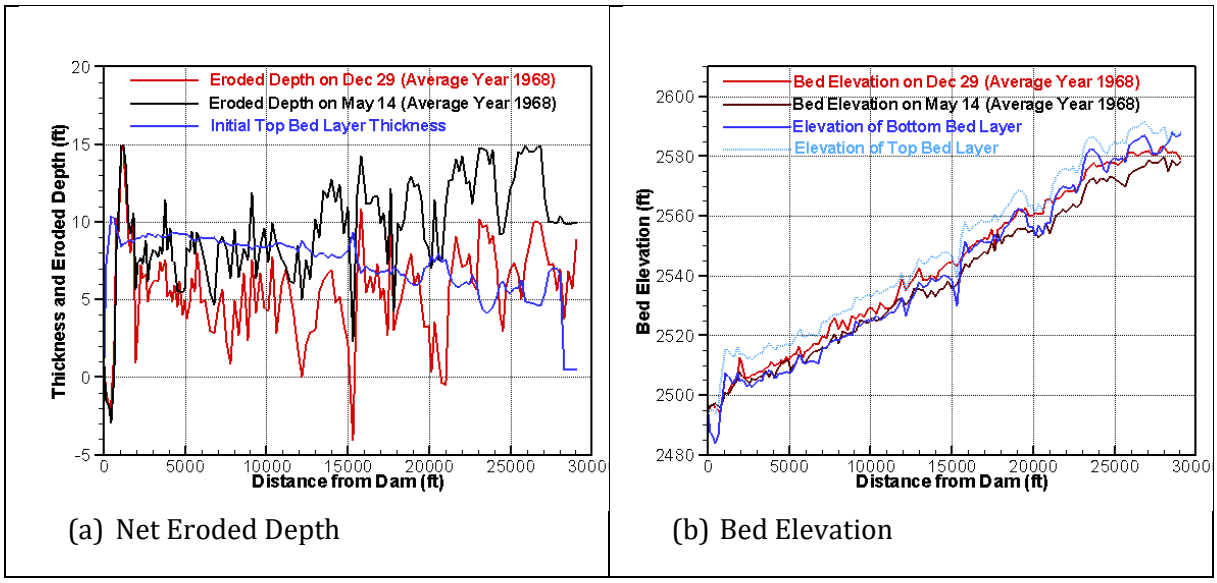

Figure 25. Simulated net depth of erosion and deposition (left) and the predicted bed elevation (right) along the thalweg of the incised channel on two dates, compared with the initial thickness of the top bed layer deposit and the top and bottom bed layer elevations.

In summary, the 2D depth-averaged model SRH-2D is used to conduct a channel form development prediction in the Copco 1 reservoir during a proposed drawdown. A total of nine simulation runs have been carried out, representing three hydrological scenarios (Dry-Year, Average-Year, and Wet-Year) and three reservoir bed erodibility conditions (Easy-Erosion, Medium-Erosion, and Hard-Erosion). Progressive erosion process is predicted that is consistent with previous studies. The predicted incised channel is found similar to the pre-dam channel alignment. Majority of the reservoir sediment deposits within the pre-dam channel are eroded after about 45 days of drawdown, particularly for the upstream half of the

reservoir. The eroded sediment provides most of the suspended sediment delivered downstream. The sediment pulse predicted has an average peak of about 6,000 ppm and a duration of about 1.5 months for hydrology up to the Medium-Year, and an average peak of 4,000 ppm and a similar duration for the Wet-Year. Model results are not sensitive to the range of erodibility parameters used for the reservoir bed sediment. Deposition is also predicted in the pre-dam floodplain area, particularly in the wide area upstream of the narrow canyon. This may have implications on how revegetation and habitat restoration should be planned once the dam is decommissioned.

4.3.2 Turbidity Current Venting Study at Shihmen Reservoir

The layer-averaged version of SRH-2D was applied to simulate turbidity currents at Shihmen Reservoir, Taiwan (Lai et al. 2015; Lai and Wu 2018; Huang et al. 2019). Herein, the extensive physical model tests carried out by Taiwan Water Resources Agency (WRPI, 2011) were used for numerical model verification and demonstration.

Suspended sediment periodically moves into Shihmen Reservoir in the form of a turbid undercurrent during typhoon events. Limited sluicing capacity has led to the loss of reservoir capacity at a much faster rate than the original design had intended. Further, turbid water rises slowly during typhoon events and may reach the elevation of the water intake facilities under extreme conditions. When turbid water does reach intake facilities, the municipal and industrial water supply has to be shut down which may cause enormous political and economic problems. In 2004, for example, Typhoon Aere alone caused 11% loss of the total reservoir storage capacity and interrupted water supply for 17 days. The Typhoon Aere disaster prompted the Taiwan government to initiate a wide range of studies along with specific projects for modifications of existing outlets at the dam and construction of new sluicing outlets. Combined field, physical model and numerical modeling studies have been carried out to better understand the turbidity current characteristics at Shihmen Reservoir and help inform the sediment sluicing projects.

The physical model study of turbidity currents at Shihmen Reservoir was carried out using a 1/100 scale undistorted model. The model occupied a space of 120 by 20 meters and encompassed about 15.5 kilometer longitudinal length of the reservoir (Figure 26a). The numerical simulation selects the same solution domain as the physical model. The final mesh consists of 33,008 cells and 33,621 nodes as shown in Figure 26b. Mesh sensitivity study has shown that the model results, i.e., the predicted current velocity and thickness, do not change more than 0.5% with further refinement of the mesh. Initial reservoir topography is based on the terrain measured near the end of 2003 and represents the conditions prior to Typhoon Aere which occurred during August 23-26, 2004. Thalweg elevation along the reservoir is plotted in Figure 27. At the upstream boundary, upstream of cross section (XS) 30, measured time series flow discharge and suspended sediment concentration are shown in Figure 28, representing the Aere event, and they are used as the upstream boundary condition. The median diameter of the current sediment is about $d_{50} \sim 5\ \mu$ m. Simulation is carried out for the period of 02:00, August 24 to 21:00, August 26, 2004, a 67-hour duration in the prototype.

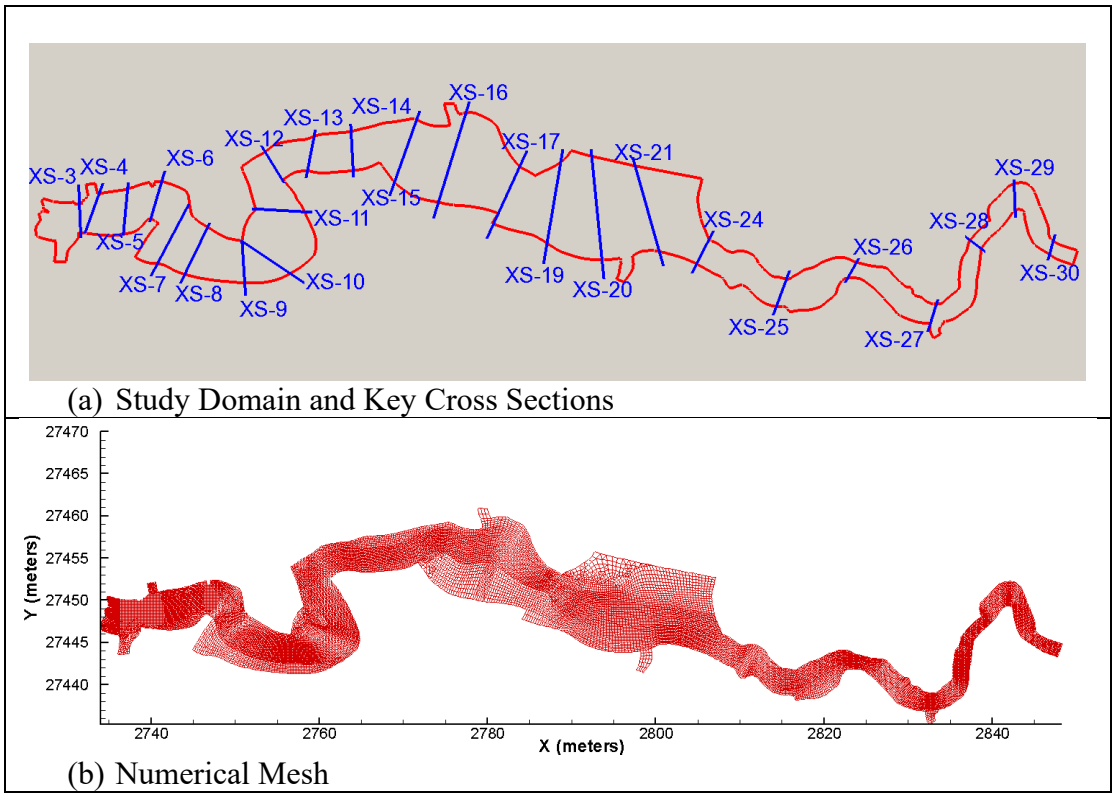

Figure 26. The study domain for both physical and numerical models, the selected cross section (XS) locations for comparison, and the mesh used for the Shihmen Reservoir modeling.

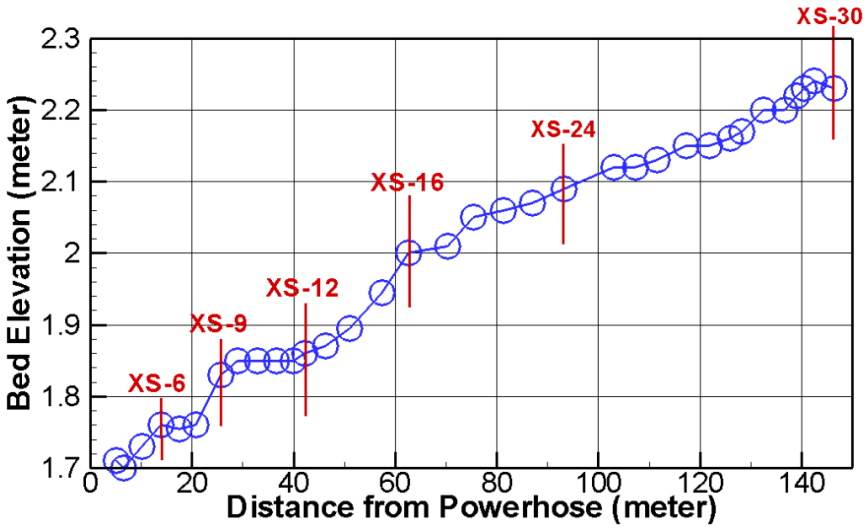

Figure 27. Reservoir thalweg bed elevation measured in December, 2003 from the powerhouse at the dam face to the upstream boundary of the study domain (physical model scale).

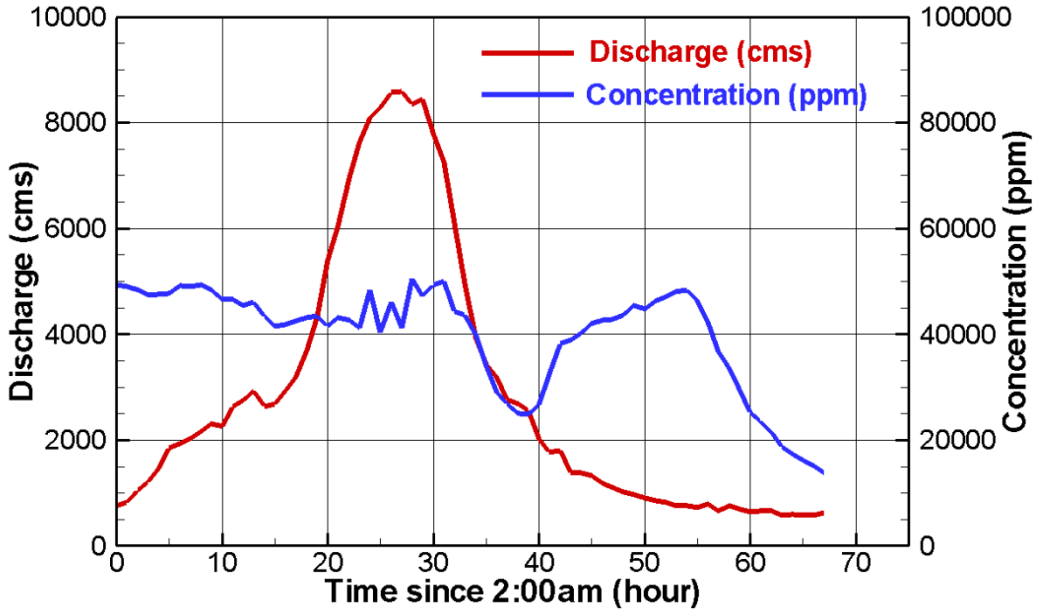

Figure 28. Time series flow discharge and sediment concentration entering the Shihmen Reservoir during Typhoon Aere in the prototype sale (time zero is at 02:00, August 24, 2004).

There are five outlets near the dam face that may divert water and sediment out of the reservoir: the spillway, the flood diversion tunnel, the powerhouse intake, the permanent river outlet, and the Shihmen Intake. The spillway has a sill elevation of 235 m, a width of 107 m and a measured maximum discharge of 5,800 m^3/s at the prototype scale. The flood diversion tunnel has a sill elevation of 220 m, a height of 8 m and a full-capacity discharge of 1,800 m^3/s. The powerhouse outlet sluices the highest amount of sediment. It has a sill elevation of 171 m, a height of 5 m and a full-capacity discharge of 380 m^3/s. The permanent channel outlet is relatively small and less important in sluicing. It has the same sill elevation as the powerhouse but with a full-capacity of 30 m^3/s. Shihmen intake is also small in its sluicing capacity. It has a sill elevation of 193.6 m, a height of 2.4 m and a full-capacity of 13 m^3/s. Other input parameters include drag coefficient of 0.055 (calibrated), time step of 0.2 s (2 s in the prototype), damping coefficient of 0.1, and front thickness of 1.0 m. Damping is used to remove the potential overshoot at the current head zone. But for this particular case, it is found that damping is not important as zero damping leads to almost the same results. In addition, the erosional rate due to the relatively large scale of the case. Simulation starts at 02:00, August 24, 2004, assuming an initially dry reservoir (i.e., zero suspended sediment concentration without undercurrent). The turbidity current enters the solution domain and then moves towards the dam.

The predicted arrival times of the turbidity current at various cross sections of the reservoir are compared with the physical model data in Figure 29. Good agreement is obtained between the model prediction and measured data. The percentage error between the numerical and physical models is less than 14% at all cross sections. The numerical model predicts that it takes 0.925 hours for the current front to reach the powerhouse from the upstream boundary

(9.25 hours in the prototype) and it is comparable to the 0.930 hours of the physical model. The turbidity current front is predicted to move at almost a constant speed with an average speed of 0.0450 m/s; this is compared with the 0.0448 m/s in the physical model scale (0.448 m/s in the prototype). It shows that the numerical model may be used to predict the current movement through the reservoir well. Such predictions are important as they help inform how the outlets may be operated to optimize sediment sluicing.

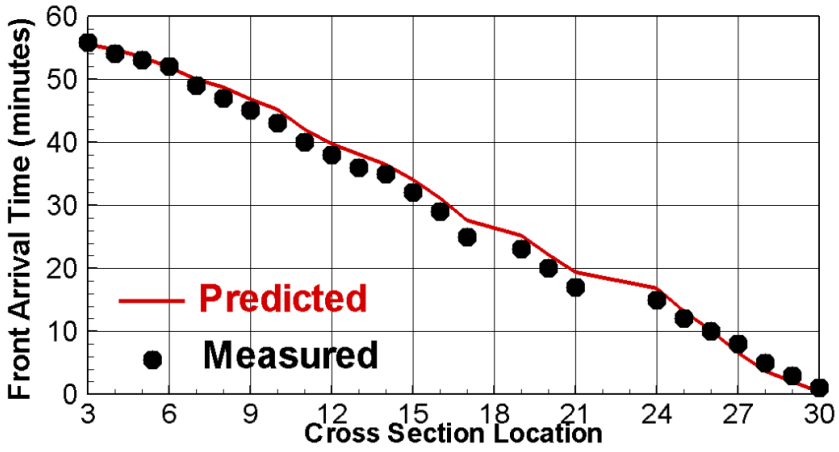

Figure 29. Comparison of numerical model predicted and physical model measured turbidity current front arrival times at various cross sections along the reservoir during Typhoon Aere (time is in the physical model scale).

Comparisons of the predicted and physical model sediment rates through all outlets are shown in Figure 30 in terms of prototype units. The agreement between the numerical model and the physical model is fair. Disagreement is observed in the variation of the sediment rate through the powerhouse after 40 hours. This may be attributed to the detrainment effect in the dam area. Major discrepancy is found in the prediction of sediment rate through the spillway and the flood diversion tunnel. The predicted rate through the spillway is much higher than the measured one. This is due to the use of a higher full-capacity discharge, 5,800 m^3/s, by the model than the actual value. The discharge at the spillway was not measured over the simulation period so a constant is used based on limited data. The predicted total amount of sediment through the flood diversion tunnel is also much higher than the measured data. It is mainly due to the difference in gate opening duration. For example, the predicted start of sluicing is at time 16 hours, about 7 hours earlier than the measured start of sluicing. The predicted start of sluicing by the numerical model is probably accurate since the model correctly predicts the current movement speed and the front arrival timing at various cross sections. We believe that the diversion tunnel gate was artificially opened sometime after the arrival of the current front during the physical model test, which unfortunately was not documented. Similar discrepancy occurs for the shut-off timing of the flood diversion gate.

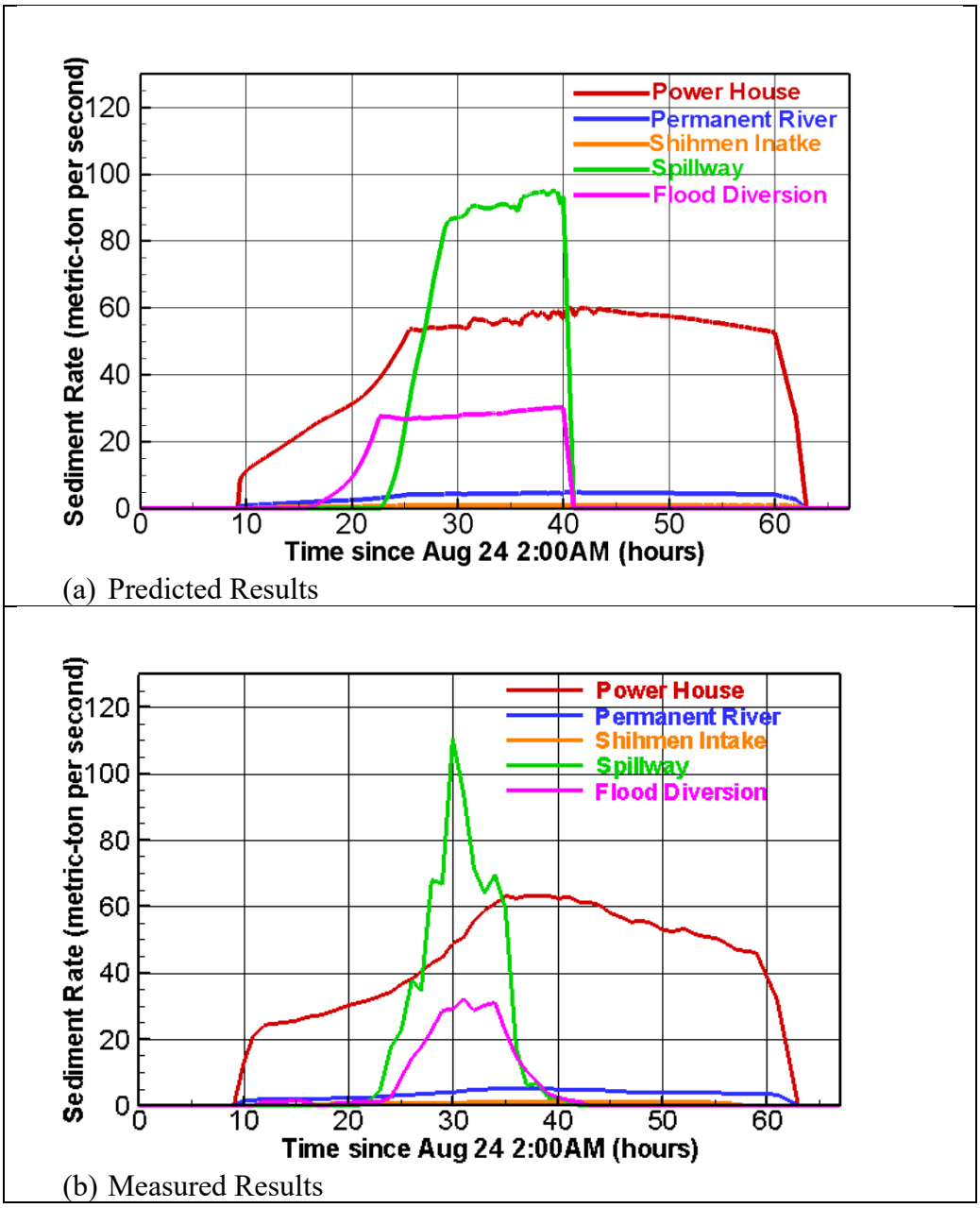

Figure 30. Comparison of numerical model predicted and physical model measured sediment rates through all sluicing outlets (time and sediment rate are in the prototype scale).

Of particular interest is the total amount of sediment that can be passed through the reservoir through all sluicing outlets, as it determines the reservoir storage loss and its life. The total sediment volumes delivered into and sluiced out of the reservoir by each outlet are compared in Table 2. The total amount of sediment passed through the reservoir is about 55.9% and 45.1%, respectively, for the numerical model and the physical model. Again, the higher predicted passing efficiency by the numerical model is primarily due to the higher amount of predicted sediment out of the spillway and diversion tunnel. The predicted and measured sediment deposition thicknesses within the reservoir after the Typhoon Aere event are compared in Figure 31. The predicted depth is about 24% smaller than the measured one since more sediment is sluiced out of the reservoir by the numerical model. The overall trend of the sediment deposition in the reservoir is reasonably predicted.

Table 2. Summary of total sediment volumes moved into and out of the reservoir during Typhoon Aere

	Total into Reservoir ($10^6\ m^3$)	Power House ($10^6\ m^3$)	Spillway ($10^6\ m^3$)	Flood Diversion ($10^6\ m^3$)	Permanent Channel ($10^6\ m^3$)	Shihmen Intake ($10^6\ m^3$)
Model Prediction	10.93	3.31	1.72	0.754	0.265	0.0569
		30.3%	15.7%	6.90%	2.42%	0.52%
Measurement	10.97	3.18	1.02	0.430	0.259	0.0593
		29.0%	9.30%	3.92%	2.36%	0.54%

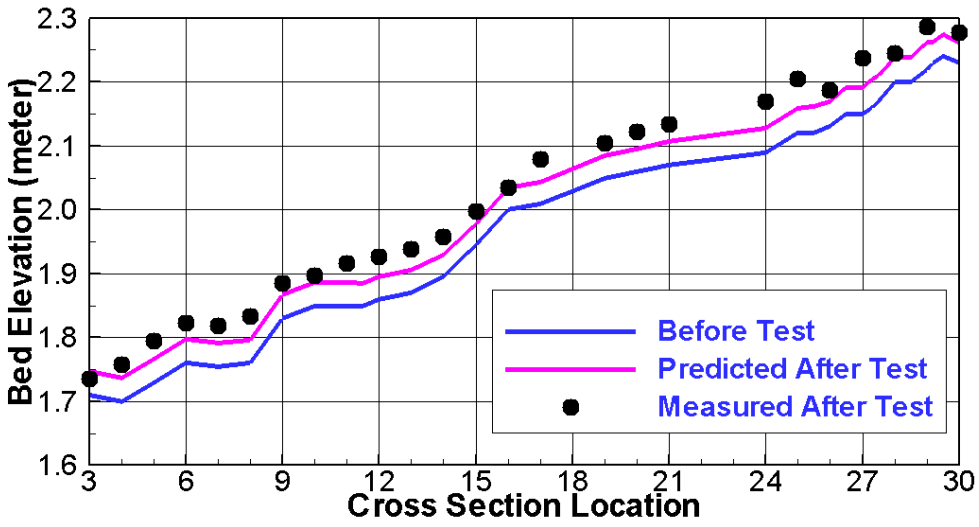

Figure 31. Comparison of numerical model predicted and physical model measured deposition depth in the reservoir along the pre-event thalweg during Typhoon Aere (bed elevation is in the physical model scale).

Sensitivity study has been carried out with regard to many model parameters. It is found that the drag coefficient and erosional rate are important while the entrainment rate is less critical. The drag coefficient is found to be important in predicting the current front movement speed but has negligible effect on the predicted outlet sediment rates. For example, the time needed for the current front to reach the powerhouse outlet is 8.20, 9.25, and 10.03 hours, respectively, with the drag coefficients of 0.035, 0.055 and 0.075. The erosional rate is important for predicting the erosion and deposition characteristics during current movement towards the reservoir. It also impacts the current movement speed. It is found that increased erosional rate leads to increased sediment volume out of the reservoir and faster current movement speed.

4.4 3D CFD Models

In this document, 3D CFD models refer to the those which solve the Reynolds-averaged Navier-Stokes (RANS) equations without the use of the hydrostatic assumption. The 3D CFD models are very general and accurate as empiricism is limited to turbulence closure as part of the mathematical formulation. 3D CFD models of this type contrast with other 3D hydraulic models which invoke the hydrostatic assumption (see, e.g., Lai and Wu 2019).

General guidelines recommended for 3D CFD modelling are listed below:

- 3D models are applicable to all types of hydraulic flushing studies: drawdown or pressure flushing and turbidity current venting.
    - In contrast, 1D and 2D models are restrictive as they are not applicable to pressure flushing, as these models assume that the velocity is uniform throughout the pool depth. 1D and 2D models may produce reduced accuracy if the width of the reservoir pool is not narrow or drawdown is only partial.
- Adjustable model parameters are few in general with a typical 3D flow modeling for calibration or validation. Input parameters specific to 3D models that may impact the results are as follows:
    - Mesh size
    - Time step
    - Turbulence model
    - Multiple sediment transport related parameters similar to the 2D models.

In the following, an application of the 3D model is presented to simulate the pressure flushing process at the Cherry Creek Reservoir, Denver, Colorado. As reviewed, no numerical modeling studies have been reported in the past and this the case serves as a unique demonstration application.

4.4.1 Mesh Generation

First, the horizontal model domain is determined as shown in Figure 32. It represents only a portion of the reservoir near the intake where the flow is important for pressure flushing. Note that the intake itself is added to the model domain - the rectangle in the figure with a horizontal dimension of 69 ft in width and 40 ft in depth. The Intake trash rack and gate opening dimensions are shown in Figure 33. The five gates are extended out so that water release amounts may be implemented properly using the numerical boundary conditions. Without the extension, boundary conditions have to be applied right at the gate openings which may lead to heightened uncertainty of simulated results.

A 2D mesh is generated first covering the horizontal model domain as shown in Figure 34. Once the 2D mesh is obtained, the bed elevation (terrain) is interpolated onto the mesh and is also displayed in the figure. The 2D horizontal mesh consists of 9,855 mixed quadrilaterals and triangles.

The 3D mesh is generated automatically by U2RANS using the sigma-mesh technique. That is, the same number of vertical mesh points are used at each 2D mesh point between the bed elevation and the water surface. In the simulation, a total of 47 uniform points are used so that the vertical mesh size is about 1 foot in the deepest area between 5504 ft and 5550 ft. A view of the final 3D mesh is shown in Figure 35.

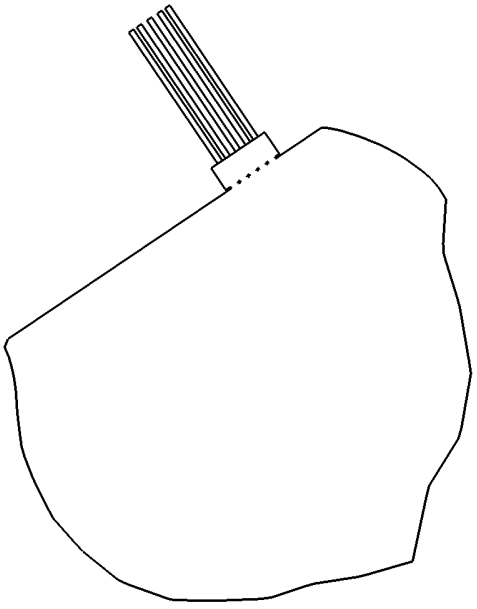

Figure 32. Model domain selected.

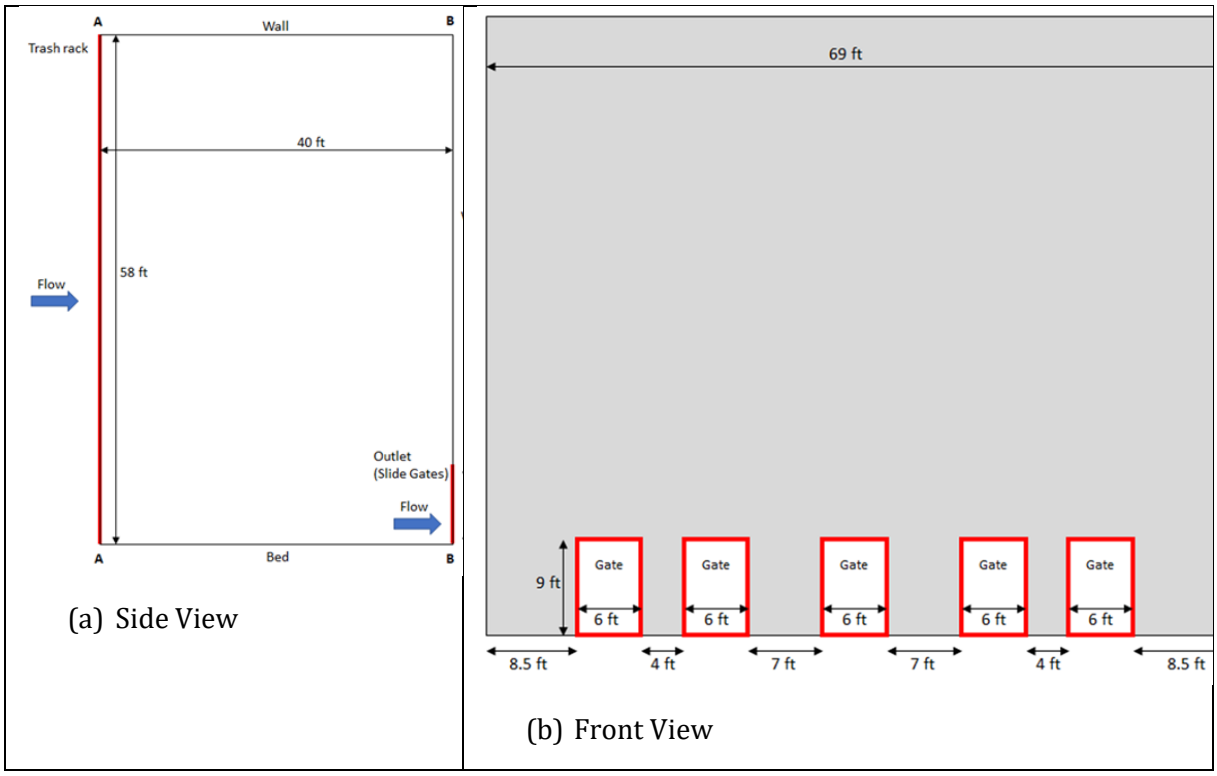

Figure 33. Geometry of the intake tower and the five low gates for pressure flushing.

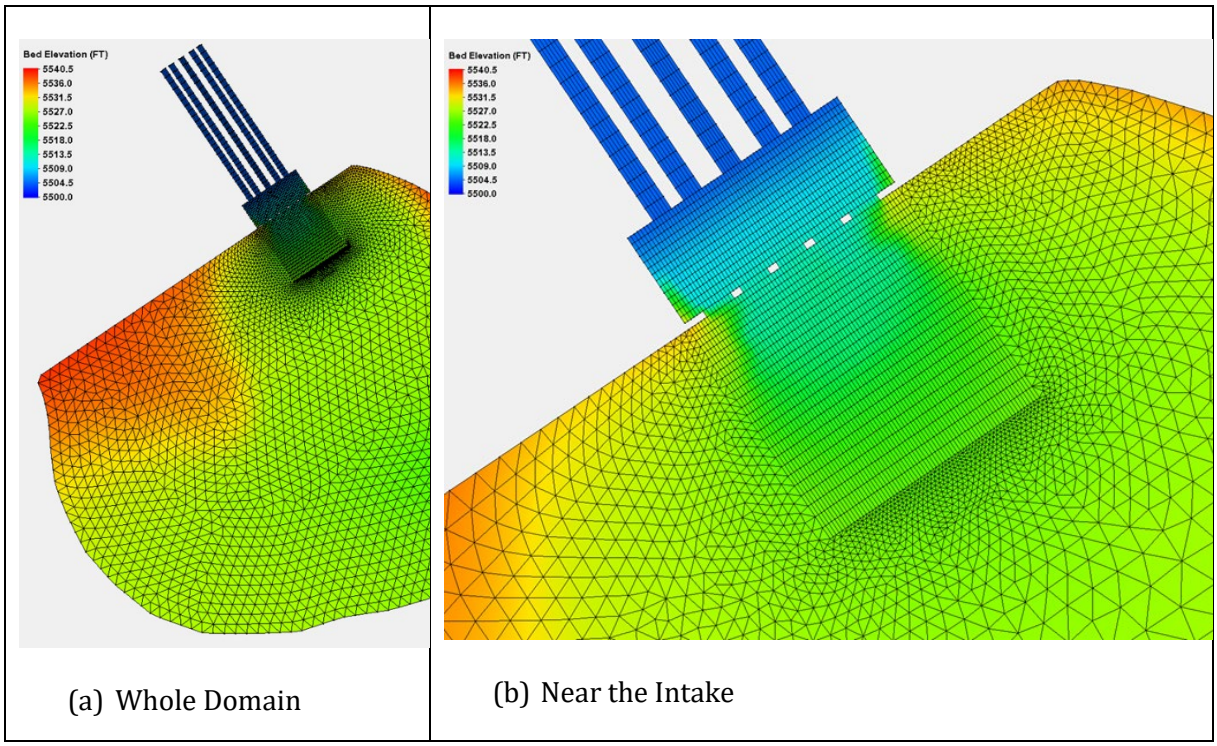

Figure 34. 2D mesh covering the horizontal model domain along with the terrain of the bed.

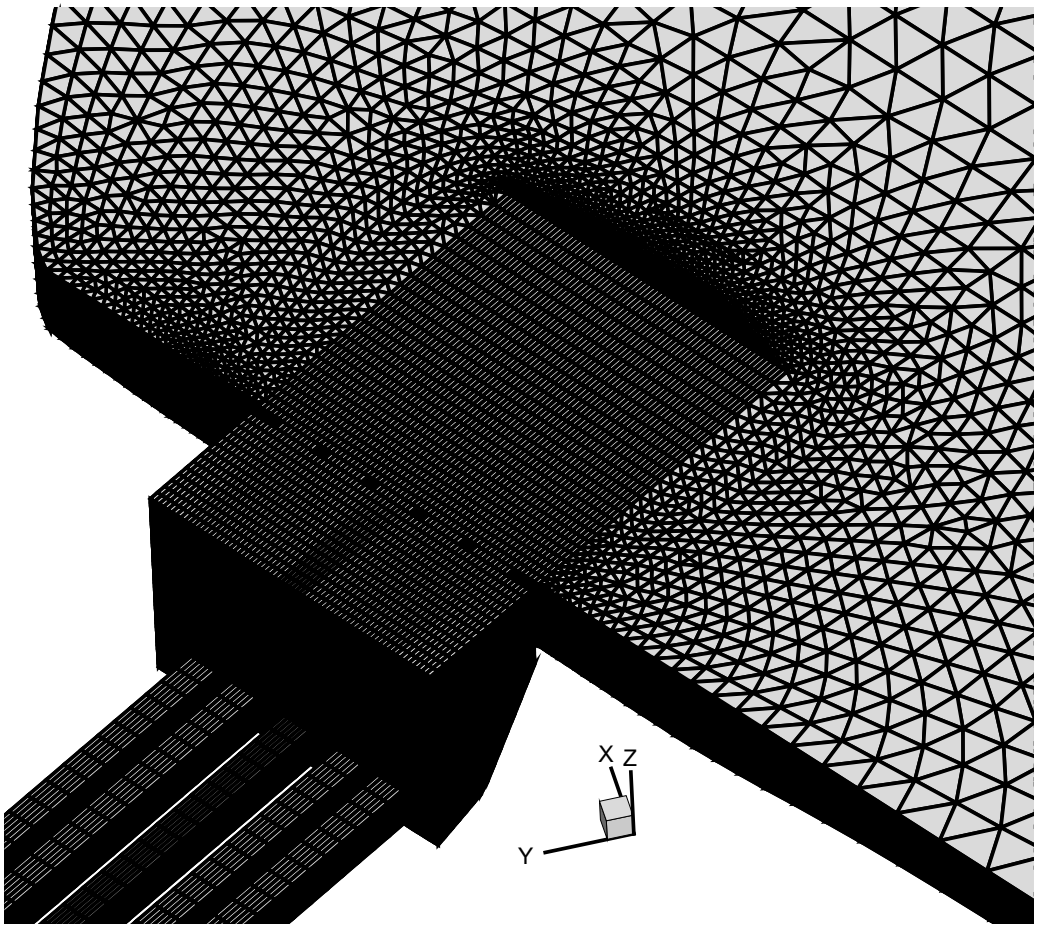

Figure 35. Close-up view of the 3D mesh near the intake.

4.4.2 Model Inputs

Two sets of modeling are carried out corresponding to two pressure flushing operations at the Cheery Creek Reservoir: 2017 low-discharge and 2018 high-discharge flushing. The flushing release rates are inputs to the model as the boundary conditions, while other model parameters (to be discussed below) remain the same for all modeling runs unless it is explicitly mentioned. Only the 2018 flushing results are discussed; readers may refer to Lai and Greimann (2020) for the 2017 results.

The 2018 flushing was conducted on May 23 with a nominal discharge of 1,300 cfs. The actual flow release through the intake gates is shown in Figure 36. The release was through one of five gates and follows the gate sequence of 3, 1, 2, 4, 5 when the gates are numbered from right to left looking towards the intake.

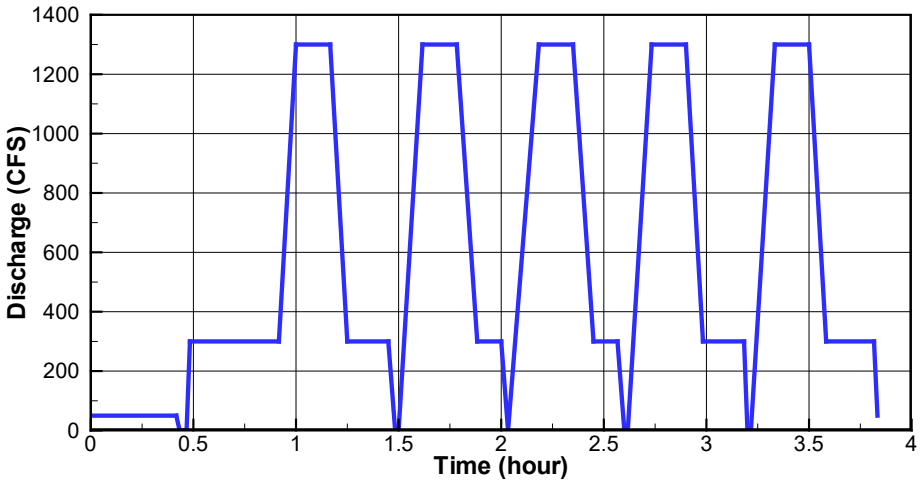

Figure 36. Actual 2018 flow release rate.

The sediments in the Cheery Creek Reservoir consists of clay, silt and sand. According to Armstrong (2017), the diameters of clay, silt, and sand are less than 0.002 mm, between 0.002 mm and 0.075 mm, and above 0.075 mm. Based on the bed gradations in the near-surface samples, the fractions for clay, silt and sand are 45%, 50%, and 5%, respectively. In this study, therefore, one cohesive sediment class is selected for the modeling, as about 95% of the sediments are in the clay and silt sizes. According to Armstrong (2017), the average of measured surface sediment specific density was about 2.51; the bulk density was 32.5 lb/ft^3 (520.6 kg/m^3).

The sediment thickness distribution is an input; the model domain is partitioned into three zones (Figure 37) for the purpose: the reservoir (red), the intake upstream of the gates (gray), and the after-gates (green). The thickness in the reservoir is large according to the survey and the erosion in the area is almost negligible, so 16.4 ft thickness is the input which does not impact the results. The after-gate area is specified as having no sediments deposited and non-erodible during the simulation. The sediment thickness of the intake (gray) zone is important; unfortunately, no measured data are available. The baseline thickness input in the intake is set up as follows. The thickness at the trash rack is obtained by averaging the measured bed elevation in the area and subtracting out the intake elevation of 5,504 ft. This showed that about eight (8) ft of sediments were deposited near the trash rack and is taken as the thickness. This thickness is assumed to be constant inside the intake except near the gates. A linear drop of thickness from 8 to 0 ft is assumed near the gate over a 4 ft distance. The baseline bed elevation (thickness) distribution in the intake and it's vicinity are displayed in Figure 38.

The next important input is the erodibility properties of the sediment. In the present modeling, constant critical shear stress and erodibility are specified as inputs. The two parameters are based on the JET test results of Armstrong (2017). The test showed that the critical shear stress and erodibility (detachment rate) varied widely at different locations (see Table 3). The measured data at the DH-17-2-1 were used in the present study as it is closer to the intake.

That is, the critical shear stress is 0.013 psf (0.62 Pa) and the erodibility/detachment rate is 200.6 ft/hr-psf (3.547e-4 m/s-Pa). The results are more sensitive to the erodibility than the critical shear stress; and some sensitivity results will be reported later in addition to the baseline setup.

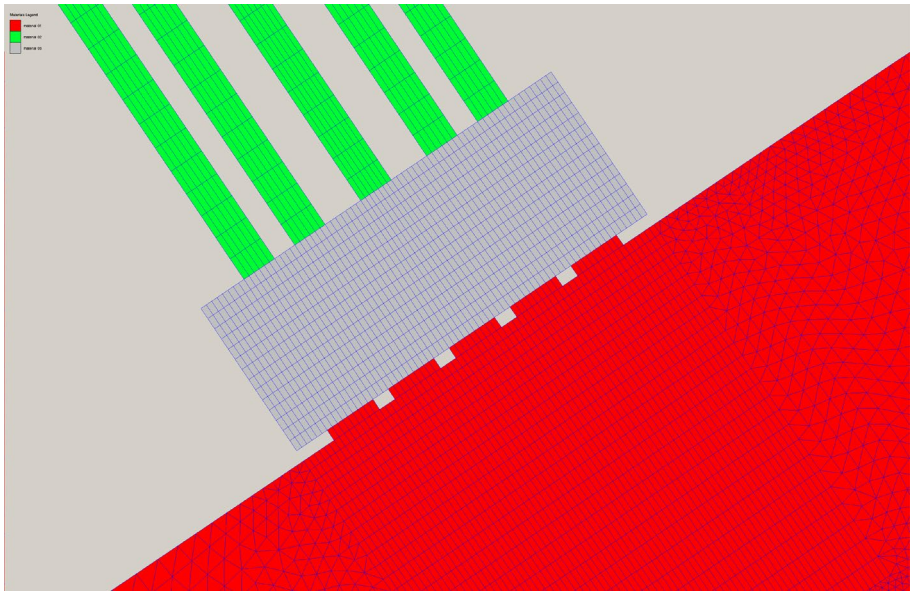

Figure 37. Three spatial zones used to specify the sediment thickness distribution.

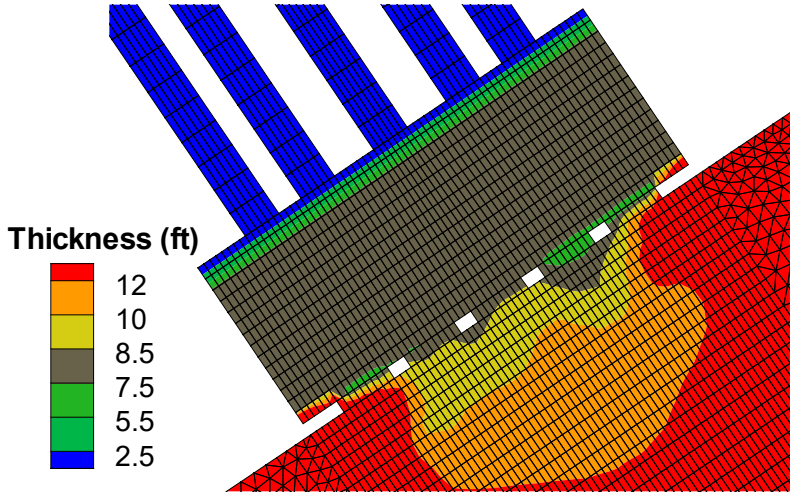

Figure 38. Thickness of the erosible sediments inside the intake (thickness is about 8 ft in the intake).

Table 3. JET test results of critical shear stress (lb/ft2 or psf) and detachment rate (ft/hr-psf) at three locations near the bed surface

Sample #	Depth (ft)	Detachment Rate (ft/hr-psf)	Surface Critical Shear Stress (psf)
DH-17-2-1	0.0	200.6	0.,013
DH-17-3-1	1.1	3.642	0.048
DH-17-4-1	0.3	18.45	0.06

4.4.3 Results and Discussion

First, the simulated sediment concentration during the 2018 flushing is compared with the field data. Note that the numerical model concentration is obtained right after the gates (within the outlet works), while the measured sediment concentration is within the Cherry Creek about 0.25 mile downstream of the dam outlet.

The measured and simulated sediment concentrations are compared in Figure 39. It is seen that the numerical model agrees with the data well though the concentration is under-predicted over the first 2-gate period and over-predicted over the next 3-gate period. The total amount of sediment release is close to the measured data. It is possible that the initial measured high concentration is partially contributed by the sediments stored downstream of the release outlet, not entirely due to the reservoir release.

The erosion pattern (scour zone) produced by the 2018 pressure flushing is shown in Figure 40. The numerical modeling shows that the scour zone is still limited to within the intake with the much higher 2018 release rate of 1,300 cfs. This is qualitatively confirmed by the fact that both the 2018 field measurements in the reservoir were unable to detect measurable scours upstream of the trash rack in the reservoir. Quantitative comparison, however, is not possible as the field measurements were not able to reach inside the intake.

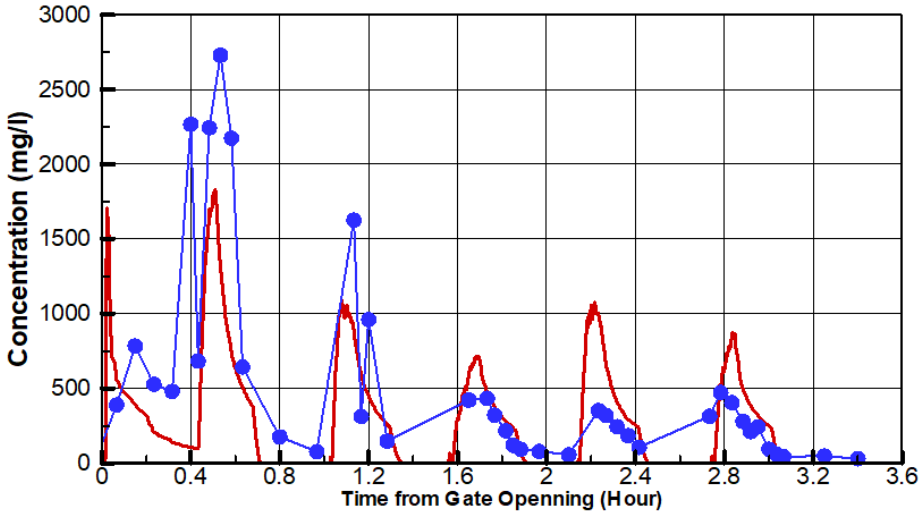

Figure 39. Baseline model predicted and field measured sediment concentration downstream of the release gate during the 2018 pressure flushing (Red line: numerical model; blue symbol and line: measurement).

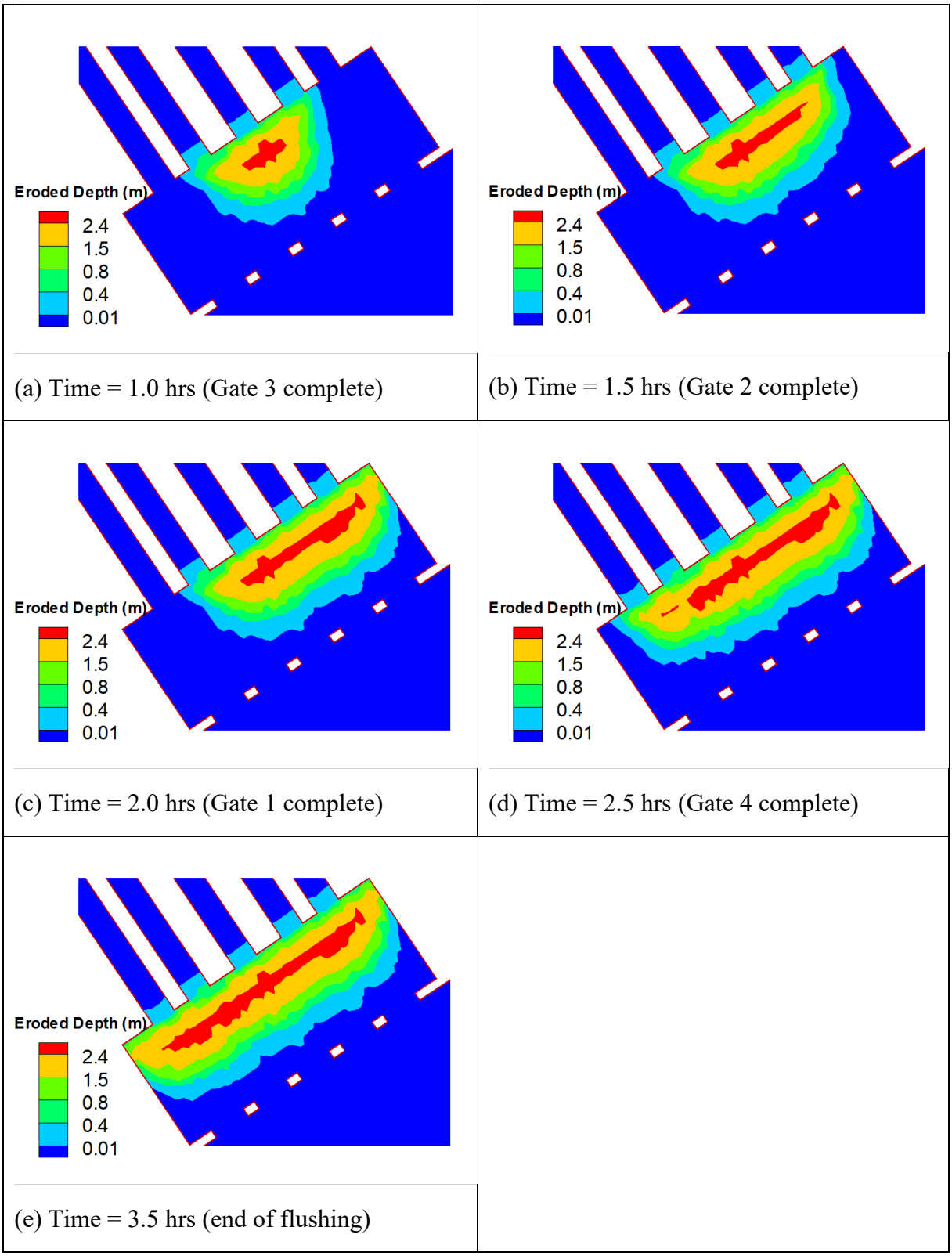

Figure 40. Predicted scour zone development in time by the baseline model during the 2018 flushing (contours represent the eroded depth in meter).

4.4.4 Concluding Remarks

The numerical simulation of pressure flushing leads to the following key findings:

- The 3D CFD model is demonstrated to work well in simulating the pressure flushing process at the Cherry Creek Reservoir.
- The model-predicted sediment release concentration is compared with the measured sediment concentration downstream in the river. The agreement is reasonable and points to the potential of the 3D model for future pressure flushing applications.
- Pressure flushing is not an efficient large-scale sediment removal option in reservoirs. Even the large 2018 release (1,300 cfs) flushing operations failed to remove sediment deposits outside the intake in the reservoir. The field surveys confirmed this as the measured differences outside of the intake tower between the pre- and post-flushing bed elevations did not have detectable scours.
- Pressure flushing does produce scour cones upstream of the gates but limited to within the intake. Pressure flushing thus is effective if the objective is to clean up the sediment deposits within the intake tower and prevent clogging from occurring in front of the gates.
- The scour cone upstream of the trash rack at Cherry Creek is at an approximately equilibrium conditions, which would be expected because flushing of the gates is performed on an annual basis.

The numerical model may be used to develop an effective strategy of flushing. Based on the above results, for example, it suggests that if the discharge would be 1,300 cfs like the 2018 release schedule, a 3-gate release, gates 3, 1 and 5, would be more efficient than the current 5-gate schedule. Other options to consider to maximize the efficiency of the flushing would be to flush every other year or to decrease the duration of the flushing. Most of the work performed by the flushing occurs immediately after the gates are opened.

5. References

Ackers, P., and Thompson, G. (1987). Reservoir sedimentation and influence of flushing. Sediment Transport in Gravel-Bed Rivers. John Wiley and Sons New York. 1987. p 845-868, 5 fig, 13 ref.

Ahadpour Dodaran, A., Park, S.K., Mardashti, A., and Noshadi, M. (2012). Investigation of dimension changes in under pressure hydraulic sediment flushing cavity of storage dams under effect of localized vibrations in sediment layers. Int J Ocean Syst Eng 2(2):71–81.

Ahn, J. (2012). "Numerical modeling of reservoir sedimentation and flushing processes." Colorado State University.

Ahn, J., Yang, C. T., PRIDAL, D. B., and REMUS, J. I. (2013). "Numerical modeling of sediment flushing from Lewis and Clark Lake." International Journal of Sediment Research, Elsevier, 28(2), 182–193.

Alavian, V., Jirka, G.H., Denton, R.A., Johnson, M.C., and Stefan, H.G. (1992). Turbidity currents entering lakes and reservoirs. J. Hydraulic Engineering, 118(11), 1464-1489.

Annandale, G.W. (1987). Developments in Water Science- Reservoir Sedimentation. BV Rand Afrikaans University: Elsevier Science Publishers.

Annandale, G.W. (2001). Reservoir conservation and sediment management. Water week.

Armstrong, B. (2017). Cherry Creek Reservoir Sediment Erosion Testing Results. Technical Memorandum No. 8530-2017-22, US Bureau of Reclamation, Denver, CO.

Artruc, T. C. (2020). Numerical Modeling of Lateral Erosion during Reservoir Drawdown.

Atkinson, E. (1996). "The feasibility of flushing sediment from reservoirs." HR Wallingford Ltd.

Basson, G.R. (2009). Management of siltation in existing and new reservoirs. General Report. 23rd Congress of the International Commission on Large Dams, Int. Com. on Large Dams, Brasilia.

Boeriu, P., Roelvink, D., Mulatu, C. A., Thilakasiri, C. N., Moldovanu, A., and Margaritescu, M. (2011). Modeling the flushing process of reservoirs. The Romanian Review Precision Mechanics, (40), 54.

BOR (Bureau of Reclamation). (1954). Some Hydraulic Engineering Aspects of Density Currents. Hydraulic Laboratory Report No. Hyd-373, Bureau of Reclamation, Denver. Colorado.

Boyd, P.M., and Gibson, S.A. (2016). Applying 1D sediment models to reservoir flushing studies: measuring, monitoring, and modeling the spencer dam sediment flush with HEC-RAS. Coastal and Hydraulics Laboratory (US).

Bradford, S.F., Katopodes, N.D. (1999). Hydrodynamics of turbidity underflows. I: Formulation and numerical analysis. J. Hydraulic Engineering, 125(10), 1006-1015.

Brignoli, M.L. (2017). Improving sustainability of sediment management in Alpine reservoirs: control of sediment flushing operations to mitigate downstream environmental impacts. Università degli Studi dell'Insubria.

Buckee, C., Kneller, B.C., and Peakall, J. (2001). Turbulence structure in steady, solute-driven gravity currents. Spec. Publ. Int. Assoc. Sedimentol., 31, 173 – 187.

Chang, H.H., Harrison, L.L., Lee, W., and Tu, S. (1996). Numerical modeling for sediment-pass-through reservoirs. Journal of Hydraulic Engineering, American Society of Civil Engineers, 122(7), 381–388.

Chaudhary, H. P., Isaac, N., Tayade, S. B., and Bhosekar, V. V. (2019). Integrated 1D and 2D numerical model simulations for flushing of sediment from reservoirs. ISH Journal of Hydraulic Engineering, Taylor & Francis, 25(1), 19–27.

Chen, C.-N. and Tsai, C.-H. (2017). Estimating sediment flushing efficiency of a shaft spillway pipe and bed evolution in a reservoir. Water, Multidisciplinary Digital Publishing Institute, 9(12), 924.

Chikita, K. (1990). Sedimentation by river induced turbidity currents: field measurements and interpretation. J. Sedimentology, 37:891-905.

Dahl, T.A. and Ramos-Villanueva, M. (2019). Overview of historical reservoir flushing events and screening guidance. Coastal and Hydraulics Laboratory (US).

Dewals, B., Erpicum, S., Archambeau, P., Detrembleur, S., Fraikin, C., and Pirotton, M. (2004). Large scale 2D numerical modelling of reservoirs sedimentation and flushing operations. Proceedings of the 9th International Symposium on River Sedimentation.

Ellison, T.H., and Turner, J.S. (1959). Turbulence entrainment in stratified flows. J. Fluid Mech., 6, 423-448.

Emamgholizadeh, S., Bina, M., Fathi-Moghadam, M., and Ghomeyshi, M. (2006). Investigation and evaluation of the pressure flushing through storage reservoir. ARPN J Engg Appl Sci., 1(4), 7–16.

Emamgholizadeh, S. and Fathi-Moghadam, M. (2014). Pressure flushing of cohesive sediment in large dam reservoirs. J Hydrologic Engg., 19(4), 674–681. DOI: 10.1061/(ASCE)HE.1943-5584.0000859.

Esmaeili, T., Sumi, T., Kantoush, S. A., Kubota, Y., and Haun, S. (2015). "Numerical study on flushing channel evolution, case study of Dashidaira reservoir, Kurobe river." 土木学会論文集 B1 (水工学), 公益社団法人 土木学会, 71(4), I_115-I_120.

Esmaeili, T., Sumi, T., Kantoush, S. A., Kubota, Y., Haun, S., and Rüther, N. (2017). "Three-dimensional numerical study of free-flow sediment flushing to increase the flushing efficiency: a case-study reservoir in Japan." Water, Multidisciplinary Digital Publishing Institute, 9(11), 900.

Fang, D. and Cao, S. (1996). An experimental study on scour funnel in front of a sediment flushing outlet of a reservoir. Proc., 6th Federal Interagency Sedimentation Conf., Las Vegas, NV, I-78–I-84.

Fan, J. and Morris, G.L. (1992). Reservoir sedimentation. II: reservoir desiltation and long-term storage capacity. J Hydraul Eng ASCE 118(3):370–384.

Fathi-Moghadam, M., Emamgholizadeh, S., Bina, M. and Ghomeshi, M. (2010). Physical modelling of pressure flushing for desilting of non-cohesive sediment, Journal of Hydraulic Research, 48:4, 509-514, DOI: 10.1080/00221686.2010.491691.

Fietz, T.R., and Wood, I.R. (1967). Three-dimensional density current. J. Hydr. Div., 93(HY6):1-23.

Garcia, M.H. (1993). Hydraulic jumps in sediment-driven bottom currents. J. Hydraul. Eng., 119(10), 1094 – 1117.

Garcia, M. H. (1994). Depositional turbidity currents laden with poorly sorted sediment. J. Hydraul. Eng., 120(11), 1240 – 1263.

GEC (Gathard Engineering Consulting). (2006). Klamath River Dam and Sediment Investigation, Technical Report, 40031st Ave. NW, Seattle, WA, 96 pages + Appendices A to K, November.

Ghoreishi, S. H., and Tabatabai, M. M. R. (2010). Model study reservoir flushing. JOURNAL OF WATER SCIENCES RESEARCH (JWSR), 2(1), 1–8.

Groenenberg, R. (2007). Process-based modeling of turbidity current hydrodynamics and sedimentation. Ph.D. Thesis, Civil Engineering and Geotechnology, Delft University of Technology.

Groenenberg, R., Sloff, K., and Weltje, G.J. (2009). A high-resolution 2-DH numerical scheme for process-based modeling of 3-D turbidite fan stratigraphy. Computers & Geosciences, 35 (2009), pp.1686-1700.

Guertault, L., Camenen, B., Paquier, A., and Peteuil, C. (2014). 1D Modelling of fine sediments dynamics in a dam reservoir during a flushing event. Proceedings of 7th International Conference on Fluvial Hydraulics, Lausanne, Switzerland, CRC Press, Lausanne, Switzerland, 147–154.

Hajikandi, H, Vosoughi, H, Jamali, S (2018). Comparing the Scour Upstream of Circular and Square Orifices, International Journal of Civil Engineering (2018) 16:1145–1156, https://doi.org/10.1007/s40999-017-0269-5.

Haun, S. and Olsen, N.R.B. (2012). Three-dimensional numerical modelling of reservoir flushing in a prototype scale, International Journal of River Basin Management, 10:4, 341-349, DOI: 10.1080/15715124.2012.736388.

Huang, C., Lai, Y.G., Lai, J., and Tan, Y. (2019). Field and Numerical Modeling Study of Turbidity Current in Shimen Reservoir during Typhoon Events. J. Hydraul. Eng., 145(5): 05019003.

Huang, J.C. and Greimann, B.P. (2012). User's manual for SRH-1D V2.0, Sedimentation and River Hydraulics Group, Technical Service Center, Bureau of Reclamation, Denver, Colorado.

Huang, J., Greimann, B., and Kimbrel, S. (2019). Simulation of Sediment Flushing in Paonia Reservoir of Colorado. Journal of Hydraulic Engineering, 145(12).

Huppert, H. E., and Simpson, J.E. (1980). The slumping of gravity currents. J. Fluid Mech., 99, 785 – 799.

Iqbal, M., Ghumman, A. R., Haider, S., Hashmi, H. N., and Khan, M. A. (2019). Application of Godunov type 2D model for simulating sediment flushing in a reservoir. Arabian Journal for Science and Engineering, Springer, 44(5), 4289–4307.

Isaac, N., Eldho, T. I., and Gupta, I. D. (2014). Numerical and physical model studies for hydraulic flushing of sediment from Chamera-II reservoir, Himachal Pradesh, India. ISH Journal of Hydraulic Engineering, 20(1), 14–23. doi:10.1080/09715010.2013.821788.

Jansson, M.B., and Erlingsson, U. (2000). Measurement and quantification of a sedimentation budget for a reservoir with regular flushing. Regul Rivers Res Manag 16:279–306.

Kamble, S.A., Kunjeer, P.S., Sureshkumar, B. and Isaac, N. (2017). Hydraulic model studies for estimating scour cone development during pressure flushing of reservoirs, ISH Journal of Hydraulic Engineering, DOI: 10.1080/09715010.2017.1381577.

Kantoush, S.A. (2008). Experimental study on the influence of the geometry of shallow reservoirs on flow patterns and sedimentation by suspended sediments, Ph.D. thesis, EPFL, Suisse.

Kondolf, G.M., Gao, Y., Annandale, G.W., Morris, G.L., Jiang, E., Zhang, J., Cao, Y., Carling, P., Fu, K., and Guo, Q. (2014). Sustainable sediment management in reservoirs and regulated rivers: Experiences from five continents. Earth's Future, Wiley Online Library, 2(5), 256–280.

Krone, R.B. (1962). Flumes studies of the transport of sediment in estuarial shoaling processes. Technical Report, Hydraulic Engineering Laboratory, University of California, Berkeley, California.

Kuenen, P.H., and Migliorini, C.I. (1950). Turbidity currents as a cause of graded bedding. J. Geology, 58, 91-127.

Lai, J.S. and Shen, H.W. (1995). An experiment study on reservoir drawdown flushing. International Journal of Sediment Research, 10(3), 19–36.

Lai, J.S. and Shen, H. W. (1996). Flushing sediment through reservoirs. Journal of Hydraulic Research, Taylor & Francis, 34(2), 237–255.

Lai, Y.G., Weber, L.J., and Patel, V.C. (2003). Non-hydrostatic three-dimensional method for hydraulic flow simulation - Part I: formulation and verification. J. Hydraulic Engineering, 129(3), 196-205.

Lai, Y. G., and Bauer, T. R. (2007). Erosion analysis upstream of the San Acacia Diversion Dam on the Rio Grande River, Project Report, Technical Service Center, Bureau of Reclamation, Denver, CO.

Lai, Y.G. (2008). SRH-2D Theory and User's Manual version 2, Technical Service Center, Bureau of Reclamation, Denver, CO.

Lai, Y.G. (2010). "Two-Dimensional Depth-Averaged Flow Modeling with an Unstructured Hybrid Mesh." J. Hydraulic Engineering, ASCE, 136(1), 12-23.

Lai, Y.G. and Greimann, B.P. (2012). Modeling channel formation on the Klamath River due to reservoir drawdown. United States Society of Dams Annual Meeting and Conference, New Orleans, Louisiana, April 23-27, 2012.

Lai, Y. G. (2014). A Two-Dimensional Layer-Averaged Turbidity Current Model. Technical Report No. SRH-2014-03, Technical Service Center, U.S. Bureau of Reclamation, Denver, Colorado.

Lai, Y.G., Huang, J., and Wu, K. (2015). Reservoir Turbidity Current Modeling with a Two-Dimensional Layer-Averaged Model. J. Hydraulic Engineering. Vol.141(12). 04015029 1-15.

Lai, Y.G. and Wu, K. (2018). A numerical modeling study of sediment bypass tunnels at shihmen reservoir, Taiwan. Int J Hydro. Vol.2(3): 00056. DOI: 10.15406/ijh.2018.02.00056.

Lai, Y.G. and Wu, K. (2019). A Three-Dimensional Flow and Sediment Transport Model for Free-Surface Open Channel Flows on Unstructured Flexible Meshes. Fluids 2019, 4, 18; doi:10.3390/fluids4010018.

Lai, Y.G. (2020). A Two-Dimensional Depth-Averaged Sediment Transport Mobile-Bed Model with Polygonal Meshes. Water 2020, 12, 1032; https://doi.org/10.3390/w12041032.

Lai, Y. G. and Greimann, B.P. (2020). Modeling of Cherry Creek Reservoir Pressure Flush. Report No. ENV-2020-83, Technical Service Center, U.S. Bureau of Reclamation, Denver, CO.

Lambert, A.M., Kelts, K.R., and Marshall, N.F. (1976). Measurements of density underflows from Walensee Switzerland. J. Sedimentology, 23, 87-105.

Liu, J., Minami, S., Otsuki, H., Liu, B., and Ashida, K. (2004). “Prediction of concerted sediment flushing.” Journal of Hydraulic Engineering, American Society of Civil Engineers, 130(11), 1089–1096.

Madadi, M.R., Rahimpour, M., and Qaderi, K. (2017). Improving the Pressurized Flushing Efficiency in Reservoirs: An Experimental Study. Water Resour Manage, 31:4633–4647. DOI 10.1007/s11269-017-1770-y.

Mahmood, K. (1987). Reservoir sedimentation: impact, extent, and mitigation. Technical paper. International Bank for Reconstruction and Development, Washington, DC (USA).

Major, J., J. O'Connor, G. Grant, K. Spicer, H. Bragg, A. Rhode, D. Tanner, C. Anderson, and J. Wallick. (2008). Initial Fluvial Response to the Removal of Oregon’s Marmot Dam, EOS – Transactions of the American Geophysical Union, 89(27), 24.

Malcherek, A. (2007). Sediment transport und Morphodynamik, Scriptum Institut fur Wasserwesen, Universitat Munchen.

Marino, B. M., Thomas, L.P., and Linden, P.F. (2005). The front condition for gravity currents. J. Fluid Mech., 536, 49 – 78.

Mehta, A.J., and Partheniades, E. (1973). Depositional behavior of cohesive sediments. Technical Report No. 16, Coastal and Oceanographic Engineering Laboratory, University of Florida, Gainesville, Florida.

Merkel, U.H. and Kopmann, R. (2012). A continuous vertical grain sorting model for Telemac and Sisyphe. River Flow 2012 – Murillo (Ed.). Taylor & Francis Group, London, ISBN 978-0-415-62129-8. Pp.457-463.

Meshkati, M.E., Dehghani, A.A., Naser, G., Emamgholizadeh, S., and Mosaedi, A (2009). Evolution of developing flushing cone during the pressurized flushing in reservoir storage. World Acad Sci Eng Technol., 58, 1107–1111.

Meshkati, M. E., Dehghani, A. A., Sumi, T., Mosaedi, A. and Meftah, M. (2012). Experimental investigation of pressure flushing technique in reservoir storages. Water and Geoscience, pp. 132–137. ISBN: 978-960-474-160-1. Reservoir sedimentation- Schleiss, eds., Taylor & Francis Group, London, ISBN 978-1-138-02675-9.

Middleton, G.V. (1966). Experiments on density and turbidity currents: I. Motion of the head. Can J. Earth Sci., 3:523-546.

Minami, S., Noguchi, K., Otsuki, H., Fukuri, H., Shimahara, N., Mizuta, J., and Takeuchi, M. (2012). Coordinated sediment flushing and effect verification of fine sediment discharge operation in Kurobe River. Proceedings of the ICOLD Conference, Kyoto, Japan, 6–8.

Morris, G. L. and Fan, J. (1998). Reservoir sedimentation handbook: design and management of dams, reservoirs, and watersheds for sustainable use. McGraw Hill Professional.

Morris, G.L., and Hu, G. (1992). HEC-6 modeling of sediment management in Loíza. Hydraulic Engineering: Saving A Threatened Resource - in Search of Solutions, Proceedings of the Hydraulic Engineering Sessions at Water Forum '92, ASCE, 630-635.

Olsen, N.R.B. (1999). Two-dimensional numerical modelling of flushing processes in water reservoirs. Journal of Hydraulic research, Taylor & Francis, 37(1), 3–16.

Olsen, N.R.B. and Haun, S. (2018). Numerical modelling of bank failures during reservoir draw-down. EDP Sciences.

Parker, G., Fukushima, Y., Pantin, H. M. (1986). Self-accelerating turbidity currents. J. Fluid Mech., 171, 145-181.

Parker, G., Garcia, M.H., Fukushima, Y., and Yu, W. (1987). Experiments on turbidity currents over an erodible bed. J. Hydraul. Res., 25(1), 123 – 147.

Partheniades, E. (1965). Erosion and deposition of cohesive soils. Journal of the Hydraulics Devision, ASCE, Vol. 91(1), 105-139.

Paull, C. K., Ussler III, W., Greene, H.G., Keaton, R., Mitts, P., and Barry J. (2003). Caught in the act: The 20th December 2001 gravity flow event in Monterey Canyon. Geo-Mar. Lett., 22, 227 - 232.

Powell, D.N. and Khan, A. (2012). Scour upstream of a circular orifice under constant head. J Hydraul Res 50(1):28–34. DOI: 10.1080/00221686.2011.637821

Powell, D.N. and Khan, A. (2015). Flow field upstream of an orifice under fixed bed and equilibrium scour conditions. J Hydraul Eng. 141(2): 04014076. DOI:10.1061/(ASCE)HY.1943-7900.0000960 04014076

PWA (Phillip Williams and Associates, Ltd). (2009). A River Once More: Restoring the Klamath River Following Removal of the Iron Gate, Copco, and J. C. Boyle Dams, California State Coastal Conservancy and California Department of Fish and Game.

Randle, T.J., Bountry, J.A., Ritchie, A., and Wille, K. (2015a). Large-scale dam removal on the Elwha River, Washington, USA: Erosion of reservoir sediment. Geomorphology, Elsevier, 246, 709–728.

Randle, T.J., Kimbrel, S., and Collins, K. L. (2015b). Reservoir sustainability workshop and national reservoir sedimentation team. The 3rd Joint Federal Interagency Conference, (Figure 4), 1–11.

Reclamation (1998) Earth Manual Part 1, Third Edition, Earth Sciences and Research Laboratory Geotechnical Research, Technical Service Center, Denver, Colorado, 1998, U.S. Department of the Interior, Bureau of Reclamation.

Reclamation. (2011). Hydrology, Hydraulics and Sediment Transport Studies for the Secretary's Determination on Klamath River Dam Removal and Basin Restoration, Technical Report No. SRH-2011-02. Prepared for Mid-Pacific Region, US Bureau of Reclamation, Technical Service Center, Denver, CO.

Saam, L., Mouris, K., Wieprecht, S., and Haun, S. (2019). Three-dimensional numerical modelling of reservoir flushing to obtain long-term sediment equilibrium. Proceedings of the 38th IAHR World Congress, Panama City, Panama, 1–6.

Sequeiros, O.E., Naruse, H., Endo, N., Garcia, M.H., and Parker, G. (2009). Experimental study on self-accelerating turbidity currents. J. Geophys. Res., 114, C05025, doi:10.1029/2008JC005149.

Shammaa, Y., Zhu, D.Z., and Rajaratnam, N. (2005). Flow upstream of orifices and sluice gates. J. Hydraul. Eng., 10.1061/(ASCE)0733-9429 (2005)131:2(127), 127–133.

Shen H.W. (1999). Flushing sediment through reservoirs. Journal of Hydraulic Research, 37 (6), 743-757.

Sumi, T. (2008). Evaluation of Efficiency of Reservoir Sediment Flushing in Kurobe River. Proceedings 4th International Conference on Scour and Erosion (ICSE-4). November 5-7, 2008, Tokyo, Japan, 608–613.

Talebbeydokhti, N., and Naghshineh, A. (2004). Flushing sediment through reservoirs. Iranian Journal of Science and Technology, Transaction B: Engineering, Taylor & Francis, 28(B1), 119–136.

van Rijn, L. C. (1993). Principles of sediment transport in rivers, estuaries, and coastal seas, Aqua Publications, Amsterdam, The Netherlands.

White, R. (2001). Evacuation of sediments from reservoirs. Thomas Telford.

White, W.R. (1990). Reservoir sedimentation and flushing. Hydrology in Mountainous Regions. Artificial Reservoirs; Water and Slopes. IAHS Publ, (194).

Wisser, D., Frolking, S., Hagen, S., and Bierkens, M.F.P. (2013). Beyond peak reservoir storage? A global estimate of declining water storage capacity in large reservoirs. Water Resources Research, Wiley Online Library, 49(9), 5732–5739.

WRPI, (2011). Planning and Physical Model Test Results of Flood Diversion and Sediment Sluicing Facilities upstream of Shihmen Reservoir (in Chinese). Water Resources Planning Institute, Water Resources Agency, Dept. of Economics Affair, December, 2011.

Xu, J.P., Noble, M.A., and Rosenfeld, L.K. (2004). In-situ measurements of velocity structure within turbidity currents. Geophysical Research Letters, 31, L09311, doi:10.1029/2004GL019718.

Xu, J.P. (2011). Measuring currents in submarine canyons: Technological and scientific progress in the past 30 years. Geosphere, v. 7, 868-876.

Zyserman, J. and Fredsøe, J. (1994). “Data Analysis of Bed Concentration of Suspended Sediment.” Journal of Hydraulic Engineering, 120(9), 1021–1042.